KU Leuven
Biomedical Sciences Group
Faculty of Medicine
Department of Neurosciences

KU LEUVEN

DOCTORAL SCHOOL
BIOMEDICAL SCIENCES

ANATOMICAL CONNECTIVITY OF THE VENTRAL MIDBRAIN IN MACAQUE

- Muhammad Zubair

Supervisor: Wim Vanduffel, Ph.D.
Co-supervisor: Tadashi Isa, Ph.D.
Kyoto University - Kyoto, Japan

Jury members: Sebastian Haesler, Ph.D.
Mathieu Vandenbulcke, Ph.D.

Bechir Jarraya, Ph.D.
Université de Versailles - Paris, France
Julie Duque, Ph.D.
Université catholique de Louvain - Leuven, Belgium

November 2021

SUMMARY

Animals adapt their behavior to adjust to dynamically changing environments. One of the important neurotransmitter systems that are implicated in shaping this behavior is dopamine (DA). In the current manuscript, we investigate this neurotransmitter system, which is involved in a wide range of functions, including but not limited to: motor control, decision-making, attention, memory and sensory processing. During the last few decades, neurophysiologists and anatomists have explored the DA neurotransmitter network. Undoubtedly, these studies have provided key knowledge on the DA network and its functions, but still, voids remain in complete understanding. We aimed to reveal the DA connectome by using recently developed viral vector mediated tracers. The first purpose of this dissertation is to gain better insights into the brain-wide structural connections originating in the ventral midbrain DA system using anterograde viral vector-based methods.

In **chapter 2**, we investigated the detailed anatomical connectivity of the midbrain DA system. Therefore, we injected adeno associated viral vector (AAV) mediated tracers into the macaque's midbrain, using magnetic resonance imaging (MRI) guidance. Subsequently, we carefully mapped the brain-wide

anatomical connections originating from the (injected) midbrain region. This in-depth study revealed dopaminergic projections at both areal- and laminar-level. We found that the lateral ventral midbrain (including substantia nigra, pars compacta (SNc)) projects densely to somatomotor cortex and dorsal striatum. In contrast, the medial midbrain (primarily the ventral tegmental area (VTA)) projects to dorsal prefrontal and temporal cortical areas, with surprisingly sparse projections to the striatum. In general, the orbitofrontal and occipito-parietal cortex received strong and weak projections, respectively. Overall, the ventral midbrain is found to project to many brain regions, although in a very heterogeneous manner.

Our second study is completely independent from the first one and explores training-based changes in neuronal processing in early visual cortical areas, which are most likely partially driven by dopaminergic signals. Hence this study aims not to investigate the anatomical features of the dopaminergic system, but rather a functional consequence of its activation under normal circumstances. Visual processing involves both retinal feedforward and non-retinal feedback signal inputs. It is largely unknown, however, how non-saccadic somatomotor signals influence early visual processing in NHPs. In **chapter 3**, we designed an event-related functional magnetic resonance imaging (fMRI) paradigm to investigate the modulations in the

neuronal activity in early visual areas after associating an effector with a visual stimulus. We found lateralized activity modulations in the visual cortical areas ipsilateral to somatomotor areas activated by the associated effector. The (enhanced) activity in ipsilateral early visual areas most likely reflect the influence of somatomotor signals induced by the effector which is associated with the visual stimulus.

In conclusion, the first study findings reported in this dissertation enhanced our understanding of the midbrain DA structural network and the second study revealed the influence of somatomotor signals in early visual processing.

SAMENVATTING

Dieren veranderen hun gedrag om zich aan te passen aan dynamisch veranderende omgevingen. Eén van de belangrijke neurotransmittersystemen die betrokken zijn bij dit gedrag is dopamine (DA). In het huidige manuscript onderzoeken we dit neurotransmittersysteem, dat betrokken is bij een breed scala aan functies, waaronder, maar niet beperkt tot: motorische controle, besluitvorming, aandacht, geheugen en sensorische verwerking. In de afgelopen decennia hebben neurofysiologen en anatomen het DA-neurotransmitternetwerk verkend. Ongetwijfeld hebben deze studies belangrijke kennis opgeleverd over het DA-netwerk en de functies, maar toch ontbreekt er informatie. We wilden het DA-connectoom onthullen met behulp van recente methodes gebaseerd op virale vectorem. Het eerste doel van dit proefschrift is om een beter inzicht te krijgen in de volledige structurele hersenverbindingen die hun oorsprong vinden in het DA-systeem van de ventrale middenhersenen met behulp van anterograad virale vector gebaseerde methoden.

In **hoofdstuk 2** onderzochten we de gedetailleerde anatomische connectiviteit van het DA-systeem van de middenhersenen. Daarom hebben we een virale vector in de middenhersenen van de makaak geïnjecteerd, met behulp van magnetische resonantie beeldvorming (MRI). Vervolgens hebben we de

anatomische verbindingen in kaart gebracht die afkomstig zijn uit het (geïnjecteerde) midden hersengebied. Deze studie onthulde dopaminerge projecties op zowel area- als laminair niveau. We vonden dat de laterale ventrale middenhersenen (inclusief substantia nigra, pars compacta (SNc)) geconcentreerd naar de somatomotorische cortex en het dorsale striatum projecteren. Daarentegen projecteren de mediale middenhersenen (voornamelijk het ventrale tegmentale gebied (VTA)) naar dorsale prefrontale en temporale corticale gebieden, met verrassend schaarse projecties naar het striatum. Over het algemeen ontvingen de orbitofrontale en occipito-pariëtale cortex respectievelijk sterke en zwakke projecties. Over het algemeen blijkt de ventrale middenhersenen naar veel hersengebieden te projecteren, maar op een zeer heterogene manier.

Visuele verwerking berust zowel op retinale feedforward als niet-retinale feedback signalen. Het is echter grotendeels onbekend hoe somatomotorische signalen (buiten oogbewegingssignalen) de vroege visuele verwerking in NHP's beïnvloeden. In **hoofdstuk 3** hebben we een event-related functioneel magnetische resonantie beeldvorming (fMRI) paradigma ontworpen om de modulaties in de neuronale activiteit in vroege visuele gebieden te onderzoeken na het associëren van een effector met een visuele stimulus. We vonden unilaterale activiteitmodulaties in

de visuele corticale gebieden ipsilateraal t.o.v. somatomotorische gebieden geactiveerd door de geassocieerde effector. De (verhoogde) activiteit in ipsilaterale vroege visuele gebieden weerspiegelt hoogstwaarschijnlijk de invloed van somatomotorische signalen geïnduceerd door de effector die geassocieerd is met de visuele stimulus.

De resultaten gerapporteerd in dit proefschrift verhogen onze kennis over het structurele DA netwerk van de middenhersenen, en onthullen de invloed van somatomotorische singalen in vroege visuele verwerking.

ACKNOWLEDGEMENTS

I would like to pay my special regards to Wim for seeing the potential and believing in me. It was his trust and constant motivation that pushed me at every step to climb up the hill. In this way, I am heavily in debt to John, who guides at each step with patience. It was a perfect balance of a hard time, guidance, support and help by you guys that finally pays off.

I am genuinely grateful to the most caring and loving people, Isa-sensei and Kaoru-san, who make my stay way easier in Japan. I was lucky to be mentored by Kaoru in the lab, whom I always found highly dedicated to the work. Despite having a hectic all-day schedule, she always took out time whenever I need her. I am highly obliged to have Isa-san to be my co-promoter. It would not be possible to complete the project without his supervision and project planning. This common research passion and dedication by Isa and Kaoru always motivates me to immerse myself in work and enjoy it completely. I would never forget our late-night lab work, evening (online) meetings with Wim, looking forward to the results after protocol optimization, working on the weekends, tissue slicing started in the morning and ended up in the evenings or sometimes even in the night. I also enjoyed their company outside the lab, going out for sushi and lab colleagues' get-togethers in the lab kitchen. It was this care, love

and support from all of my Kyoto lab colleagues and friends that make Japan a second home to me.

Many thanks to Chantal and Anne for taking care of my monkeys whenever I travelled home or for work. I was always amazed by Chantal's magical hands who know how to bring monkey back to work, after I give up on them. She was always there to help me in the behavioral trainings and sometimes preparation for the scanning sessions. In all these years, I think the person whom I bother the most was Astrid. As she takes care of all my flight bookings/re-bookings, many of the reimbursements. I would thank her for being always determined to bring me back from Japan when I was stuck there due to COVID restrictions, following a lot of paperwork, emails to the authorities, airline and travel companies.

I am grateful of having Sjoerd as my PhD colleague, with whom it was always easy to work with, as I found him always exceptionally helpful and supportive. His sincere suggestions always helped me in tackling the problems and getting out of the uncomfortable situations. Undoubtedly, we were two individuals from very different world of thoughts, but I guess this diversity is the beauty that bring colors to our society. I want to thank all my lab colleagues, including Qi, Xiaolian, Pascaline, Puiu, Marina, Marcelo, Eline, Tao, Matteo, Alessia, and Robert. The weekly fMRI sessions with Koen's group including Prosper, Saloni, Ding,

Sona and Lotte, were informative and knowledgeable. Special thanks to my other lab mates who joined me on this voyage including, Satwant, Kasper, Francesco, Valentina, Flavio, Irene, Mela, Mahsa, Arno, Mansoureh, Jerome, Elvira, Benjamin, Amir, Sofie, Lara, Michael, Jerome, Celia, Marta, Anna and Rajani. I want to pay credits to all those people including Wouter, Marc, Stijn, Piet, Gerrit, Christophe, Inez, Astrid, Sara, Elsie, Marc, Ronnie, Kenneth and Jan without whom the running of this lab is not even possible.

I also want to pay special thanks to the chair of my supervisory committee Prof. Dirk Daelemans and jury members: Prof. Sebastian Haesler, Prof. Mathieu Vandenbulcke, Prof. Bechir Jarraya and Prof. Julie Duque, for dedicating their valuable time to read my thesis and provide valuable comments.

In the end, I would send love to my niece (Aroosh (ma' Gappu)), little nephew (Daoud) pay thanks to my beloved and supporting wife (Anam Khan), blessed father (Fakhar-ud-Din) and mother (Shehnaz Jahan), loving brothers (Umair and Uzair) and sister (Ayesha Khan) who were always there to support, take care of things, fulfill home responsibilities in my absence, motivate me, pray for me with patience in this long voyage. My achievements and success would never be possible without their constant support, motivation, trust and love. Undoubtedly, in this whole time away from home, I have missed you guys at all those events

and celebrations, but your love always makes me feel like I was among you all the time. I never felt bored in Leuven, having an excellent company with Usman, as we share our passion for cooking, food, travel, sports, and movies. Talking and chatting with my best friends Usama, Haroon and Kashif, all sitting on different continents, make me realize how close our friendship was, even being physically far away from each other.

I want to end the acknowledgement section with a quote, that always makes me motivated in hopeless situations.

"There will come a time when you believe everything is finished; that will be the beginning"

- Louis L'Amour (1908 – 1988 CE)

To my parents and wife

TABLE OF CONTENTS

CHAPTER I: General Introduction 3

1.1 Dopamine 5

1.2 Classification of midbrain dopaminergic neurons 6

1.3 Interspecies differences on the distribution of midbrain dopamine neurons 7

1.4 Major midbrain dopaminergic pathways 10

1.5 Anatomical connections of the midbrain system 11

1.5.1 Current knowledge on midbrain afferent projections 12

1.5.2 Current knowledge on midbrain efferent projections 16

1.6 Need to investigate dopaminergic efferent connections 18

1.7 Non-retinal inputs contribution in early visual processing 20

1.8 Methods 25

1.8.1 Immunohistochemistry and immunofluorescence process 25

1.8.2 Neuronal tract-tracing technique 29

1.8.3 functional magnetic resonance imaging (fMRI) 30

1.9 Objectives 32

CHAPTER II: Ventral midbrain projections in the macaque brain 39

2.1 Introduction 41

2.2 Materials and Methods 44

2.2.1 Subjects 44

2.2.2 Viral vector preparation 45
2.2.3 MRI/CT-guided targeting and injection procedures 45
2.2.4 Histological processing 48
2.2.5 Anti- RFP immunohistochemistry through DAB staining 49
2.2.6 Double labelling IHC with anti-RFP and anti-TH antibodies 50
2.2.7 Histological assessment and data analysis 51
2.3 Results 52
2.3.1 Injection sites 52
2.3.2 Cell-type specificity within injection sites 55
2.3.3 Cortical and subcortical projections 56
2.3.4 Prefrontal cortex 57
2.3.5 Somatomotor cortex 65
2.3.6 Occipito-parietal cortex 69
2.3.7 Temporal cortex 72
2.3.8 Subcortical regions 77
2.3.9 IHC double labelling of nerve terminals 85
2.4 Discussion 88
2.5 Supplementary information 98
CHAPTER III: Somatomotor signals modulate early visual cortical activity 113
3.1 Introduction 115
3.2 Results 117
3.2.1 Hand-color association: behavioral performance 119

3.2.2 Eye positions 119
3.2.4 Hand-color association: group fMRI analysis 123
3.3 Discussion 132
3.4 MATERIALS AND METHODS 139
3.4.1 Subjects 139
3.4.2 Color-hand association task 140
3.4.3 fMRI data acquisition 142
3.4.4 GRE and anatomical data acquisition 143
3.4.5 fMRI preprocessing and analysis 144
3.5 Supplementary information 146
3.6 STAR METHODS 157
CHAPTER IV: Discussion 161
4.1 Ventral midbrain dopaminergic efferent projections 162
4.1.1 Significant findings relative to previous studies 162
4.1.2 Linking DA anatomical and effective connectivity studies 167
4.1.3 Limitations of the study and future perspectives 169
4.1.4 Midbrain dopaminergic neurons shaping motor activity 175
4.1.5 Parkinson's Disease and its treatment 175
4.2 Effector-induced modulations in the early visual processing 180
4.2.1 Significant findings in light with the previous work 181
4.2.2 Open questions and future work perspectives 188

4.3 General conclusion 188
References 191
APPENDIX 221

LIST OF ABBREVIATIONS AND ACRONYMS

1	somatosensory area 1
2	somatosensory area 2
3a	somatosensory area 3a
3b	somatosensory area 3b
5PE	superior parietal lobule area
6M	area 6 of ctx (suppl. motor)
7	inferior parietal lobule area
8AD	subregion of the DPFC
8AV	subregion of the DPFC
8B	subregion of the DPFC
9L	subregion of the DPFC
9M	subregion of the DPFC
11	subregion of the OFC
12	subregion of the OFC
13L	subregion of the OFC
13M	subregion of the OFC
14	subregion of the OFC
23a-c	subregion of the PCC
24a-d	subregion of the ACC
25	subregion of the ACC

31	subregion of the PCC
32	subregion of the ACC
35	subregion of the Ent
44	subregion of the VLPFC
45A	subregion of the VLPFC
45B	subregion of the VLPFC
46d	subregion of the DPFC
46v	subregion of the DPFC
47l	subregion of the VLPFC
47O	subregion of the VLPFC
A1	auditory area 1
A8	cell group A8 (=RRF)
A9	cell group A9 (=SNc)
A10	cell group A10 (=VTA)
AAV	adeno-associated virus
ACC	anterior cingulate cortex
AIP	anterior intraparietal area
AK	auditory koniocortex
Amyg	amygdala
AO	anterior olfactory cortex
AQL	anterior quadrangular lobule
aT	anterior thalamus
Aud	auditory cortex

BOLD	blood-oxygen-level-dependent
CA	field CA of the hippocampus
Cd	caudate nucleus
Cereb	cerebellum
Cl	claustrum
CT	computed tomography
D99	macaque brain template
DA	dopamine
DAB	diaminobenzidine
Dg	dentate gyrus
dLGN	dorsal LGN
DPFC	dorsal prefrontal cortex
ECL	Ent, caudal limiting field
EGP	external globus pallidus
EI	Ent, intermediate part
ELC	Ent, lateral, caudal division
EM	electrical microstimulation
Ent	entorhinal cortex
ER	Ent, rostral part
F1	motor area 1
F2	motor area 2
F3	motor area 3
F4	motor area F4

F4/5	agranular frontal area F4/5
F5p	motor area F5, posterior part
F6	motor area F6
F7	motor area 7
FEW	family-wise error rate
fMRI	functional MRI
FST	fundus of superior temporal sulcus
GFP	green fluorescent protein
GI	granular insula cortex
GLM	general linear model
GP	globus pallidus
GRE	gradient echo
GrL	gracile lobule
Gu	gustatory cortex
Hipp	hippocampus
IA	agranular insula
ID	dysgranular insula
IG	granular insula
IGP	internal globus pallidus
IHC	immunohistochemistry
ins	insula
IPa	IP associated area of STS
IPar	intraparietal cortex

IPro	insular proisocortex
IPS	intraparietal sulcus
ISL	inferior semilunar lobule
IT	inferotemporal areas
ITG	inferior temporal gyrus
L-DOPA	levodopa
LGN	lateral geniculate nucleus
LIP	lateral intraparietal area
LIPd	LIP, dorsal
LIPv	LIP, ventral
mdT	medial dorsal thalamus
MGN	medial geniculate nucleus
MIP	medial intraparietal area
mml	medial medullar lamina
MRI	magnetic resonance imaging
MST	medial superior temporal area
MTG	medial temporal gyrus
NAc(c)	nucleus accumbens (core)
NAc(s)	nucleus accumbens (shell)
NB	nucleus basalis
NGS	normal goat serum
OFC	orbitofrontal cortex
OPAI	orbital periallocortex

OPro	orbital proisocortex
PaAC	para-auditory area, caudal part
PaAL	para-auditory area, lateral part
PaAR	para-auditory cortex, rostral part
PAG	periaqueductal gray
PaIL	parainsular area, lateral part
PaIM	parainsular area, medial part
Par	parietal cortex
PBS	phosphate buffered saline
PCC	posterior cingulate cortex
PD	parkinson's disease
PE	parietal area PE
PF	parietal area PF
PFC	prefrontal cortex
PG	parietal area PG
PGa	PG associated area of the sts
PGM	parietal area PG, medial part
Pir	piriform cortex
ProK	prokoniocortex
ProM	promotor area
Pu	putamen
Pul	pulvinar nuclei
ReI	retroinsular area

RFP	red fluorescent protein
RPE	reward prediction error
RRF	retrorubral field
Rt	reticular nucleus (prethalamus)
S2	secondary somatosensory ctx
SEM	standard error of the mean
SII	secondary somatosensory ctx
Sim	simple lobule
SNc	substantia nigra, pars compacta
SNr	substantia nigra, pars reticulata
Somato	somatosensory cortex
ST1	superior temporal region 1
ST2	superior temporal region 2
ST3	superior temporal region 3
STG	superior temporal gyrus
STN	subthalamic nucleus
Strait	striatum
STS	superior temporal sulcus
Sub	subiculum
TAa	temporal area TAa
TE	temporal area TE
TE1	temporal area TE1
TE	echo time

TEa	temporal area TEa
TEM	temporal area TE, medial part
TEO	temporal area TE, occipital part
TF	temporal area TF
TFO	temporal area TF, occipital part
TG	temporal gyrus
TH	temporal area TH
TH	tyrosine hydroxylase
THO	temporal area TH, occipital part
TL	temporal area TL
TLR	temporal area TL, rostral
TO	temporal-occipital cortex
TP	temporal pole
TPO	temporal-parietal-occipital
TPt	temporoparietal area
TR	repetition time
V	lobule V
V1	visual area 1
V2	visual area 2
V2d	V2, dorsal part
V2v	V2, ventral part
V3	visual area 3
V3A	visual area 3A

V3d	visual area 3, dorsal part
V3v	visual area 3, ventral part
V4	visual area 4
V4v	visual area 4, ventral part
V5	visual area 5 (=MT)
V6	visual area 6
V6A	visual area 6A
Vg/mL	viral genomes per mL
VI	declive
VIIB	tuber
VIP	ventral intraparietal sulcus
Vis	visual cortex
vIT	ventral lateral thalamus
VLPFC	ventral lateral prefrontal cortex
VP	ventral pallidum
VTA	ventral tegmental area

The unprepared mind cannot see the outstretched hand of opportunity.

-Alexander Fleming (1881 – 1955 CE)

CHAPTER I: General Introduction

The brain is the most complex organ of the body, which works as a central command unit for controlling not only very fundamental vital functions (i.e. respiration, digestion etc.) but also to perform exceedingly complex cognitive tasks (i.e. driving, solving mathematical equations, reading, etc.). Some of these cognitive tasks are learned by associating reward with a stimulus or a behavior. Reward-based learning (Schultz, 2015) is supported by a reward network originating in the ventral midbrain. More specifically activity of dopamine (DA) neurons in the ventral tegmental area (VTA) encodes reward prediction errors (RPE) (Schultz, 1997, Schultz, 2016), first introduced in seminal NHP studies of Wolfram Schultz. In rodents, the role of dopamine (DA) in reward-based learning (Steinberg et al., 2013, Tsai et al., 2009, Witten et al., 2011) has been causally demonstrated, which has been later confirmed in primates (Stauffer et al., 2016). Despite the importance of DA in reward-based learning, our current knowledge about the anatomical connections of this neurotransmitter system in primates is still largely unknown due to existing challenges relative to rodents (i.e. brain size, targeting specific cell-types, expression level of opsins, typically mall number of subjects, etc.) (Galvan et al., 2017). Recently, it has also been shown that stimulation of the

DA network concurrently with a task-irrelevant visual cue induces cortical plasticity in mid-stage visual areas of the macaque (Arsenault and Vanduffel, 2019). Although this form of cortical plasticity that was observed may reflect be mediated by direct dopaminergic innervations to these regions, this still needs to be tested.

Finally, although extraretinal signals influence processing in early visual areas, we don't have much knowledge about possible modulations in stimulus representations induced by the association of an effector (i.e. motor action) with a visual stimulus.

In this dissertation, our first study aims to increase our knowledge on the anatomical profile of the ventral midbrain DA system by using viral vector mediated axonal tract tracers. Apart from the midbrain DA anatomical connectivity exploration, in our second study, we tested our hypothesis that the association of an action with a visual stimulus can modulate the stimulus representation in occipital cortex. The two studies discussed in this manuscript are independent, where the first one provides an in-depth insight into the ventral midbrain connectome while the second one shows the involvement of somatomotor input in visual processing, most likely driven by dopaminergic signals. Time did not permit to prove the dopaminergic nature of the

learning-induced alterations in visual representations, hence this will be pursued in future studies.

1.1 Dopamine

The midbrain dopaminergic neurons constitute the main source of dopamine (DA) (Chinta and Andersen, 2005). The dopaminergic neurons synthesize DA by conversion of tyrosine to L-DOPA which in turn is finally converted to DA.

DA is a neuro-transmitter and modulator that plays a pivotal role in driving some essential motor control and cognitive functions, like reward signaling (Schultz et al., 1997), non-associative learning (Waelti et al., 2001), working memory (Williams and Goldman-Rakic, 1995, Wang et al., 2004, Sawaguchi and Goldman-Rakic, 1991, Arnsten et al., 1995, Goldman-Rakic, 1997), motivation and reinforcement-based learning (Arsenault et al., 2014).

DA neurons also play a vital role in the reward system by responding to reward-predicting stimuli (Schultz, 1997): they become active in response to an unpredicted reward or to sensory stimuli predicting reward (Schultz, 1998, Satoh et al., 2003, Takikawa et al., 2004). When a mismatch is detected between actual and expected rewards, dopaminergic neuron

encodes RPE (Schultz, 2007). Yet, the activity of DA neurons is not entirely dependent on the RPE signal, they are also sensitive to aversion, uncertainty and novelty (Schultz, 2007, Bromberg-Martin et al., 2010). For example, in NHPs, a study found two types of DA neurons, motivational salience and value coding, responding to aversive events by activation and inhibition, respectively (Matsumoto and Hikosaka, 2009). However, later studies shows the activity of DA neurons in an aversive event is not related to the aversiveness (Fiorillo et al., 2013, Fiorillo, 2013).

1.2 Classification of midbrain dopaminergic neurons

The main origin for most of the DA neurons is the midbrain or mesencephalon, the most anterior part of the brainstem. Based on cellular morphology and general topography, the DA neurons in the midbrain are classified into three major subgroups: retrorubral field (RRF; A8 cell group), the substantia nigra (SN; A9 cell group), and (VTA; A10 cell group), in rat (Dahlström, 1964), in monkeys (Hubbard and di Carlo, 1973, Felten et al., 1974) and in humans (Nobin, 1973). The absolute number of mesencephalon DA neurons and their distribution varies considerably among different species (**Table 1.1**) (Murris, 2020). The total number of midbrain DA neurons is estimated to be

three- to seven-fold higher in rhesus monkey and an additional two times more in humans compared to that in rodents (German et al., 1988, German et al., 1989). It is important to mention, however, that it is quite challenging to exactly define the borders of the mesencephalon DA nuclei (especially between VTA, SN, and RRF) due to their irregular boundaries.

1.3 Interspecies differences on the distribution of midbrain dopamine neurons

In rats, a detailed quantification of the midbrain DA neurons in six midbrain nuclei has been performed: (i) RRF: corresponding to the A8 cell group (ii) substantia nigra pars compacta (SNc) and (iii) substantia nigra reticulata (SNr): corresponding to the A9 cell group (iv) VTA (v) central linear nucleus (CLi) and (vi) interfascicular nucleus (IF): corresponding to the A10 cell group (German and Manaye, 1993). It was reported that the majority (73%) of the cells in the VTA of rats are dopaminergic. An average number of dopaminergic (TH-immunostained) neurons in the above-mentioned midbrain nuclei are shown in **Table 1.2**. In monkeys, the total number of dopaminergic (TH^+) neurons were determined for four mesencephalon regions (RRF, SN (further subdivide into dorsal and ventral SN), and VTA) (Francois et al., 1999). More than two-thirds (72%) of these TH^+ neurons were located in the ventral SN. The rest 14%, 4% and 10% were found in VTA, dorsal SN, and RRF, respectively (see **Table 1.3**). Thus, the

absolute number and distribution of midbrain DA neurons across different dopaminergic nuclei varies considerably amongst these species, i.e. In rodents, VTA consists mainly (65%) dopaminergic neurons interspersed with GABAergic (33%) and glutamatergic neurons (2-3%) (Kawano et al., 2006, Morales and Root, 2014, Nair-Roberts et al., 2008). On the other hand, the percentage of midbrain DA neurons located in the VTA is lower in primates than in rodents (German and Manaye, 1993, Francois et al., 1999).

Species		VTA	SN
Mouse	M. musculus	12,500	10,000
Rat	R. rattus	20,000	20,000
Monkey	M. mulatta	50,000	150,000
Human	H. sapiens	100,000	300,000

Table 1.1: Cell count: Inter-species differences in absolute number of VTA and SN neurons (Murris, 2020)

Mesencephalic region	Mean ± SD	Percentage
RRF	1,341 ± 90	6
SNc	9607 ± 622	43
SNr	849 ± 23	4
CLi	1,292 ± 134	6
VTA	7,423 ± 547	34
IF	1,494 ± 161	7
Total	**22,006 ± 1,300**	**100**

Table 1.2: An average number and fraction of TH-immunostained (dopaminergic) neurons in six midbrain nuclei of the rat (German and Manaye, 1993).

Mesencephalic region	Mean ± SD	Percentage
RRF	9,080 ± 1070	10
ventral SN	66,920 ± 4620	72
dorsal SN	3,580 ± 2,180	4
VTA	12,800 ± 1,670	14
Total	**92,380 ± 4,820**	**100**

Table 1.3: An average number and fraction of TH-positive neurons in four mesencephalic regions of the monkey (Francois et al., 1999).

1.4 Major midbrain dopaminergic pathways

The midbrain dopaminergic neurons have widespread efferent (outgoing) projections with the remainder of the brain. These projections are classified as nigrostriatal, mesolimbic and mesocortical pathways. The nigrostriatal pathway originates in the SN (comprising both SNc and SNr) and projects towards the dorsal striatum (caudate and putamen). The other two pathways (mesolimbic and mesocortical), collectively known as mesocorticolimbic, have a common origin in the VTA. The mesolimbic pathways are directed to the ventral striatum (nucleus accumbens (NAc) and olfactory tubercle), amygdala and hippocampus, whereas, the mesocortical pathways projects to the cerebral cortex (Williams and Goldman-Rakic, 1998, Berger et al., 1988). The general outline of these efferent projections from the midbrain DA neurons is illustrated in **Figure 1.1**.

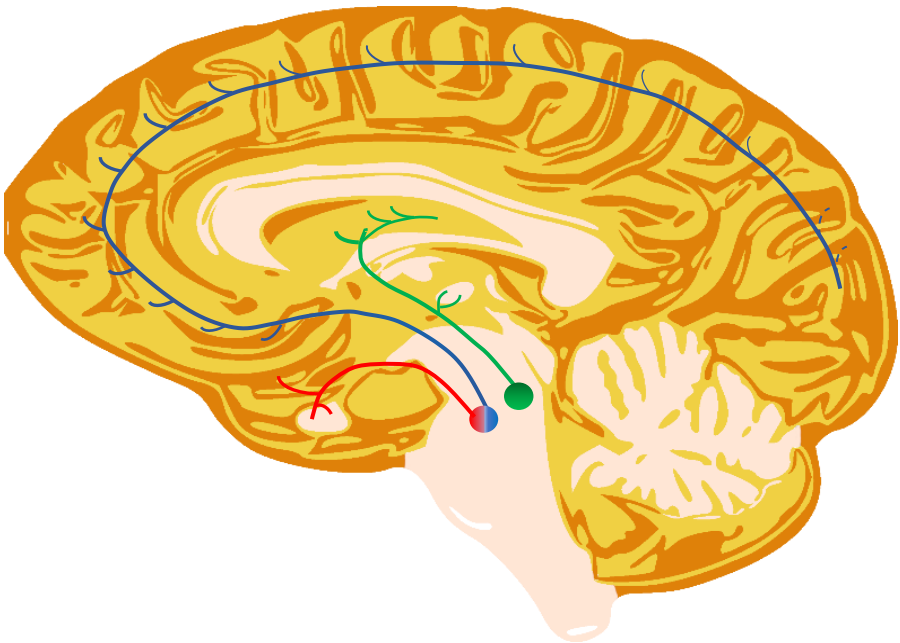


Figure 1.1: Overview of midbrain dopaminergic efferent projections in the brain. Mesocortical pathway (blue): VTA to cortical areas, Mesolimbic (red): VTA to ventral striatum, Nigrostriatal (green): SN to dorsal striatum.

1.5 Anatomical connections of the midbrain system

A key aspect to understand brain functions is the anatomical connectivity between neurons, between columns and between areas. Besides the mere anatomical connectivity, knowledge about the flow of information between different parts of the brain, including the direction in which signals are flowing, is also

crucial for understanding the functional role of regions. In contrast to rodents (Björklund et al., 1984, Berger et al., 1985b, Berger et al., 1985a, Descarries et al., 1987), primate studies lack detailed information regarding the exact mesencephalic origin of the dopaminergic connections (i.e. do they originate either in the VTA or the SN) and their whole-brain projection pattern. In this section, we shall outline previous studies on the midbrain afferent (incoming) and efferent (outgoing) projections in both rodents and NHPs. These are mainly the anatomical connectivity studies that have been performed based on a combination of immunohistochemistry (IHC) **(section 1.7.1)** and neuronal track-tracing **(section 1.7.2)** techniques.

1.5.1 Current knowledge on midbrain afferent projections

The projections to the midbrain neurons have been examined most thoroughly in rodents. As mentioned before, in rodents, 65% of the neurons in the VTA are dopaminergic. Different subpopulation of neurons in the VTA have different afferent connections, projection targets and neurotransmitter content (see **Figure 1.2**). Afferent projections to VTA were observed in the lateral hypothalamus (Fadel and Deutch, 2002). Other afferent inputs originate in the dorsal pons, where two nuclei. i.e. the laterodorsal tegmentum nucleus (LDT) and pedunculopontine

tegmental nucleus (PPTg), provide notable numbers of cholinergic, glutamatergic as well as GABAergic projections to the VTA (Cornwall et al., 1990, Oakman et al., 1995, Semba and Fibiger, 1992). Noted, the LDT primarily projects to the VTA whereas, the PPTg projects to both VTA and SNc (Oakman et al., 1995). One of the studies using a retrograde tracer injected in the VTA, revealed labelled neurons in prefrontal cortex (PFC) and the medulla oblongata (Geisler and Zahm, 2005). Moreover, the VTA also receives sparse afferent glutamatergic projections from the PFC (Geisler and Zahm, 2005, Sesack and Pickel, 1992), nucleus accumbens (NAc) and superior colliculus (Geisler and Zahm, 2005), lateral hypothalamus (Rosin et al., 2003) and several other brainstem structures. Presumably, VTA receives GABAergic inputs from the NAc (Conrad and Pfaff, 1976) and ventral pallidum (VP), as the labeled NAc fibers were found diffusely scattered in the VTA or spread laterally into the SN with very few labeled neurons situated in the lateral VP (Geisler and Zahm, 2005). The VTA also receives serotonergic inputs from the dorsal raphe nucleus and noradrenergic inputs from the locus coeruleus (LC) (Geisler and Zahm, 2005, Phillipson, 1979). Some other inputs to the VTA arise from the hypothalamus (Phillipson, 1979), amygdala (Wallace et al., 1992), and cerebellar nuclei (Geisler and Zahm, 2005).

In primates, the striatum is found to be the major source of afferent projections to the midbrain regions (especially VTA/SN)

(Haber, 2014), where it has been found that the dorsal striatum innervates more to the ventral region of the midbrain while the ventral striatum ends up dorsally (Lynd-Balta and Haber, 1994). Moreover, the dorsolateral striatum which receives extensive midbrain projections, projects sparsely to the ventrolateral pars reticulata (Haber et al., 2000). In contrary to the striatum, the cortical afferent projections to the midbrain DA cells does not appear to be robust. A restricted PFC afferent dopaminergic projection to the midbrain regions was observed (Frankle et al., 2006). Other afferent projections to the midbrain were reported from the VP and the external globus pallidus (EGP) projecting to the SN (Parent, 1986). Among several other small inputs to the VTA/SN, also GABAergic projections from the rostromedial tegmental nucleus (RMTg) have been reported (Jhou et al., 2009).

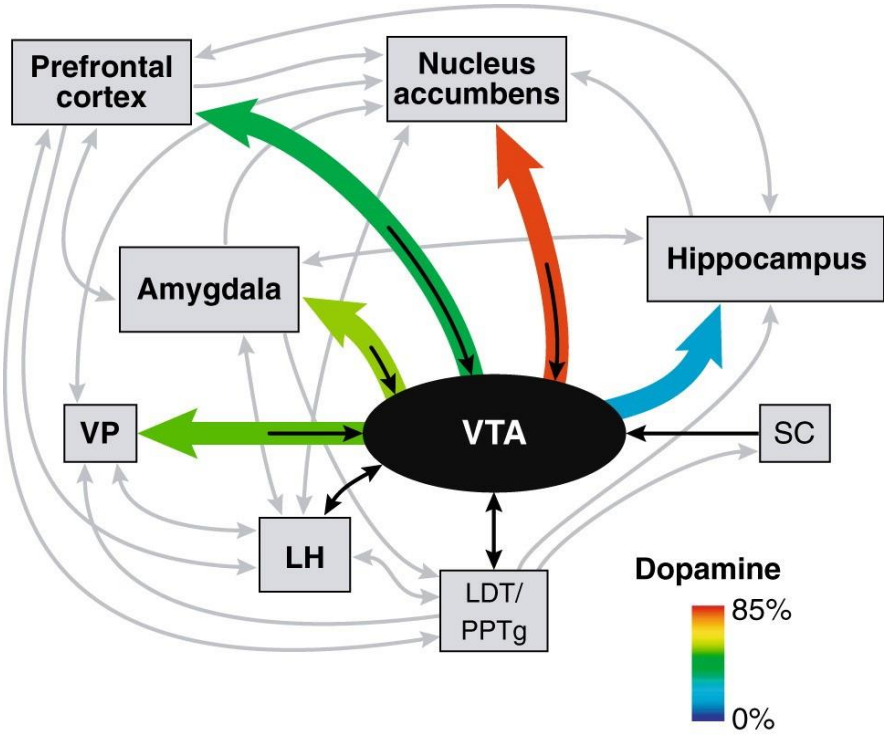


Figure 1.2: Major afferent and efferent projections of the VTA in rodents. Anatomical pathways to and from the VTA are represented by the color/black arrows. Rest of the connections are illustrated with gray color uni- or bi-directional arrows. An estimation of the percentage of projecting dopaminergic neurons (identified cytochemically) is shown by the color scale in the right bottom corner. **Abbreviations:** SC=superior colliculus; PPTg= pedunculopontine tegmental nucleus; VP=ventral pallidum; LDT=laterodorsal tegmental nucleus; LH=lateral hypothalamus. (adapted from Howard et.al., 2007)

1.5.2 Current knowledge on midbrain efferent projections

The VTA and SN are deeply integrated structures of the midbrain that are the main source of limbic forebrain and striatal dopamine. In rodents, the ventromedial striatum (NAc core and shell) receives dense projections from the midbrain VTA, the other areas include parts of PFC, lateral hypothalamus, and amygdala (Berger et al., 1974, Fuxe et al., 1974, Lindvall et al., 1978). The regions receiving sparse projections include entorhinal cortex, hippocampus and lateral septal area (Beckstead et al., 1979, Swanson, 1982). In studies using retrograde markers injected in the forebrain target sites, showed that each target receives input from distinct group of VTA neurons (Fallon et al., 1984, Swanson, 1982). A variable proportion of VTA-dopaminergic neurons projects to different locations (**Figure 1.2**). In rodents, DA projections from the VTA to NAc are the strongest (65-85%), then comes the lateral septal area (72%), followed by amygdala (53%), entorhinal cortex (46%), PFC (30-40%), and lastly the hippocampus (6-18%) (Fallon et al., 1984, Swanson, 1982, Gasbarri et al., 1994). Interestingly, it was observed that the electrical or chemical stimulation of the VTA evokes glutamatergic excitatory postsynaptic potentials (EPSPs) in PFC of rats (Lavin et al., 2005). Similarly, in mouse, it was shown that VTA stimulation mediate fast excitatory signals via glutamatergic synapses

(Chuhma et al., 2004). These studies raise the possibility that glutamate is co-transmitted in some dopaminergic VTA projection neurons, as already claimed earlier (Sulzer et al., 1998). Other studies have shown that also efferent GABAergic projections exist from the VTA to both PFC and NAc (Van Bockstaele and Pickel, 1995, Carr and Sesack, 2000).

In primates, the cortex is quite extensively innervated with midbrain DA terminals (Gaspar et al., 1989, Lewis et al., 1987). The majority of the DA cortical projections originate in the VTA and the dorsal SNc (Lidow et al., 1991, Gaspar et al., 1992, Levitt et al., 1984, Porrino and Goldman-Rakic, 1982) as illustrated in **Figure 1.3**. Moreover, the medial and lateral VTA/SN project to the medial and lateral striatum, respectively (Lynd-Balta and Haber, 1994, Parent et al., 1983). However, the dorsoventral topography is inverse, whereby the dorsal and ventral SNc neurons project to the ventral and dorsal caudate nucleus and putamen, respectively. In particular, the ventral tier projects mainly to the dorsolateral striatum. It was noted that, the striatal areas receive DA projections in differential ratios (Haber et al., 2000). Relatively recent findings concerning the midbrain dopaminergic (afferent and efferent) connections are reviewed in (Yetnikoff et al., 2014).

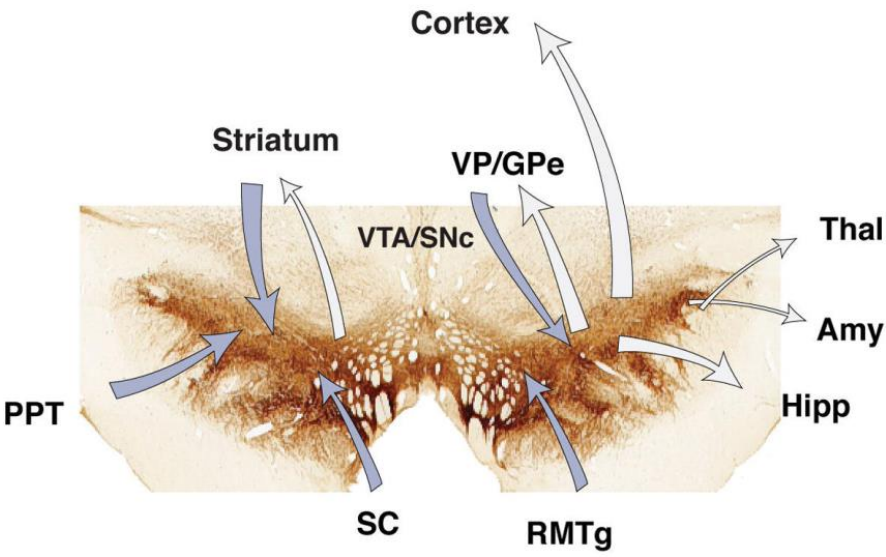


Figure 1.3: Schematic illustrating afferent and efferent connections of the midbrain dopamine neurons in macaque. Grey arrows=inputs; light grey arrows=outputs; Arrows represent general input and outputs and are not intended to represent topography. The wideness of arrow represents a rough density of the projections. **Abbreviations:** VTA=ventral tegmental area; VP=ventral pallidum; GPe=globus pallidus, external segment; Amy=amygdala; PPT=Pedunculopontine nucleus; Hipp=hippocampus; SNc=substantia nigra, pars compacta; SC=superior colliculus; Thal=thalamus; RMTg=rostromedial tegmental nucleus. (adapted from Haber, 2014)

1.6 Need to investigate dopaminergic efferent connections

The midbrain (especially) VTA is heavily studied in rodents, using novel genetic-based tools to identify the projections of the

dopaminergic VTA neurons (Aransay et al., 2015), with the most advanced viral vectors not yet available for primate research. Primate studies on VTA mainly focused on their electrophysiological properties and barely relied on causal or refined genetic-based experimental tools (Stauffer et al., 2016, Arsenault et al., 2014). Remarkably, only a few studies in the late 80's, with less sensitive technologies, examined the efferent projections of the VTA in primates (Berger et al., 1988, Lewis et al., 1987). Retrograde tract tracing techniques have been only used in the macaque to identify the mesofrontal dopaminergic projections (Williams and Goldman-Rakic, 1998). The latter type of studies focused on the injected regions; thus, they provided only a limited overview of all the regions that receive input from the VTA. Moreover, the use of retrograde tract-tracing techniques limited scientists to explore the connectome of a specific region throughout the brain. Consequently, the large-scale, brain-wide efferent connectivity of primate VTA remained surprisingly underexplored, despite the importance of the VTA in many cognitive and motor processes. With the recent advent and development of viral vectors for primates (Davidsson et al., 2019), we took the advantage to use them in the NHPs research. In our study, the injection of state-of-the-art viral vector constructs and subsequent anterograde tract-tracing allowed us to look for the anatomical connections in detail, including subcortical regions (see **Chapter 2**).

1.7 Non-retinal inputs contribution in early visual processing

The previous study focused on the anatomical connections of dopaminergic nuclei in the ventral midbrain. The second study bears, admittedly only in an indirect manner at this moment, at a presumptive functional consequence of dopaminergic activity: i.c., can associative learning between a stimulus and a specific effector lead to a modulation of activity in early visual cortex? Early visual processing is dependent on both retinal and non-retinal inputs. These non-retinal inputs include attention, memory, auditory, oculomotor, saccadic eye-movement and locomotion signals etc. In rodents, studies have shown that locomotion can modulate early visual processing (Saleem et al., 2013, Keller et al., 2012, Niell and Stryker, 2010, Ayaz et al., 2013), as discussed below. Also in NHPs higher-order visual area (V4) shows feature-dependent categorization sensitivity (Mirabella et al., 2007). This study, however, did not incorporate a possible involvement of the effector in the modulation of visually-driven activity. This motivated us to test the hypothesis whether the association of a visual stimulus feature with a specific effector can modulate activity in the visual processing.

To make sense of the outside world and react appropriately, multiple sensory inputs are integrated in the brain to produce a meaningful, unified and coherent representation of the situation. Traditionally, it has been assumed that this integration of information mainly happens in higher-order areas in the neocortex. Integration of multiple inputs have been observed in several neural circuits (Wolpert et al., 1995, Chen et al., 2013, Ernst and Banks, 2002, Angelaki et al., 2011) and typically involves mixed neuronal representations (Rigotti et al., 2013, Angelaki et al., 2009, Pouget et al., 2002). It has become evident, however, that neuronal activity in early visual areas does not merely dependent on a retinal stimulus, but is shaped by other nonvisual factors such as attention (McAdams and Reid, 2005, Roberts et al., 2007), impending reward (Shuler and Bear, 2006), and sensory inputs from other modalities (Ghazanfar and Schroeder, 2006, Iurilli et al., 2012).

In rodents, studies showed that primary visual (V1) neurons process multimodal information that integrates information about the visual stimulus with locomotion signals (Saleem et al., 2013, Keller et al., 2012, Niell and Stryker, 2010, Ayaz et al., 2013). Nevertheless, the exact nature of such locomotion-related signals is disputed. The observation of V1 responses to locomotion in the absence of a visual stimulus (in complete dark environment) (Saleem et al., 2013) suggested that the locomotor signals may

even drive, not just modulate activity of these neurons (Keller et al., 2012, Saleem et al., 2013). Other studies suggested that V1 signals the mismatch between the actual visual stimuli and those that should have been encountered given the locomotion (Keller et al., 2012), or that locomotion markedly reduced surround suppression, allowing the primary visual neurons to integrate over larger regions of visual space (Ayaz et al., 2013).

In primates, early investigations of the cerebral cortex recognized the importance of integrating information from multiple sensory modalities. Remarkably, a number of anatomical studies propose that in primary cortical areas of macaque, the substrate exists for multisensory integration (Cappe and Barone, 2005, Falchier et al., 2002, Rockland and Ojima, 2003). This integration of information from different sensory modalities is essential for primary and higher-order cortical operations and is considered an integral part of cognition. In NHPs, also higher order cortical areas (i.e. DLPFC, OFC, posterior cingulate gyrus, FST, and parahippocampal gyrus) receive inputs from multiple unimodal areas (Jones and Powell, 1970).

The primate's visual system also incorporates multiple inputs required to perform complex cognitive or motor tasks. For example, for successful navigation visual input needs to be combined with non-visual factors (i.e. subject's moving speed,

body balance, proper moves etc.) (Israel et al., 1997). As an example, consider the scenario of walking through a crowded street without bumping into others. To do so, visual and motor information needs to be integrated to control proper limb movements. Likewise, while performing a visuomotor task, the visual information can influence the motor system through different task-dependent pathways (Toni et al., 2001, Passingham et al., 1998). This visual information flows through the dorsal system when spatially congruent visuomotor transformations are involved (Milner and Goodale, 2006). Another route involves the ventral stream, extending into the ventral prefrontal cortex (Murray et al., 2000, Petrides, 1997, Passingham and Toni, 2001) for decision making based on the identification of external contexts (e.g. the identification of people or objects that may obstruct the walker).

As mentioned before, visual processing depends on retinal and non-retinal inputs. The non-retinal input signals (i.e. attention, emotion, context, reward value, memory of the subject) modulate neuronal processing in early visual cortical areas. Electrophysiological (Roelfsema et al., 1998, Ito and Gilbert, 1999, Gilbert et al., 2000, Martinez et al., 1999) and imaging studies (Martinez et al., 1999, Somers et al., 1999, Smith et al., 2000) have shown that the visual processing in the primates' early visual cortical areas is influenced by attention to features (McAdams

and Maunsell, 1999, Mirabella et al., 2007) or spatial location of stimulus (Williford and Maunsell, 2006, Sundberg et al., 2009) (reviewed in (Posner and Gilbert, 1999)). Some imaging studies, while showing faces with emotions, demonstrate the interaction between brain centers linked to emotion (i.e. amygdala) and visual processing in occipital cortex (Vuilleumier et al., 2004, Pessoa and Ungerleider, 2004). Moreover, working memory (Harrison and Tong, 2009, Cocchi et al., 2011) and identity-based contextual association and position of surrounding objects (Quek and Peelen, 2020) were also found contributing in the visual processing. The estimation of the subjective reward value and reward outcomes is another factors contributing in the processing of visual information (Stănişor et al., 2013).

Other major non-retinal sensory inputs that contributes to early visual processing includes, auditory (Ibrahim et al., 2016), oculomotor (Noudoost et al., 2014), saccadic eye-movements (Sylvester et al., 2005, Reppas et al., 2002) and locomotion. Neuroanatomical studies in macaque confirms the interconnections between auditory, sensorimotor and visual cortices (Kuypers et al., 1965). Moreover, anatomical tracing studies revealed audiovisual convergence in visual cortex, mainly in primary (V1) and secondary (V2) visual areas (Falchier et al., 2002, Rockland and Ojima, 2003).

Currently, in NHPs, we do not know much about the involvement of the somatomotor input as one of the non-retinal input we suspect to be involved in the early visual processing. In **chapter 3**, we have tried to solve a part of this puzzle by testing our hypothesis that the early visual neurons may change their response properties when an effector (motor action) is associated with the visual stimulus.

1.8 Methods

1.8.1 Immunohistochemistry and immunofluorescence process

Immunohistochemistry (IHC) is a powerful microscopy-based technique for the identification and visualization of cellular components, for instance proteins or other macromolecules, in tissue samples. The main steps of the classical IHC process are i) sample preparation, ii) staining and iii) detection (visualization) as illustrated in **Figure 1.4**. The sample preparation involves a fixation process and is an important step as the antigen exhibition relies on the quality of the tissue sample. The staining step involves the binding of antibodies with the targeted epitope. Normally, binding of antibodies is performed sequentially in two steps: first the primary antibody is allowed to bind to the epitope of the targeted antigen. Then comes the secondary antibody which is coupled to a reporter molecule. At

the detection stage, this reporter molecule produces a colored precipitate when treated with a chemical substrate, or just show the respective fluorescence color in case of fluorophore as a coupled reporter.

The IHC process is heavily dependent on the quality and specificity of the antibodies, as their choice can directly affects the results, reliability and interpretation. Even if antibodies can detect the correct molecule of interest, they may vary in their specificity for their intended target. The choice of antibodies with high-specificity is essential for obtaining reliable results as they produce more “on-target” bindings and less background signal. There are two main types of antibodies: polyclonal (heterogeneous mixture of antibodies that can bind to different epitopes on the target), monoclonal (bind to the same epitope of the target). Both antibodies are being used in the IHC process but should be carefully selected considering their strengths and weaknesses. As polyclonal antibodies tend to bind multiple epitopes on the same target, they are considered as very potent. However, there is a possibility of increased off-target binding due to poorly defined epitopes with varying epitope-specificities. In contrast, monoclonal antibodies are known to have high specificity for the targeted epitope, but sometimes makes the results difficult to interpret, due to low sensitivity if the target epitope is relatively rare.

The IHC staining process is being executed by following one of two alternative tissue handling approaches. The first one requires to apply the staining on slide-mounted samples. In contrast, the free-floating (Bulmer, 1964, Nadelhaft, 1984) method allows the sample to be stained while suspended in the solution. In fact, the free-floating technique allows a better antibody penetration, thus, is recommended when dealing with thicker sections (<20 µm) and if one aims to acquire information on dendritic and axonal projections. This staining technique is also efficient when dealing with several sections simultaneously. As our goal was to find the axonal projections, we used the free-float staining method for the sliced tissues of 40 µm thickness.

The IHC detection step is based on the secondary antibody that carries a pre-bound reporter molecule, i.e. enzyme or fluorophore. The visualization of the reporter molecule localizes indirectly the target and facilitates to observe the target's expression pattern among heterogeneous cell populations. The target-antibody interaction is visualized either by an observable stain or a fluorescent signal under a fluorescence microscope. The reaction of a secondary antibody carrying the reporter molecule is in itself a signal amplification step since several secondary antibodies can bind to the primary antibody which results in a stronger signal by multiple reporter molecules.

However, dependent on the sensitivity of the experiment and desirable signal amplification the secondary antibody may instead carry linker molecules which are able to recruit a large number of reporter molecules in subsequent steps.

Additionally, the counterstaining process can enhance the contrast between the signal and its background which facilitates the interpretation of morphology and cell structure within the IHC treated sample. The most common type of counterstains are hematoxylin and neutral red that stains cellular cytoplasm with a pale bluish and pinkish color, respectively and the cell nuclei in a dark bluish and pinkish color, respectively. The fluorescence stained sections do not require counterstaining, since the detection is not based on light microscopy. The immunohistochemically treated sections are coverslipped with care to avoid any air bubbles that could possible distort the imaging and degrade the condition of the section in the long run.

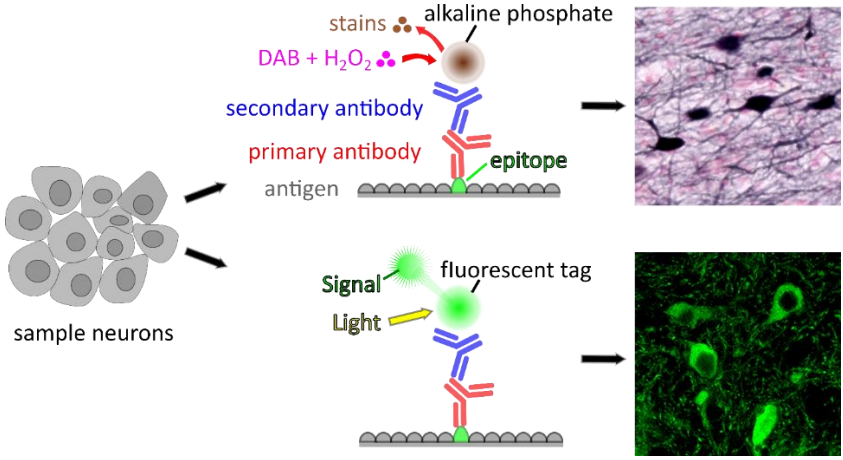


Figure 1.4: Illustration of the IHC technique. (top) indirect immunohistochemistry, diaminobenzidine (DAB) is oxidized by hydrogen peroxide in a reaction catalyzed by an alkaline phosphate (i.e. Ammonium nickel phosphate) which results in the indirect visualization (usually dark-brown stain color) of the cell, **(bottom)** immunofluorescence, a fluorescent reporter (green fluorescent protein) attached to the secondary antibody aids the visualization of the stained cells under a fluorescent microscope.

1.8.2 Neuronal tract-tracing technique

Neuronal tract-tracing technique is used to identify and visualize anatomical connections between brain regions. In this technique, a tracer is injected in a target region of the brain with compounds that is intracellularly transported across the neuron. This enables to visualize the spread of the injected compound throughout the neuron, the morphology of the neuron including its axonal and dendritic details. Most

importantly, it reveals areas connected with the injection site. Over the past decades, these tracer injections have been used to establish 'connectomes' in different animal species.

In general, based on the type of tracers, two main tract-tracing techniques can be distinguished: anterograde (from cell bodies to their terminals) and retrograde (from terminals to the cell bodies) as illustrated in **Figure 1.5**. The main purpose of both these techniques is to detect and visualize connections between a target population of neurons and their connections.



Figure 1.5: Anterograde and retrograde neuronal tract tracing. The tracer spreads as shown by the arrows, **(left)** either away from the cell body (anterograde) or **(right)** towards it (retrograde).

1.8.3 functional magnetic resonance imaging (fMRI)

fMRI is a non-invasive neuroimaging technique to investigate the functional properties of multiple brain areas simultaneously by offering good spatial resolution. It is an indirect measure of

changes in cerebral blood flow (CBF), cerebral blood volume (CBV) and blood oxygenation that (mainly) follows changes in neural activity (Ogawa et al., 1993). At baseline level or resting state, a certain proportion of oxygenated to deoxygenated blood is maintained. However, when a brain region becomes active, the metabolic demands of that region requires oxygen consumption to fulfill the energy demands resulting in higher concentration of deoxygenated blood level and an increase of CBF and CBV in that brain area.

In humans, the most often used fMRI contrast is blood-oxygen-level-dependent (BOLD). BOLD fMRI relies on the different magnetic properties of oxygen-rich and oxygen-poor blood. Oxygenated blood is weakly diamagnetic (i.e. has little or no magnetic effect), which does not distort the MR signal contrary to the deoxygenated blood which is paramagnetic (i.e. weakly magnetic) resulting dephasing of the spinning protons and local MR signal loss. Thus, fMRI is sensitive for an increase or decrease in oxygenated blood in a specific brain region, typically as a result of changing neuronal activity.

For non-human studies, however, instead of BOLD imaging, contrast-agent enhanced fMRI is often being used. In this technique, a contrast agent that contains iron (e.g. MION;

Monocrystalline Iron Oxide Nanoparticles) is injected into the bloodstream of the animal prior to scanning. The iron in the blood distorts the local magnetic field. Hence an increase in neuronal activity, followed by an increase in local blood volume, causes a local decrease in the fMRI signal. Thus, the effect produced by contrast-agent enhanced fMRI is opposite to that of BOLD. Contrast agents increase the statistical power (approximately by 10 folds), spatial resolution and localization of fMRI-detectable events compared to the BOLD technique (Vanduffel et al., 2001).

1.9 Objectives

In our lab, previous studies using VTA-electrical microstimulation (VTA-EM) have shown increased fMRI activity throughout most of the dopaminergic reward network (Arsenault et al., 2014). Moreover, stimulation effects depend on the stimulation frequency and state of the subject (Murris et al., 2020). In addition, changes in cortical representations and improvements in stimulus discriminability is also shown by pairing a visual stimulus with VTA-EM (Arsenault and Vanduffel, 2019, Murris et al., 2021). As a continuation to investigate the VTA dopaminergic network and modulations of sensory cortex induced by dopaminergic and other non-retinal signals, we will **(1)** map the midbrain (especially VTA and SN) dopaminergic efferent

projections throughout the brain, and in an independent study **(2)** test our hypothesis that associating an effector with a visual stimulus modulate neuronal representations in early visual cortical areas.

(1) Recently, well established tools to find the VTA-DA projections have been used in rodents (Aransay et al., 2015). With the advent and development of these advanced (high-sensitive) techniques becoming viable in primate studies (Davidsson et al., 2019) we are in a position to explore the VTA-DA connectome markedly better than before in order to update our relatively limited knowledge on midbrain efferent connections (see **section 1.5.2**). The effective connectivity of the VTA dopaminergic neurons, as a proxy for anatomical connectivity (Vanduffel et al., 2002), has also been measured by electrically stimulating the VTA (VTA-EM), which yielded stimulation-induced activities throughout many of the known anatomically connected regions (including the reward network; (Arsenault et al., 2014)). As mentioned earlier (see **section 1.3**), the VTA also contains subsets of non-dopaminergic neurons (i.e., GABAergic, glutamatergic). Electrical stimulation being a non-cell type-specific technique, VTA-EM cannot guarantee that the resulting fMRI activities are caused by dopaminergic neurons. The effective connectivity measures can be a result of activating both non-dopaminergic and dopaminergic neurons, which are

heterogeneously distributed within the VTA. Moreover, we also found that the effective connectivity measures also depend on stimulation frequency and state of the subject (Murris et al., 2020), complicating the interpretation of stimulation results. This highlights the need to improve our knowledge of the VTA-dopaminergic anatomical pathways and for a better understanding of the efferent connectivity profile of the ventral midbrain. In **Chapter 2** of this dissertation, to increase our understanding of the whole-brain connectivity of dopaminergic system in primates, we shall trace the detailed axonal terminals of the midbrain dopaminergic neurons using anterograde viral vector-based tractography.

(2) Our lab showed that pairing a task-irrelevant stimulus with VTA-EM is sufficient to drive stimulus-specific plasticity and improve stimulus discriminability (Arsenault and Vanduffel, 2019). This led us to hypothesize that also the pairing an effector (relying on a motor response in which the dopaminergic system plays a pivotal role) to a visual stimulus might modulate the representation of a retinal stimulus. In **Chapter 3**, we tested this hypothesis by designing a color-discrimination task in which a color-cue is coupled with a specific hand response (visuomotor association) and we looked for modulations in the visual stimulus representation depending on which hand was paired with the color-cue.

All outstanding work, in art as well as in science, results from immense zeal applied to a great idea.

-Santiago Ramón y Cajal (1852 – 1934 CE)

CHAPTER II: Ventral midbrain projections in the macaque brain

Muhammad Zubair[1,2,3], Sjoerd R Murris[1,2], Kaoru Isa[3], Hirotaka Onoe[4], Yoshinori Koshimizu[3], Kenta Kobayashi[5], Wim Vanduffel[1,2,6,7], Tadashi Isa[3,4,8]

[1] Laboratory of Neuro- and Psychophysiology, Department of Neurosciences, KU Leuven Medical School, Leuven 3000, Belgium

[2] Leuven Brain Institute, KU Leuven, Leuven 3000, Belgium

[3] Department of Neuroscience, Graduate School of Medicine, Kyoto University, Kyoto 606-8501, Japan

[4] Human Brain Research Center, Graduate School of Medicine, Kyoto University, Kyoto 606-8507, Japan

[5] Section of Viral Vector Development, National Institute for Physiological Sciences, Okazaki, 444-8585, Japan

[6] Athinoula A. Martinos Center for Biomedical Imaging, Massachusetts General Hospital, Charlestown, MA 02129, USA

[7] Department of Radiology, Harvard Medical School, Boston, MA 02144, USA

[8] Institute for the Advanced Study of Human Biology (WPI-ASHBi), Kyoto 606-8501, Japan.

Published as:

Zubair, M., Murris, S. R., Isa, K., Onoe, H., Koshimizu, Y., Kobayashi, K., Vanduffel, W., Isa, T. Divergent whole brain projections from the ventral midbrain in macaques. *Cerebral Cortex,* 2021.

Divergent whole brain projections from the ventral midbrain in macaques

To understand the connectome of the axonal arborizations of dopaminergic midbrain neurons, we investigated the anterograde spread of highly sensitive viral tracers injected into the ventral tegmental area (VTA) and adjacent areas in three macaques. In two monkeys, injections were centered on the lateral VTA with some spread into the substantia nigra, while in one animal the injection targeted the medial VTA with partial spread into the ventromedial thalamus. Double-labeling with antibodies against transduced fluorescent proteins and tyrosine hydroxylase indicated that substantial portions of transduced midbrain neurons were dopaminergic. Interestingly, cortical terminals were found either homogeneously in molecular layer I, or more heterogeneously, sometimes forming patches, in the deeper laminae II-VI. In the animals with injections in lateral VTA, terminals were most dense in somatomotor cortex and the striatum. In contrast, when the medial VTA was transduced, dense terminals were found in dorsal prefrontal and temporal cortices, while projections to striatum were sparse. In all monkeys, orbitofrontal and occipito-parietal cortex received strong and weak innervation, respectively. Thus, the

dopaminergic ventral midbrain sends heterogeneous projections throughout the brain. Furthermore, our results suggest the existence of subgroups in meso-dopaminergic neurons depending on their location in the primate ventral midbrain.

2.1 Introduction

The mammalian midbrain houses several nuclei that contain predominantly dopaminergic cells. These mesencephalic clusters are classically divided into three major subgroups: the ventral tegmental area (VTA or A10), the substantia nigra (SN or A9: including both the pars compacta (SNc) and pars reticulata (SNr)) and the retrorubral field (RRF or A8) (Dahlström, 1964). Individual axons originating from dopaminergic cell bodies within these midbrain nuclei branch into many cortical and subcortical target areas (Matsuda et al., 2009, Aransay et al., 2015). In addition, the omnipresence of dopamine (DA) receptors and terminals throughout the brain in rodents (Weiner et al., 1991), non-human primates (Berger et al., 1988, Brown et al., 1979, Lidow et al., 1991) and humans (Gaspar et al., 1989) emphasizes the importance of these midbrain subgroups, which are the nearly exclusive source of DA within our brain.

A wide range of functions is associated with dopamine, such as: reward and reward prediction error signaling (Schultz, 2015),

working memory (Gamo et al., 2010, Sawaguchi and Goldman-Rakic, 1991), inhibitory control (Chamberlain et al., 2006), motor behavior (Kunori et al., 2014), attention (Noudoost and Moore, 2011) and motivation and effort (Vancraeyenest et al., 2020, Walton and Bouret, 2019). In attempts to ascertain the functional contribution of the midbrain to cortical and subcortical processing, previous studies combined electrical or optogenetic stimulation of the VTA in macaque monkeys with concurrent physiological (including functional magnetic resonance imaging, fMRI) and/or behavioral measures. Stimulation of this structure has a reinforcing effect within both instrumental and Pavlovian conditioning paradigms (Arsenault et al., 2014, Stauffer et al., 2016). Furthermore, concurrent brain-wide fMRI activation induced by VTA stimulation was detected in a network of mainly reward-related areas in monkeys (Arsenault et al., 2014). Comparable rodent studies (i.e., through optogenetics) have found, however, that the fMRI effects of midbrain photostimulation are more widespread than expected and potentially extend beyond this canonical reward network (Decot et al., 2017, Lohani et al., 2017). These seemingly incompatible findings could be the result of the testing conditions, such as stimulation parameters (amplitude, frequency, duration etc.) and the state of the animal (Murris et al., 2020). Perhaps the potentially largest contributor, however, to these heterogeneous functional and behavioral effects

evoked by stimulating the DA system relates to the affected nuclei and/or cell-types that are specifically activated within the midbrain. Recent rodent studies linking a conditioned visual stimulus to photostimulation of the more dorsal lateral midbrain (mostly SNc) lead to an increase in undirected locomotion in the animals, whereas photostimulation of the more ventral medial midbrain (mostly VTA) resulted in more active stimulus-directed learning (Keiflin et al., 2019, Saunders et al., 2018b).

To tackle outstanding questions on the multifaceted nature of the DA-system, it is crucial to precisely understand its underlying structural architecture. Thus far, however, despite the pioneering studies on the dopaminergic forebrain projections by Goldman-Rakic and colleagues (Levitt et al., 1984, Lidow et al., 1991), the efferent connectivity profile of the dopaminergic midbrain has remained under-investigated in primates. The injection of retrograde tracers has revealed strong projections from the midbrain to a handful of regions including the prefrontal cortex (Williams and Goldman-Rakic, 1998, Frankle et al., 2006), the striatum (Haber et al., 2000) and sparse projections to higher visual area (Gattass et al., 2014) in primates. Still, the caveat of retrograde tracers is that they do not permit a full brain exploration and the density of innervation in individual cortical laminae is impossible to assess with retrograde tracing.

The recent advent and development of viral vectors within neuroscience allows for improved anterograde tracing of neural projections (Davidsson et al., 2019). Here, we took advantage of these technological developments and injected the midbrain of three monkeys, with adeno-associated virus (AAV). We found that projections originating from the VTA (with some inclusion of neighboring nuclei) cover the entire brain, but with clearly heterogeneous patterns of regions with high- and low-density innervation, and with profound differences across layers. There are hotspots with dense projections and patchy expression of reporter genes in regions such as the striatum and orbitofrontal cortex. We also found obvious differences in the projection patterns across subjects, likely due to small variations in midbrain injection sites.

2.2 Materials and Methods

2.2.1 Subjects

Three female macaque monkeys (Macaca fuscata; M1: 4.2 kg, 4 years old; M2: 6.7 kg, 7 years old; M3: 9.4 kg, 9 years old) were used in the present study (Supplementary Material **S2.1**). Animal care and experimental procedures were performed in accordance with the ILAR's Guide for the Care and Use of Laboratory Animals and were approved by the committee for

animal experiments at the Graduate School of Medicine in Kyoto University, Japan. Monkeys are fed daily with standard primate chow, water and supplemented with fruits.

2.2.2 Viral vector preparation

AAV vectors were packaged as previously described (Kobayashi et al., 2016). Briefly, the packaging (pAAV2.1 or pAAV-DJ and pHelper) and transfer plasmids (pAAV-CAG-DsRed2 and pAAV-CAG-hChR2(H134R)-tdTomato) were transfected into HEK293T cells. The pAAV2.1 was prepared by mixing pAAV-RC1 and pAAV-RC2 plasmids; the weight ratio of pAAV-RC1 to pAAV-RC2 is 1:9. After incubation, harvested cells were lysed and purified by serial ultracentrifugation with cesium chloride. The purified particles were dialyzed with 0.001% Pluronic-F68 Solution (Sigma-Aldrich; St. Louis, MO USA) in phosphate-buffered saline (PBS), and then concentrated through ultrafiltration. The copy number of the viral genome (vg) was determined using a TaqMan Universal Master Mix II (Applied Biosystems; Foster City, CA USA).

2.2.3 MRI/CT-guided targeting and injection procedures

For the precise injection of AAV vectors into the VTA, we performed magnetic resonance imaging (MRI) and computed tomographic (CT) imaging by using a 3-Tesla MRI scanner (Verio,

Siemens, USA) and a 320-detector-row CT scanner (Aquilion ONE, Toshiba Medical Systems Corporation, Japan), respectively. For all surgeries, anesthesia of the monkeys was initially induced by intramuscular injections of xylazine hydrochloride (2mg/kg), ketamine hydrochloride (5mg/kg) and atropine sulphate (0.04 mg/kg), and subsequently maintained through the inhalation of isoflurane (1.0 - 1.5%) from a ventilator. Vital functions (i.e., heart rate, respiration rate, oxygen saturation, body temperature, and end-tidal carbon dioxide) were monitored throughout surgeries. First, the MR and CT images were obtained while the animals' head was fixed in custom-designed an acrylic MRI-compatible stereotactic apparatus under anesthesia. A custom-built 8-channel birdcage radiofrequency coil with a 10 cm inner diameter (Takashima Seisakusho Co., Ltd, Japan) was used for MRI. High-resolution 3D T1- and T2-weighted images were obtained through a 3D fast spin-echo sequence with two echoes. The separate CT and MR images were overlaid by applying a linear, rigid coregistration algorithm (PMOD Technologies, Zürich, Switzerland), in which the MR image was aligned on the subject's skull visible on the CT image. The merged image could subsequently be used to determine the exact positioning of a chamber on the skull, that allowed to target the VTA. This chamber could hold a stereotactic plastic grid for fixing an injection needle, with holes at 1 mm intervals (6-YGD-D1, Crist, USA). For monkeys 1 and 2, two chambers were tilted back

30 degrees in the sagittal plane and 25 degrees in the coronal plane for each hemisphere. For monkey 3, a single chamber was positioned vertically on the skull above the VTA.

A second series of MRI/CT images was acquired under anesthesia, but after chamber implantation and with the grid in place, to determine the exact position of the needle within the grid and depth of the injection along the track. To verify and visualize the exact injection site for the VTA of each monkey, a craniotomy was made under the grid and a gadolinium solution (OMNISCAN, Daiichi-Sankyo, Japan) at a concentration of 0.02 µmol/µL was injected into the intended position (rate: 0.1 µL/min, total volume: 0.5 µL). A subsequent acquisition of a T1-weighted image following the injection, revealed the spread of the contrast agent (**Figure S2.1**) and therefore gave us a good indication of the center-of-mass of the injections.

Exact specifications of the viral vectors, the injections and the animals that were used are provided in Supplementary Material S1. After the injection sites relative to the grid were decided, the monkey was anesthetized again and the AAV vectors were injected into the intended location: the VTA. The injection needles were prepared as previously described (Vancraeyenest et al., 2020). Briefly, the Hamilton needles (28G, 140mm; point style 2; no hub) were attached to a polytetrafluoroethylene tube

and connected to another Hamilton syringe (10µL, Model 701, Cemented NDL, 26sG, 2 in, point style 2) that were jointly attached to a micro-infusion pump (Legato 130 Syringe Pump, KdScientific). By attaching the injection needle to a micromanipulator (Narishige; Tokyo, Japan), we were able to accurately lower the needle to the previously calculated targets within the midbrain. After lowering the needle to the target site, the actual injection of the vector was conducted after a five-minute interval to allow for stabilization of the tissue from needle insertion. Subsequently, the vector was injected at a rate of 100 nl/min. Following the initial injection, another five-minute interval ensured that the viral vector was absorbed, and then, the needle was lifted. Postoperatively, the animals were treated with intramuscular analgesics (5mg/kg, ketoprofen) and antibiotics (5mg/kg Ampicillin) and kept under quarantine for at least seven days.

2.2.4 Histological processing

Approximately 40 days after the viral vector injections, the animals were deeply anesthetized with ketamine and euthanized through intravenous administration of sodium pentobarbital (35 mg/kg). The animal was then transcardially perfused using 0.05M phosphate buffered saline (PBS) followed by 4% paraformaldehyde in 0.1 M phosphate buffer (PB pH 7.4). The

brain was subsequently extracted from the skull, saturated with 10, 20 and 30% sucrose solutions in PB for cryoprotection, and later sectioned into 40 µm coronal slices with a sliding microtome (REM-710; Yamato, Japan) along the stereotactic coordinates from the rostral to caudal end of the cortical tissue including subcortical structures and parts of the cerebellum.

2.2.5 Anti- RFP immunohistochemistry through DAB staining

For immunohistochemistry (IHC) of vector transfected neurons, a first antibody to the DsRed2 or tdTomato, red fluorescent protein (RFP) was used with subsequent enhancement through diaminobenzidine (DAB) staining. All procedures below were performed at room temperature, unless stated otherwise. Every 24th section from anterior to posterior was incubated in a blocking solution of 10% normal goat serum (NGS) in PBS with 0.3% of Triton X-100 (PBS-T). Sections were then washed with PBS-T and incubated in 1:5000 rabbit polyclonal anti-RFP (Rockland Immunochemicals; Gilberstville, PA USA) in 2% NGS/PBS-T solution overnight at 4°C. On the next day, sections were washed in PBS-T and incubated in 1:200 biotinylated goat anti-rabbit IgG (Vector Laboratories; CA, US) in 2% NGS/PBS-T for two hours. Afterwards, sections were incubated with 1:200 vectastain elite ABC kit (Avidin-Biotin Complex – Vector

Laboratories: CA, US) in PBS-T for one hour and visualized with DAB containing 1% nickel ammonium sulfate (0.01% DAB, 1.0% nickel ammonium sulfate, 0.0003 % H2O2) in tris-buffered saline. To enable comparison of the staining strength throughout the series of whole-brain sections of each monkey, these reaction conditions were carefully controlled to be consistent. The sections were counterstained with 0.1% Neutral Red (Merck 101369, Frankfurt, Germany).

2.2.6 Double labelling IHC with anti-RFP and anti-TH antibodies

To check the injected area of AAVs, direct fluorescence of RFP was observed and microphotographs were taken with a fluorescence microscope (Keyence BZ-X800, BZ-X710; Osaka, Japan). Immunofluorescent staining against tyrosine hydroxylase (TH) was conducted to detect dopaminergic neurons and to outline the VTA and SNc. The anti-TH IHC method is described below. (1) To verify anti-TH immunoreactivity of the infected neurons in the midbrain and (2) to investigate anti-TH immunoreactivity of their axons at target areas, we applied IHC against the RFP to enhance the relatively weak signal in addition to the anti-TH IHC. Sections were incubated with monoclonal mouse anti-RFP (1:500, MBL, Woburn, MA USA; M155-3) and polyclonal rabbit anti-TH (1:500, Merck Millipore; Burlington,

MA USA: AB152) in 5% NGS in PBS/T after blocking incubation. Subsequently, sections were visualized with AF555 Goat anti-mouse IgG (1:200, Abcam; Cambridge, UK: ab150117) for RFP, and AF647 goat anti-rabbit IgG (1 :200, Invitrogen; Carlsbad, CA USA: A-11012) or AF488 goat anti-rabbit IgG (1:200, Invitrogen; A-11008) for TH, respectively.

2.2.7 Histological assessment and data analysis

To assess the presence of the injected vector, IHC-DAB treated sections (see above) were analyzed with a Keyence inverted microscope. Under a high-resolution (1920 x 1024 dpi) condition, the x4 magnification was sufficient to clearly visualize stained axons at the projection sites. A complete picture of each brain section was acquired through consecutive sampling and subsequent stitching of the magnified images, after which the resulting image was stored offline at its original size. In addition, regions of interest were carefully chosen and images of these representative areas were obtained at more optimal imaging conditions. To assess the areal density of the projections, we compared and equated our sections to comparable schematic coronal slices from a standard monkey atlas (Paxinos et al., 2000). In this detailed analysis, we divided the whole brain into five main subdivisions: (1) prefrontal, (2) somatomotor, (3) parieto-occipital, (4) temporal, and (5) subcortical areas. Each of

these subdivisions was then subdivided into reference regions from the same atlas. In addition, within each of the cortical regions, we determined the distribution of axon terminals for the different layers based on laminar landmarks visible through counterstaining for neurons (Neutral Red). The layers were split in three segments: the molecular layer (lamina I), intermediate layers (laminae II-III) and deeper layers (laminae IV-VI). We considered the subcortical areas as a whole since they lack the typical six-layered architecture of neocortical areas. The axonal distribution within each area and its layer segments was ranked on a scale within the range of 0-4, from no fiber expression (0) to the highest density of fibers (4). To indicate concentrated expressions of fibers in sparsely innervated regions (so-called patches), we marked the region and layer in question with an asterisk (of which the size denotes its density).

2.3 Results

2.3.1 Injection sites

AAV vectors were injected into the ventral midbrain at multiple sites through a stereotactically positioned plastic grid in three animals (see Materials & Methods). The regions infected with the vector

injection are shown for the three animals in **Figure 2.1 A-F**.

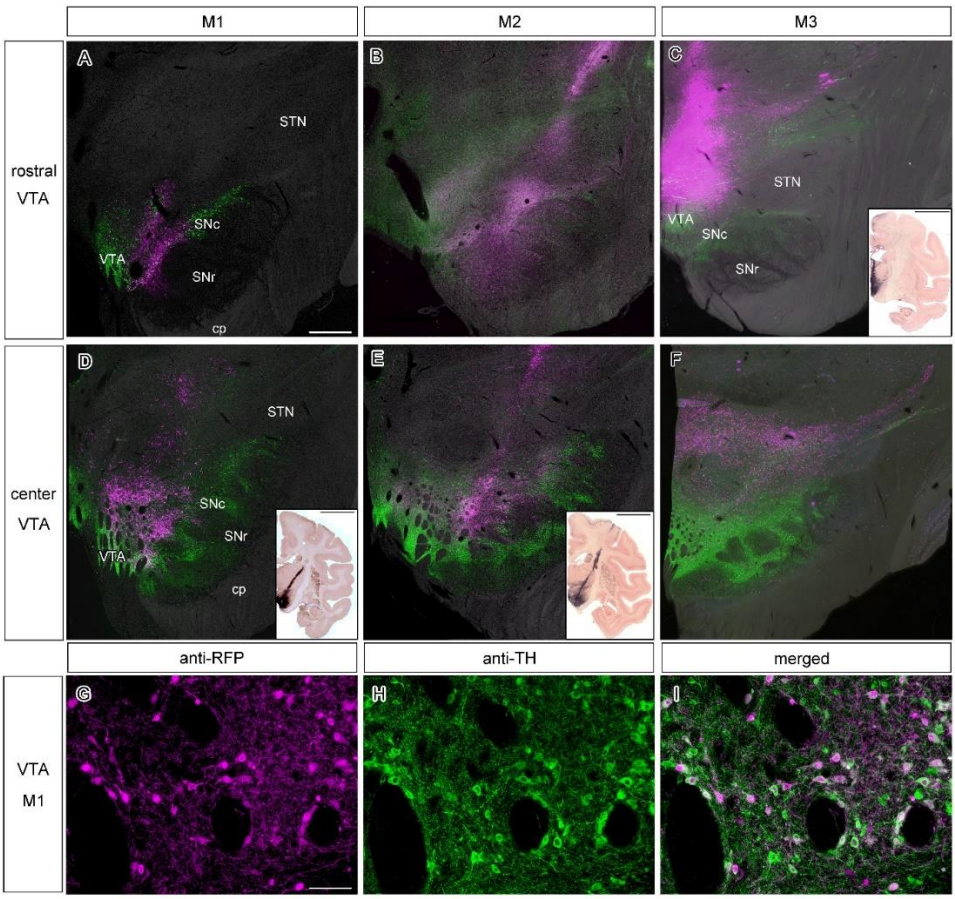


Figure 2.1: Viral vector injections targeting the VTA in three monkeys. (A-C) Photomicrographs of coronal sections in M1-3, revealing the rostral part of the VTA. Superimposition of anti-TH IHC (green), direct RFP fluorescence (magenta) on top of an inverted bright field microscope image. Scale bar in (A): 1 mm. The bottom right inset in (C) depicts a coronal slice in the vicinity in M3 through enhanced DAB staining, providing a clear overview of the injection area. Scale bar in the inset: 10 mm. **(D-F)** Additional photomicrographs of slightly more posterior coronal sections in M1-3, revealing the central portion of the VTA. Staining specifics and the scale bar are the same as in (A-C). The more diagonal injection trajectories of M1 and M2 are depicted in the

bottom right insets through enhanced DAB staining on coronal sections in the direct vicinity of the magnified images. Scale bar in the inset: 10 mm. **(G-I)** High magnification view of the VTA in M1, showing double anti-RFP and anti-TH IHC in cell bodies around the injection site. **(G)** anti-RFP IHC, **(H)** anti-TH IHC and **(I)** their merged image. Scale bar: 100 µm. **Abbreviations:** ventral tegmental area (VTA), substantia nigra pars reticulata (SNr), substantia nigra pars compacta (SNc), subthalamic nucleus (STN), cerebral peduncle (cp).

The sections were stained with IHC against tyrosine hydroxylase in which the dopaminergic cell groups of the VTA and SNc (TH+: in green) are clearly visible. The injections themselves were visualized through direct fluorescence of RFP which was integrated in the viral vectors (either DsRed2 or tdTomato; RFP+ in magenta). In M1, the injection was centered on the middle portion of the VTA along the rostro-caudal axis through laterally inclined injection tracks. The viral vector spread into the medial part of the SNc but spared the medial thalamus **(Figure 2.1 A, D)**. In M2, the injection was centered on the lateral portion of the VTA along the mediolateral axis and the central part of the VTA along the rostrocaudal axis. In addition, the vector spread into the medial two thirds of the SNc. This injection mostly spared the medial part of the VTA and medial thalamus **(Figure 2.1 B, E)**. In M3, the injection was centered on the dorso-medial, and rostral part of the VTA, excluding the SNc but including a part of the medial thalamus through vertical injection tracks **(Figure 2.1 C, F)**. Thus, the injection sites and spread of the injected vector

were relatively similar in monkeys M1 and M2, whereas the injected areas overlapped only partially with those in M3. In all three animals, the injection spared the RRF (data not shown).

2.3.2 Cell-type specificity within injection sites

Since the reporter gene introduced by AAV vector were driven by the ubiquitous promotor, it is not clear what fraction of somata at either the injection site and/or the terminals at the projection sites are dopaminergic. To estimate the portion of midbrain DA neurons that simultaneously contained the reporter gene of the infected vector (i.e., DsRed2 or tdTomato), we performed double fluorescent IHC against both TH and RFP. We then merged the images to show the co-expression within the somata (Blanchard et al., 1994, Lewis et al., 1988). **Figure 2.1 G-I** shows representative images of double-labeled neurons within the VTA of M1. Of the RFP+ cells around the injection site in M1, 76% (225/291) were TH+. In M2, this number was slightly higher, with 79% (206/262) double-labeled neurons. In M3, a smaller number of RFP+ cells 37% (100/270) showed concurrent staining for TH. Overall, these results suggest that not all, yet a considerable portion of the cells expressing RFP were dopaminergic.

2.3.3 Cortical and subcortical projections

A slice-by-slice assessment of the density of labeled fibers visualized by DAB (see Materials & Methods) revealed how cortical and subcortical structures are innervated by anterograde projections from the ventral midbrain. Stained axons in the cerebral cortex could be broadly divided into three categories: those in the most superficial or molecular layer (lamina I), in intermediate layers (laminae II-III) or in the deeper layers (laminae IV-VI). **Figure 2.2** and **2.4** collectively highlight example slices at three different magnifications of cortical projections in various areas in M1. In **Figure 2.3** representative slices highlighting cortical projections in M3 are presented. Subcortical innervations are indicated in **Figure 2.5,** focusing on the most salient results from the three animals. In general, the cortical projections found in the molecular layer tended to be more homogeneous compared to VTA projections in intermediate and deeper layers, which sometimes formed concentrated clusters of stained axons that we refer to as patches. The complete overview of cortical projections in the hemisphere ipsilateral to the injection side in subjects M1, M2 and M3 are presented in **Figure S2.2 - 2.4**, respectively. Contralateral projections relative to the injection site were only analyzed in M1 (photomicrographs are not shown in the main text because the stained axons were too sparse). However, see **Figure S2.5** for a brain-wide overview

of the stained coronal sections. The expression pattern of ventral midbrain projections across the entire brain was quantified on a scale from 0 to 4 (visualized in **Figure 2.6** and **2.8**).

2.3.4 Prefrontal cortex

In light of the previously determined connectivity between the prefrontal cortex (PFC) and the midbrain (Williams and Goldman-Rakic, 1998) together with a well-established role for DA in cognition within frontal areas (Noudoost and Moore, 2011, Ott and Nieder, 2019), we first set out to investigate the presence of axonal staining in various regions of the PFC. To this end, we divided frontal cortex into five subdivisions, which in turn all contained subregions themselves (overview in **Figure 2.6**). Descriptions of the results below largely follow the rankings presented in **Figure 2.6**.

The anterior part of the cingulate (ACC: areas 24, 25 and 32) contains a substantial number of stained axons fibers in the molecular layer for M1 and M2, but received only relatively weak midbrain projections in intermediate and deeper layers. This is in stark contrast with the findings in M3, in which the molecular layer of ACC contains very dense innervations (rank 4: 24a-c, rank 3: 24d, 32, **Figure 2.3B1**). In addition, in M3 cingulate is scattered with strongly stained patches that span mostly the intermediate

layers (laminae II-III: **Figure2.3B1ii**), which occasionally cross over into the deeper layers (laminae IV-VI).

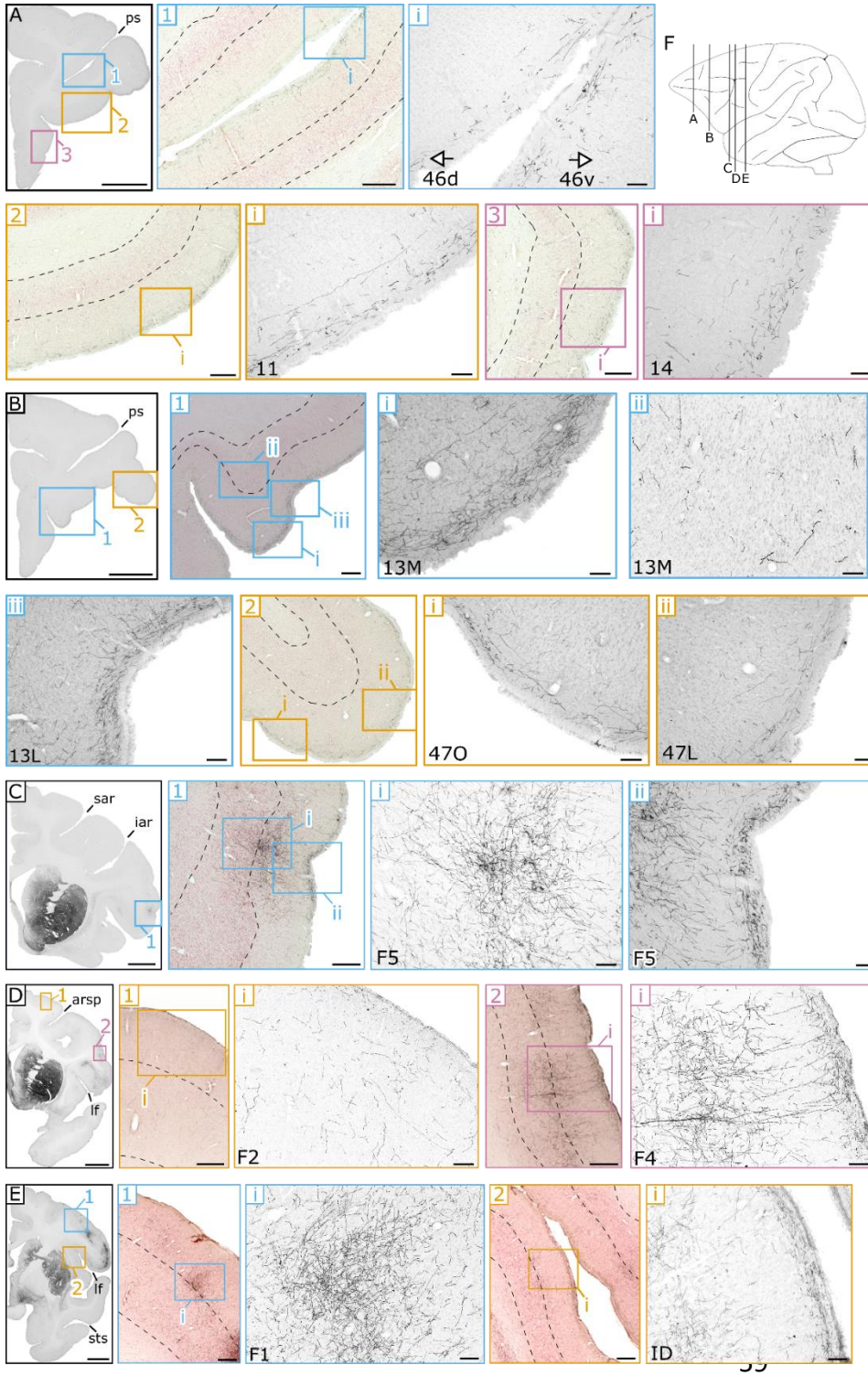

A
ps
1
2
3
1
i
i
46d
46v
F
A
B
C
DE
2
i
i
11
3
i
i
14
B
ps
1
2
1
ii
iii
i
i
13M
ii
13M
iii
13L
2
ii
i
i
47O
ii
47L
C
sar
iar
1
1
i
ii
i
F5
ii
F5
D
1
arsp
2
lf
1
i
i
F2
2
i
i
F4
E
1
2
lf
sts
1
i
F1
2
i
i
ID

Figure 2.2: Example sections of anterograde spread of the viral vector in frontal and somatomotor cortex in M1. (A) Coronal section at low magnification within the frontal cortex. Within this section, medium magnification images **(1-3)** show DAB staining of the terminals on top of counterstaining. Dotted lines represent the boundary of the intermediate (laminae II-III) and deeper layers (laminae IV-VI), and that of the deeper layers and the transition into white matter. Images at the highest resolution (roman numerals: **i-iii**) show DAB staining of the axonal fibers in more detail within PFC areas: 46d, 46v, 11 and 14. **(B)** Coronal section posterior to (A), with magnified images of PFC areas: 13M/L and 47L/O. **(C)** Coronal section highlighting a patch of fibers in motor area F5. **(D)** Coronal section containing two additional motor areas of F2 and F4. **(E)** Most posterior coronal section illustrating projections in primary motor area F1 and the dysgranular insula (ID). **(F)** A schematic sagittal view indicating the anterior-posterior position of each of the coronal sections (**A**-**E**). Scale bar: 1000 µm for **A**, **B**, **C**, **D**, and **E,** 500 µm for **A1, A2, A3, B1, B2**, **C1, D1, D2, E1,** and **E2** and 100 µm for all the other panels. **Landmark sulci**: principal sulcus (ps), superior arcuate sulcus (sar), inferior arcuate sulcus (iar), arcuate rectus spur (arsp), lateral fissure (lf), superior temporal sulcus (sts).

The bulk of the prefrontal cortex encompasses the dorsal prefrontal cortex (DPFC) and ventro-lateral prefrontal cortex (VLPFC). Compared to the ACC, the molecular layer of DPFC of M1 and M2 receives moderate projections from the midbrain (rank 1-2: areas 9M/L & 8AD, 8B), with an attenuated density in the intermediate and deeper layers. Slightly denser connected regions within the DPFC for these two monkeys are area 46 (rank 3 in M2, rank 2 in M1) and the ventral part of area 8A (rank 3 in

M2, rank 2 in M1). Within area 46, the density of the terminals seems to increase toward the fundus of the sulcus within the molecular layer (**Figure 2.2A1**). What immediately stands out for M3's DPFC compared to the other subjects, is the strong staining across all layers within area 9 (rank 4: 9M/9L). Not only does the more homogenous molecular layer color dark; deeply stained patches can be found throughout this area (**Figure 2.3A1**). The pattern in the remaining dorsal prefrontal areas in M3 are comparable to those in the other animals, with the notable exception of the deepest layer which ranks moderately, but consistently higher in this animal (rank 0-1: M1 & M2; rank 2-3: M3). The results within the third subdivision of the PFC, that of the VLPFC, do not deviate much from the more dorsal findings above. In M1 and M2, the same superficial to deeper gradient is present: with a medium density in the molecular layer (rank 2: areas 45 & 44) and decreasing innervations in the intermediate and deeper layers (rank 1: areas 45 & 44). Within this subdivision, area 47 is more innervated in M1 and M2 compared to neighboring regions, in particular the orbital part (rank 3: 47O, **Figure 2.2B2**). Again, overall staining in M3 was stronger in the VLPFC subdivision, which was most evident in area 45 (rank 3: 45A, rank 4: 45B), but interestingly also in area 47 (rank 3-4: 47O/47L, **Figure 2.3B2**).

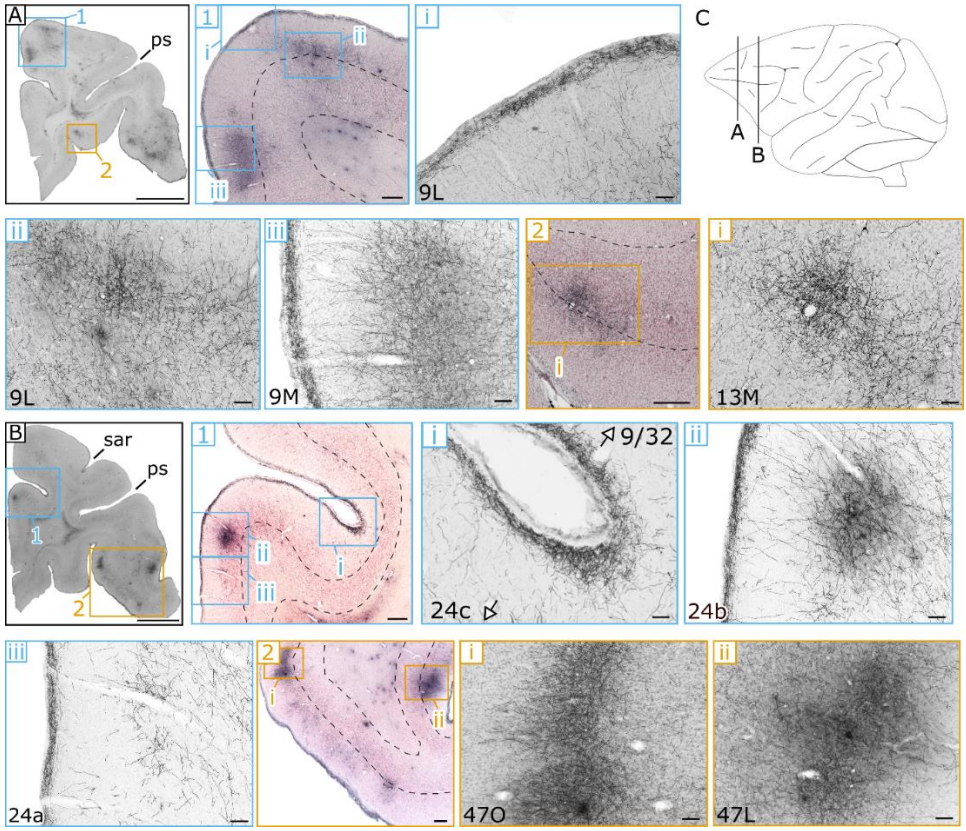


Figure 2.3 Example sections of the anterograde spread of viral vector in PFC and the anterior cingulate regions in M3. Conventions as those in Figure 2.2. **(A)** DAB staining of an anterior coronal section, in which innervations within (1) divisions of area 9 within the DPFC are shown (9M/9L) together with (2) a dense patch in the intermediate and deeper layers of OFC area 13 (13M). **(B)** Coronal section highlighting innervations in (1) the ACC (area 24a-c) and in the bordering DPFC area 9/32. In (2) the more rostral-lateral area 47 (47O/L) of the VLPFC contains concentrated patches mostly restricted to the intermediate layers. **(C)** A schematic sagittal view indicating the anterior-posterior position of each of the coronal sections (A-B). Scale bar: 1000 µm for **A** and **B**, 500 µm for **A1, A2, B1** and **B2**, and 100 µm for all the other panels. **Landmark sulci**: principal sulcus (ps), superior arcuate sulcus (sar).

To glean more insights in the latter observations, we assessed the projections within the more ventral PFC subdivision of the orbitofrontal cortex (OFC). Although the influence of DA within this frontal part of the brain has been less established than in its more dorsal counterparts (DPFC/VLPFC (Williams and Goldman-Rakic, 1998)), deficits in DA to this structure affect various cognitive functions in several animal models (Walker et al., 2009, Zeeb et al., 2010). In all monkeys, overall innervations were stronger in the OFC compared to the subdivisions in the PFC discussed above. In M1 and M2, the molecular layer was well innervated, which was particularly pronounced in area 11 (rank 3: in both M1 and M2; **Figure 2.2A2**), area 13 (rank 4: 13M in M1-M2 and 13L in M1, rank 3: 13L; **Figure 2.2B1**), but much less than PFC, and to a lesser extent in area 14 (rank 2 in M1/M2; **Figure 2.2A3**). In all of these areas, the axonal densities decrease in a typically cascading fashion towards the intermediate and deeper layers (rank 2: laminae II-III; rank 1: laminae IV-VI). The innervation pattern in M3 resembled that of the other monkeys, with the exception that innervations are typically even stronger, and there are more patchy expressions in the intermediate and deeper layers of area 13 (rank 2-3: 13M and 13L, **Figure 2.3A2**). Moreover, small patches were also present in the deepest layers of area 11 in M3. The more posterior OFC regions border the

subcortex and consist of the orbital periallocortex (OPAI), orbital proisocortex (OPro), anterior olfactory cortex (AO) and piriform cortex (Pir). Axonal terminal staining in OPAI and OPro was quite similar for all monkeys, with patchy expression in M2 (OPAI: laminae IV-VI) and in M3 (OPAI: laminae II-III). Projections within the anterior olfactory cortex, however, was divergent with relatively few axons in all layers of M1 and M2 (rank 1-2: AO), but significant innervation in M3 (rank 3-4: AO). The piriform cortex is homogenously innervated, with small patches in the deeper layers in M3 (Pir: laminae IV-VI). Interestingly this structure receives midbrain inputs that are relatively symmetrical across hemispheres (rank 2: Pir of M1c), as opposed to all other frontal structures that we assessed.

The last subdivision within the PFC contains insular and parainsular regions that are roughly located around the inlet of the lateral sulcus. In M1 and M2, axonal densities within this subdivision are unevenly divided: with, for example, very strong staining in the dorsal insula of M1 (rank 4: ID, **Figure 2.2E2**), moderate expression in the remaining part of the insula (rank 1-3: IG, IA and gustatory cortex of M1 and M2), but weak or even no expression in parainsular regions (rank 0: IPro, PaIL & PaIM in laminae II-VI of M2). In M3, on the other hand, expression is more homogenous throughout the insula, with slightly stronger innervations in the molecular layer compared to the

intermediate and deeper layers. In general, all subdivisions within PFC showed a typical trend receiving dense and diffuse projections in the molecular layer, with the remaining layers receiving patchy projections, which was more pronounced in the intermediate layers.

2.3.5 Somatomotor cortex

At first sight, we noticed that expression within the somatosensory and motor cortical areas were quite dissimilar across monkeys. We therefore decided to consider these areas as a single subdivision to facilitate comparisons in expression patterns. In the more anterior motor regions, the homogeneity of the molecular layer was less pronounced compared to the frontal areas. Rather, the motor and sensory regions consist of dark patches, which are especially prominent in M1 an M2, but mostly absent in M3.

The anterior motor region F7 shows moderate expression in all three subjects on average, with a varying distribution of axonal densities in the different layers across the three animals. For M3, F7 is the only motor region that is relatively strongly innervated (rank 3: F7 in the molecular layer and patchy expression in the intermediate layers); with the remaining part of the somatomotor cortex showing very weak projections (mostly

rank 1 except F5 and SII with rank 2). The patterns in M1 and M2 are completely different compared to M3, with strong ventral midbrain innervations in primary motor cortex (rank 4: F1, lamina I & laminae II-III in M2; patchy expression in laminae II-III of M1, **Figure 2.2E1**). The secondary motor areas also receive stronger projections in M1 and M2 compared to M3. Albeit less obvious than in F1, these areas also contained dense axonal patches mostly restricted to the intermediate layers (rank 2-3: F5 in M1 and M2, **Figure 2.2C1**; rank 1-3: F4 in M1 and M2, **Figure 2.2D2i** & rank 1-2: F2 in M1 and M2, **Figure 2.2D1i**). Besides the secondary motor areas, strong innervations were present in the more ventral premotor cortex of area ProM, which borders the somatosensory areas (rank 3-4: ProM in M1 and rank 2-3: ProM in M2). As stated above, axonal staining within somatosensory areas of M3 was mostly absent (rank 0-1: 2/1, 3a-b, 1, 2). In contrast, and especially pronounced in M1 but less so in M2, extensive patches were found in the intermediate and deeper layers of areas 2/1 (rank 4: 2/1 in M1, **Figure 2.4A2iii**), area 3a (rank 2-3: 3a in M1, **Figure 2.4A2i**), and area 3b (rank 3-4: 3b in M1, **Figure 2.4A2ii**). The more posterior primary somatosensory areas 1 and 2 contained less axonal terminals and were more equally innervated in the three animals (rank 1-2 in M1 and M2; rank 0-1 in M3). The ventrally located secondary somatosensory area showed quite extensive innervations, in particular in the deeper and intermediate layers of M1 (rank 3: SII in all layers,

patchiness in laminae II-III) and M2 (rank 2: SII in all layers, patchiness in laminae II-VI).

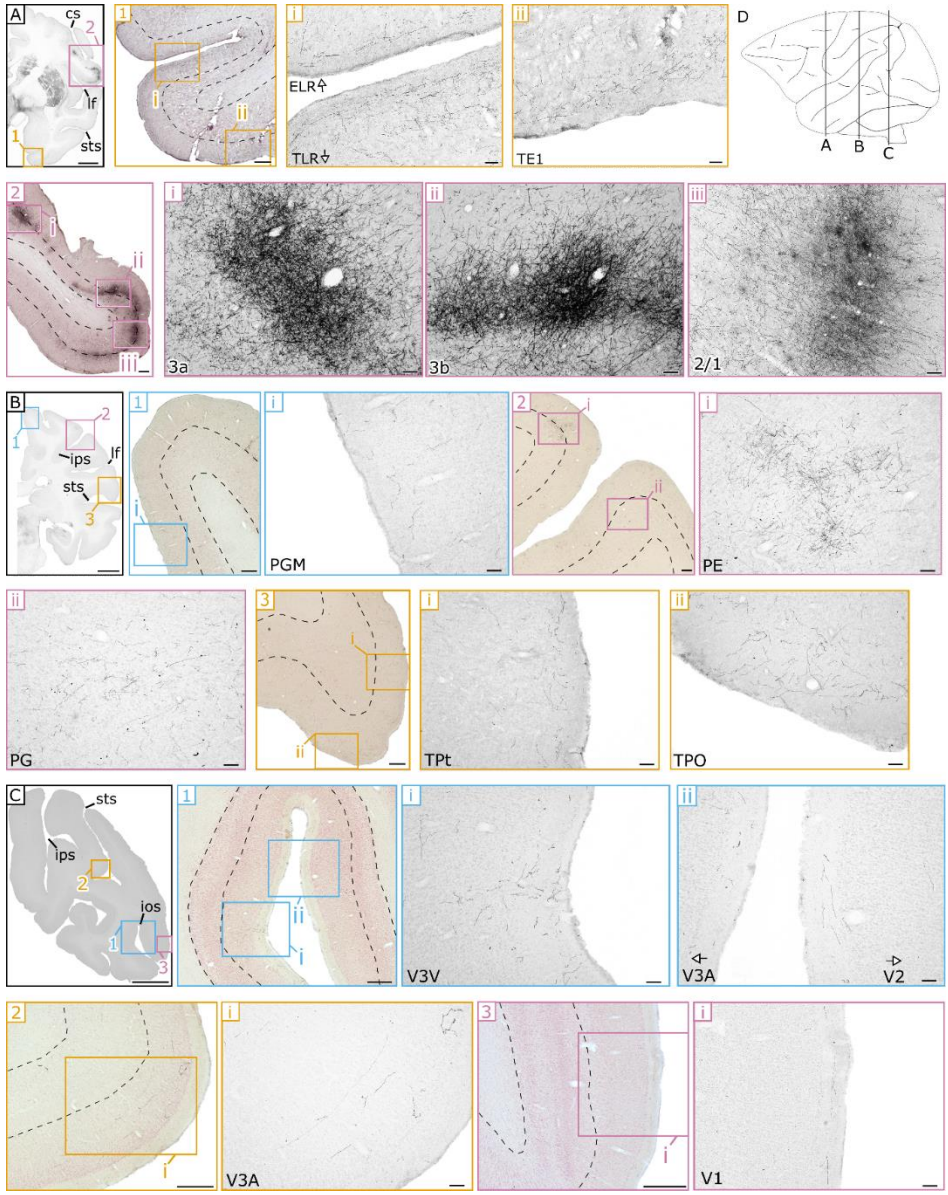


Figure 2.4 Example sections of anterograde spread of the viral vector in somatosensory, parieto-occipital and temporal regions in M1. Conventions as those in Figure 2. **(A)** anterior section showing fiber densities within (1) temporal regions including part of the entorhinal cortex (ELR) and inferior temporal regions (TLR and TE1) and (2)

parietal regions including somatosensory areas (3a, 3b, and 2/1) showing dense patches in the intermediate and deeper layers. **(B)** More posterior section highlighting varying fiber densities in (1) dorso-medial parietal area (PGM), (2) intermediate and deeper layers of two parietal areas (PE and PG) and (3) in the molecular and intermediate layers of two temporal regions (TPt and TPO). **(C)** The most posterior section showing few fibers within the (1-2) intermediate visual regions (V3V, V3A and V2) and (3) hardly any fibers in V1. **(D)** A schematic sagittal view indicating the anterior-posterior position of each of the coronal sections (A-C). Scale bar: 1000 µm for **A, B** and **C**, 500 µm for **A1, A2, B1, B2, B3, C1, C2** and **C3**, and 100 µm for all the other panels. **Landmark sulci**: central sulcus (cs), lateral fissure (lf), superior temporal sulcus (sts), intraparietal sulcus (ips), inferior occipital sulcus (ios).

2.3.6 Occipito-parietal cortex

Following the assessment of the frontal PFC subdivisions and somatosensory cortex, we extended our evaluation to the more posterior occipito-parietal areas, which, in light of the classically described anterior to posterior decrease in DA receptor distributions (Berger et al., 1988, Gaspar et al., 1989) are of particular interest. In agreement with these earlier assessments, the overall axonal densities within these more posterior regions were indeed less pronounced in all three animals, most clearly in M1 and M2.

The rankings within the posterior cingulate (PCC) differed only slightly from those described above for ACC. In M1 and M2,

diffuse projections targeted area 23, even including some parts not containing any stained axon (rank 1-2: 23a-c in M1; rank 0-2: area 23a-c in M2). A similar situation also held for the more posterior area 31 (rank 1-2: 31 in M1 and M2). Overall axonal densities in M3's PCC were stronger compared to that of other subjects, exactly as observed in ACC. This was most evident in area 23a (rank 3-4: 23a in laminae II-VI).

The parietal and intra-parietal subdivisions occupy the area between the posterior end of somatomotor cortex and the anterior boundary of dorsal extrastriate visual areas. Expression within the inferior parietal lobe areas was sparse and rather similar across monkeys. In M3, only sparse clusters of fibers could be detected within these parietal areas (rank 1-2: PE, PF, PGM and PG) that were equally divided across the laminae. In M1 and M2 more patchy and dense staining was occasionally observed, for example, in area PE (rank 2: laminae II-VI M1; **Figure 2.4B2i**, patchiness in laminae II-III for M2), area PGM (rank 2: laminae IV-VI in M1; **Figure 2.4B1i**, rank 3: lamina I in M2) and area PG (rank 1-2: laminae II-VI in M1; **Figure 2.4B2ii**). Within the retroinsular region, the pattern was reversed with strong projections in the molecular layer of M3 (rank 3: ReI in M3), but weak innervations throughout all layers of the other two monkeys (rank 1: ReI in M1 and M2). Finally, the areas within the intraparietal sulcus receive relatively few midbrain axons. Most

pronounced expression is observed in M3, followed by that of M1, and subsequently M2. Overall, staining in M3 is homogeneous but sparse, with small clusters of fibers in the anterior intraparietal area (rank 2: AIP, laminae IV-VI), the medial intraparietal area (rank 2: MIP, laminae II-III) and the ventral and dorsal part of the lateral intraparietal area (rank 2: LIPv & LIPd, laminae IV-VI). Such small axonal clusters were also present in the dorsal part of the lateral intraparietal area of M1 (rank 2: LIPd, laminae IV-VI), although innervations were generally sparse in this intraparietal subdivision. In M2, large portions of the intraparietal subdivision did not contain any labeled fibers (rank 0-1: AIP, MIP, LIPd, LIPv, VIP).

Occipitally are the visual regions, which were collectively analyzed as a last subdivision within the combined occipito-parietal cortex. Somewhat surprisingly, the general pattern of expression within dorsal visual areas can be seen as an inverted U-shape: in which the more anterior areas V5 and V6 together with the most posterior occipital areas V1 and V2 contain relatively little fibers, at least compared to the more intermediate visual areas V3 and V4. This pattern is most extreme in M2 in which overall expression is low and areas V1/V2 and areas V5 and V6 were completely void of axonal staining (rank 0: V5, V6, V1, V2). In M1, more projections are visible, but most of the anterior and posterior visual regions are

weakly innervated by the ventral midbrain (rank 0-1; V5, V6, V1 – **Figure 2.4C3i**, V2 – **Figure 2.4C1ii**). In both M1 and M2, the more intermediate visual regions show stronger staining, which is most pronounced in the molecular layer (rank 1-2: V4, V4V, V3A – **Figure 2.4C1ii** and **2.4C2i**, V3D and V3V – **Figure 2.4C1i**) although this extends to the deeper and intermediate layers in some cases (rank 2: V3D in laminae IV-VI of M1). Results in M3 deviate slightly from the other two animals. The number of fibers is higher throughout visual cortex, which is most obvious in the intermediate areas (rank 2-3: throughout all laminae in V4V and V3A), but also in the most posterior regions in which projections stretch all the way towards the most posterior end of the occipital lobe.

2.3.7 Temporal cortex

Because previous evidence suggests that especially temporal regions of rodents and monkeys differ in terms of DA receptor and terminal distributions (Berger et al., 1991), we set out to investigate projection patterns within several subdivisions along the temporal lobe, roughly from anterior to posterior. Of note is the strong innervation throughout the temporal lobe in the molecular layer of M3, together with local patchy clusters in the temporal pole (TP) and entorhinal cortex. Moreover, intriguing is

the absence of fibers in primary as well as extended auditory cortex.

Expression within the entorhinal cortex was similar in M1 and M3, with a substantial number of fibers throughout area 35 (rank 2: laminae I & IV-VI and rank 3: laminae II-III) and other subregions, including the rostral (rank 2-3: ER, M1 and M3), intermediate (rank 1-2: in EI across layers), caudo-lateral (rank 1-2: ECL throughout all layers), and limiting caudal division of entorhinal cortex (rank 2-3: ELC, M1 and M3). Unfortunately, parts of entorhinal cortex in M2, which mostly included the intermediate zone (EI), were lost during histological preparations. Nonetheless, overall staining in the remaining parts of entorhinal cortex was weak with a minor presence or sometimes absence of axonal terminals in area 35 (rank 1: 35 in all layers) and the rostral (rank 1: ER, molecular layer, rank 0: laminae II-VI), caudo-lateral (rank 1: ECL in all layers) and limiting caudal division (rank 1: laminae I-III and rank 0: laminae IV-VI) of the entorhinal cortex.

The strongest consistent innervations across the three monkeys were found in the areas of the temporal pole. The molecular layer of area TLR contained relatively dense projections in all the three animals (rank 3: TLR in lamina I, **Figure 2.4A1i**). These projections were more variable across monkeys within the

deeper layers (rank 1-3: TLR in laminae II-VI, **Figure 2.4A1i**). The remaining part of the temporal pole (collectively called TP) receives consistent, but less dense projections in the three monkeys (rank 2: all layers for M1 and M2, lamina I in M3; rank 1: laminae II-VI in M3).

Axonal terminals were limited within auditory cortex, in particular in the koniocortex in which the primary auditory cortex itself resides (AK), but also within the belt and parabelt regions (PaAR, PaAC) and in the prosiocortex (ProK). The molecular layer of auditory cortex in M3 was the notable exception, as it showed average staining (rank 2: ProK, PaAR, PaAC & AK). In M1 and M2, the molecular layer was sparsely innervated, and only a handful of fibers was visible in the primary auditory cortex (rank 1: AK), and the rostral (rank 1: PaAR) and caudal (rank 1: PaAC) parabelt regions. The deeper and intermediate layers in all of the three animals were either completely void of midbrain fibers or rarely contained isolated fibers (rank 0-1: ProK/PaAR/PaAC/AK in laminae II-VI).

Various regions along the temporal lobe spanning from the temporal pole to the intraparietal junction and anterior extrastriate visual areas were assessed within the more dorsal superior temporal gyrus (STG), and within the more ventral subdivision of the combined inferior and medial (ITG/MTG)

temporal gyrus. Starting with areas within the more dorsal part of the superior temporal gyrus: in the anterior regions of ST1 and ST2, expression was restricted to the superficial layer in M3 (rank 2: ST1/ST2). In this animal, the more posterior ST3 showed a substantial upward trend in the number of fibers throughout all layers, but particularly within the molecular layer (rank 3: ST3 lamina I & rank 2: in laminae II-IV). This was a trend in M3, which was also present for the remainder of areas within the STG located just above the STS (rank 3: TAa/TPO in lamina I; rank 1-2: in laminae II-VI). In M1 and M2, the pattern within the STG was quite similar between the two monkeys but deviated from that in M3: in these two animals, expression within ST1 and ST2 was sparse but balanced across layers (rank 2: ST1/ST2, lamina I; rank 0-1: laminae II-VI). Within the more posterior superior temporal region of ST3, no expression was observed apart form a couple of fibers in the molecular layer (rank 1: ST3, lamina I). As in M3, more axonal terminals were observed in the ventral regions of the STG bordering the sulcus of these two monkeys (rank 2: TAa/TPO, lamina I in M1 and M2; laminae II-III in M1 – **Figure 2.4B3ii**).

The association areas occupying that part of the STS where the superior temporal gyrus transitions into the inferior temporal gyrus, showed a similar pattern of expression in the three monkeys, although overall staining was higher in M3. The more

dorsal association area PG, together with the more ventral IPa within the fold of the STS, follow the general trend in which most stained fibers are harbored within the molecular layer (rank 2: PGa/IPa in M1-M2, rank 3: in M3), with more sparse innervations in the intermediate and deeper layers (rank 1-2: PGa/IPa in all three animals for laminae II-VI). Largely, the composition of fiber expressions found in the association cortex of the STS was observed throughout most of inferior temporal cortex in both the molecular (rank 3: TEa/TEM/TE1-3 in lamina I for M3; rank 2: in lamina I for M1-2, exemplified by TE1 in **Figure 2.4A1ii**) and combined intermediate and deeper layers (rank 1-2: TEa/TEM/TE1-3 in laminae II-VI for M3; rank 0-1: in laminae II-VI for M1-2). Extending into the more medial temporal gyrus, the pattern of expression remained largely the same in M3 (rank 2-3: TL/TF/TFO in lamina I; rank 1-2 in laminae II-VI), while in M1 and M2 the number of fibers decreased. This was most evident in M2 (rank 1-2: TL/TF/TFO in lamina I; rank 0-1 in laminae II-VI). Results from the most medial temporal regions of TH/THO, bordering the entorhinal cortex, were markedly different between the three animals. In M1, we discovered dense expressions throughout all layers in these two areas (rank 2-3: TH in M1; rank 3: THO in M1). In contrast, in both M3, and especially in M2, the number of fibers was relatively low, if not almost zero (rank 1: TH/THO in lamina I for M2-3; rank 0-2: laminae II-VI).

The posterior temporal areas were grouped into a temporal-occipital (TO) subdivision, located at the confluence between the caudal end of the temporal lobe, parietal cortex and higher order visual areas. The differences between animals are substantial and correspond largely to those described for the visual areas within parietal-occipital cortex. In M3, the molecular layer of these regions receives dense projections (rank 2-3: TPt/MST/FST/TEO, lamina I), that are weaker in the intermediate layers, with small clusters of fibers in the deeper layers (rank 1-2: TPt/MST/FST/TEO, laminae II-VI). In M1, and certainly M2, fibers are mostly absent and if present, they were mostly restricted to the molecular layer (rank 0-1: TPt/MST/FST/TEO in M1 and M2, see **Figure 2.4B3i** for an example of area TPt).

2.3.8 Subcortical regions

Alongside an extensive ranking of projections towards the cortex, we also identified several subcortical structures that were of interest in light of potential connectivity with the dopaminergic midbrain. Lacking the typical laminar organization of the cortex, we ranked the density in the individual subcortical regions as a whole. Within the brains of M1 and M2, it was immediately clear that the striatum was preferentially innervated, with extensive staining in both the caudate nucleus (rank 4: Cd – **Figure 2.5Ai**) and the putamen (rank 4: Pu – **Figure**

2.5Aii). Although less substantial, the dorsal striatal structures in the contralateral hemisphere of M1 also received projections, as evidenced for the putamen (rank 2: Pu) and caudate nucleus (rank 2: Cd). In addition, the ipsilateral ventral striatal nucleus accumbens (NAc) also received considerable projections (**Figure 2.5Aiv**), which was slightly more obvious in the shell (rank 4: NAc(s)) compared to the core (rank 3: NAc(c)) of this nucleus. The striatal findings of M1 and M2 are in stark contrast with those of M3, in which only sparse projections could be detected in the caudate nucleus (rank 1: Cd, **Figure 2.5Fi**), putamen (rank 1: Pu, **Figure 2.5Fii**) and the shell (rank 1: NAc(s)) and core (rank 1: NAc(c)) of the nucleus accumbens (**Figure 2.5Fiii**).

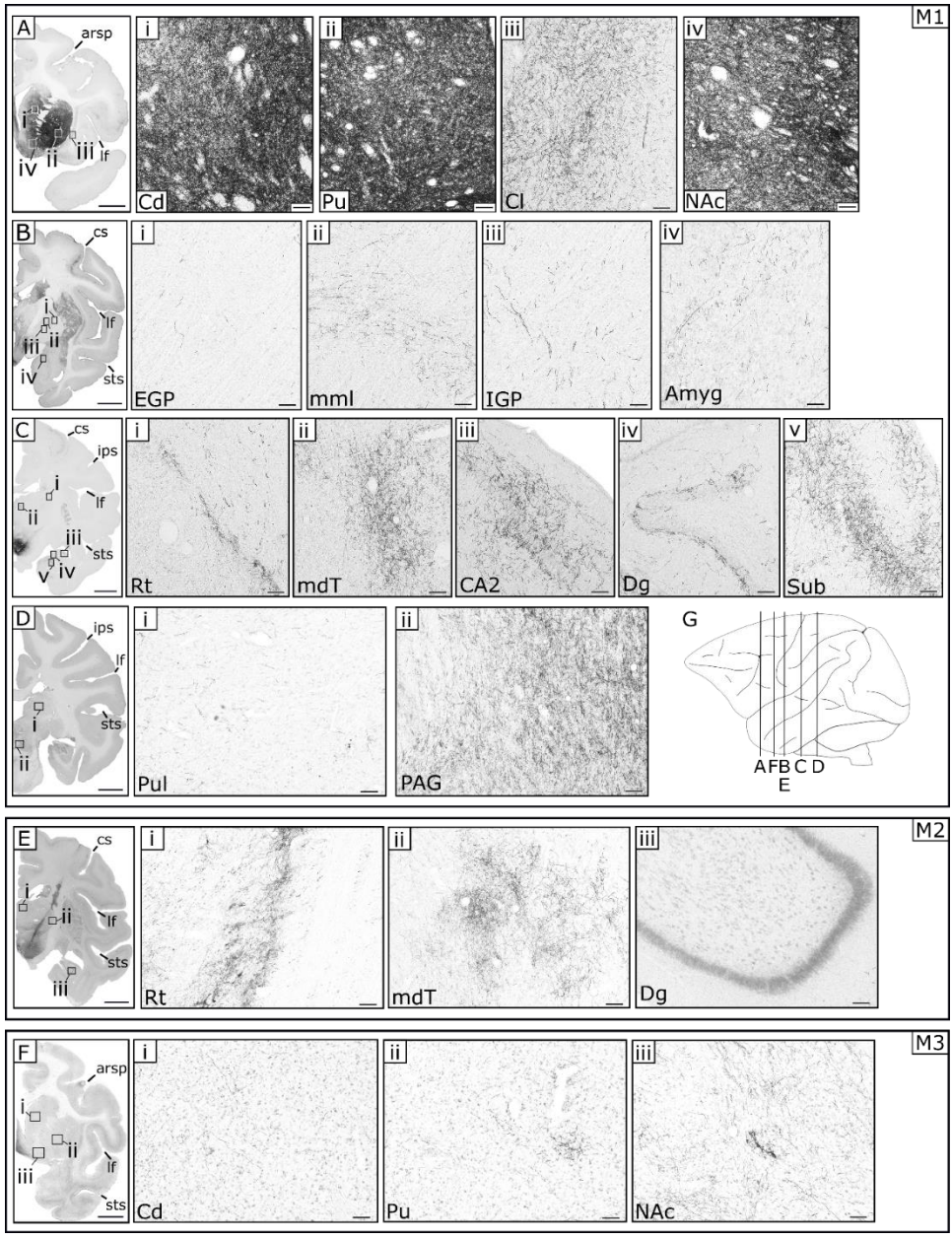


Figure 2.5: Example sections highlighting the viral vector spread in a number of selected subcortical regions in M1-3. (A) Coronal sections of M1 with magnified images (indicated with roman numerals).

Significant innervations in the dorsal striatum: (i) caudate nucleus (Cd) and (ii) putamen (Pu). Moderate stained fibers can be seen in the (iii) claustrum (Cl) and in the ventral striatum (iv) nucleus accumbens (NAc). **(B)** Coronal section of M1 with magnified images showing very weak innervations in: (i) external globus pallidus (EGP), (ii) medial medullary lamina (mml) a border between two basal ganglia nuclei, (iii) internal globus pallidus (IGP), and sparse fiber density in (iv) amygdala (Amyg). **(C)** Coronal section of M1 showing sparse innervations in parts of thalamus and hippocampus: (i) thalamic reticular nucleus (Rt), (ii) medial-dorsal thalamus (mdT), (iii) subfield CA2 of the hippocampus, (iv) the dentate gyrus (Dg) and (v) the subiculum (Sub). **(D)** Coronal section of M1 showing magnified images of the (i) pulvinar (Pul) and (ii) the periaqueductal gray (PAG). **(E)** Coronal section in M2 showing sparse innervations in parts of the thalamus: (i) Rt and (ii) mdT containing a comparable innervation pattern as that in M1, but altogether lacking stained fibers in the hippocampus (iii). **(F)** Coronal section in M3 showing weak and sparse innervations in the dorsal: (i) Cd, (ii) Pu and ventral striatum: (iii) NAc. **(G)** A schematic sagittal view indicating the anterior-posterior position of each of the coronal sections (A-F). Scale bar: 1000 µm for **A, B, C, D, E** and **F**, and 100 µm for all the other panels. **Landmark sulci**: arcuate rectus spur (arsp), lateral fissure (lf), central sulcus (cs), superior temporal sulcus (sts), intraparietal sulcus (ips).

The expression profile of the remaining structures of the basal ganglia that we ranked, were more comparable across monkeys. The external and internal parts of the globus pallidus show relatively little or even no AAV expression (rank 1: EGP in M1-2, **Figure 2.5Bi**, rank 0: M3; rank 2: IGP in M1, rank 1: M2-3, **Figure 2.5Biii**), whereas the medial medullary lamina (mml) separating the two related nuclei is clearly visible, containing a relatively higher number of fibers (rank 2: mml in M1/3 – **Figure 2.5Bii**,

rank 3: M2). We were unable to find any expression in the subthalamic nucleus, apart from those related to the trajectory of the injections (rank 0: STN). This suggests that the substantia nigra pars compacta was relatively weakly transduced by our injections, even in M1 and M2. Indeed, at least in rodents, the STN receives dopaminergic input from the latter structure (Cragg et al., 2004). Finally, the ventral pallidum, an important component of the limbic system and part of the basal ganglia, showed dense staining in all monkeys (rank 3-4: VP, M1-3), even within the contralateral hemisphere of M1 (rank 2: VP, M1c).

Three other subcortical regions, which we deemed of interest, are the claustrum (Cl), nucleus basalis (NB) and the amygdala (Amyg). Fiber density within the claustrum was high and rather homogenous from its more anterior to posterior extension in M1 (rank 3: Cl, **Figure 2.5Aiii**) and in M2-3 (rank 2: Cl). The cholinergic forebrain region of the nucleus basalis, is located ventral to the neighboring globus pallidus and ventral pallidum and received very strong projections in M3 (rank 4: NB), with a smaller, yet symmetrical distribution of fibers in M1 (rank 3: NB, M1, ipsilateral; rank 2: M1, contralateral) and almost no fibers in M2 (rank 1: NB). Although the amygdala consists of several divisions, we did not distinguish these as subregions and ranked the structure as a whole. In fact, the density of the projections was relatively low in any of the subjects (rank 1-2: Amyg in M1-3).

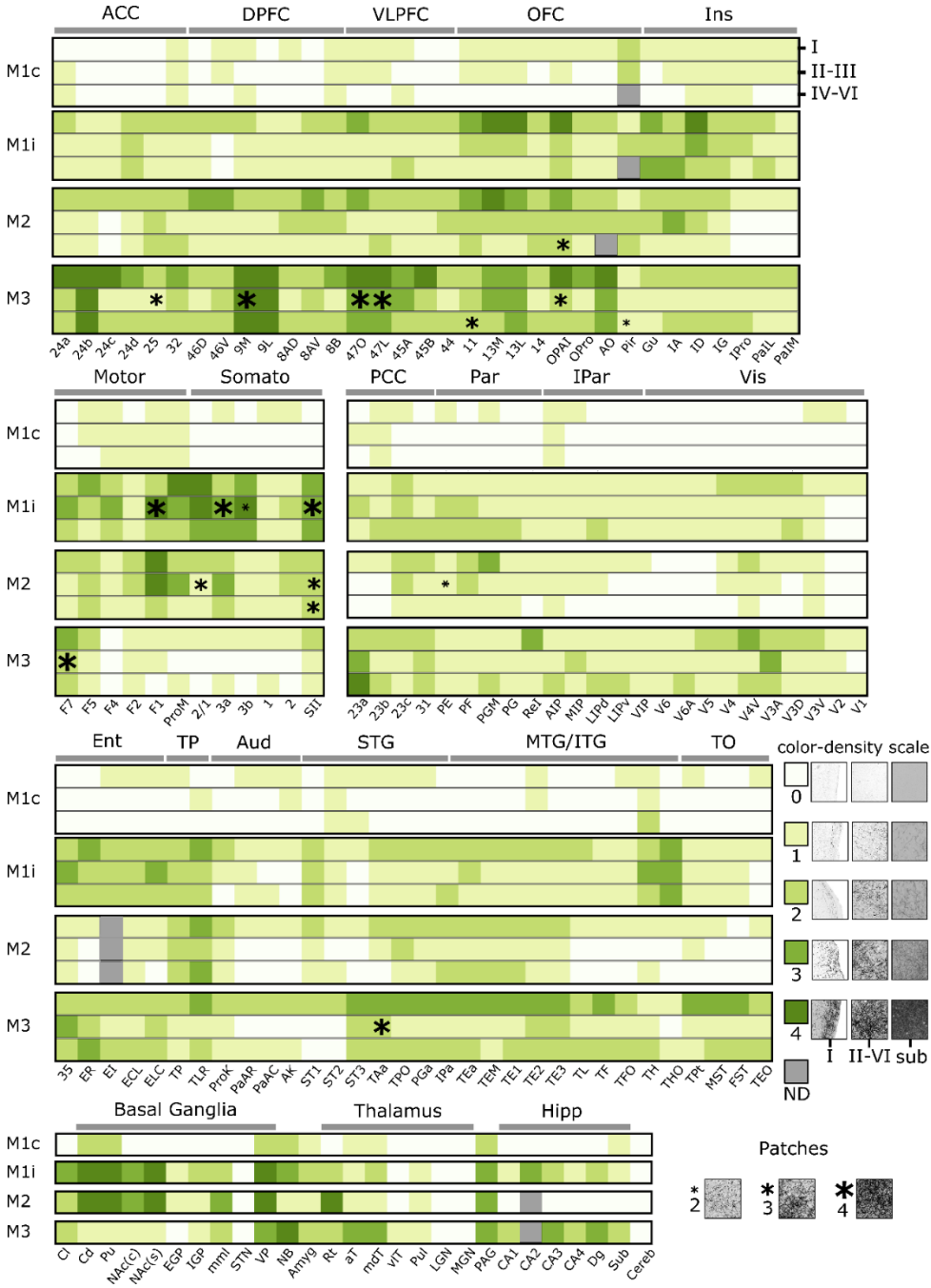

ACC
DPFC
VLPFC
OFC
Ins
M1c
M1i
M2
M3
I
II-III
IV-VI
24a 24b 24c 24d 25 32 46D 46V 9M 9L 8AD 8AV 8B 47O 47L 45A 45B 44 11 13M 13L 14 OPAI OPro AO Pir Gu IA ID IG IPro PaIL PaIM
Motor
Somato
PCC
Par
IPar
Vis
F7 F5 F4 F2 F1 ProM 2/1 3a 3b 1 2 SII 23a 23b 23c 31 PE PF PGM PG ReI AIP MIP LIPd LIPv VIP V6 V6A V5 V4 V4V V3A V3D V3V V2 V1
Ent
TP
Aud
STG
MTG/ITG
TO
35 ER EI ECL ELC TP TLR ProK PaAR PaAC AK ST1 ST2 ST3 TAa TPO PGa IPa TEa TEM TE1 TE2 TE3 TL TF TFO TH THO TPt MST FST TEO
color-density scale
0
1
2
3
4
I
II-VI
sub
ND
Basal Ganglia
Thalamus
Hipp
Cl Cd Pu NAc(c) NAc(s) EGP IGP mml STN VP NB Amyg Rt aT mdT vlT Pul LGN MGN PAG CA1 CA2 CA3 CA4 Dg Sub Cereb
Patches
2
3
4

Figure 2.6: Heatmap with estimates of fiber densities (ranking) for the areas and laminae throughout the brain of subjects M1-M3. Rankings for each of the three subjects: M1, M2 and M3 with separate rankings in M1 split for contralateral (M1c) and ipsilateral (M1i) hemispheres relative to the injection. The three layer-segments are separated per row: molecular (lamina I), intermediate (laminae II-III) and deeper layers (laminae IV-VI), as indicated for the first subject (M1c: top right). The scale for the rankings (0-4) is displayed in a legend on the right of the figure, with representative magnified photomicrograph examples of fiber densities at each of the rankings in the molecular layer (I), intermediate and deeper layers combined (II-VI) and for subcortical structures (Sub). In addition, representative examples of patchiness at different strengths (2-4), as conveyed by the size of the asterisk, are shown in the bottom of the figure. The overview consists of five major subdivisions, from top to bottom: prefrontal (ACC: anterior cingulate cortex, DPFC: dorsal prefrontal cortex, VLPFC: ventro-lateral prefrontal cortex, OFC: orbitofrontal cortex, Ins: (para)-insular regions), Somatomotor (Motor: motor cortex, Somato: somatosensory cortex), parieto-occipital (PCC: posterior cingulate cortex, Par: parietal cortex, IPar: intra-parietal cortex, Vis: visual cortices), temporal (Ent: entorhinal cortex, TP: temporal pole, Aud: (para)-auditory cortex, STG: superior temporal gyrus, MTG/ITG: medial- and inferior-temporal gyri, TO: temporo-occipital cortex) and subcortical (Basal Ganglia, Thalamus and Hipp: hippocampus). ND = no data.

To gain an in-depth insight into thalamic innervations from the dopaminergic midbrain, we split the structure into seven of its main components that could be identified based on anatomical landmarks. We found that the reticular nucleus (or pre-thalamus) ranked high in M2 (rank 4: Rt, **Figure 2.5Ei**) and a relatively high density of fibers was also present in the other two

animals (rank 2: Rt, **Figure 2.5Ci**). Other, moderately innervated thalamic divisions are the medial-dorsal (mdT) and anterior (aT) part, in which M3 received more projections (rank 3: aT/mdT) than M1 (rank 2: mdT, **Figure 2.5Cii**; rank 1: aT) and M2 (rank 1: mdT/aT, **Figure 2.5Eii** which shows the mdT). Both the pulvinar (Pul) and the ventro-lateral thalamus (vlT) contained little to no fibers (rank 1: Pul in M1-M3; rank 0: vlT in M1-2 and rank 1: M3). Finally, the two primary sensory nuclei at the foot of the thalamus were completely void of midbrain fibers, as evidenced by the absence of projections in both the lateral (rank 0: LGN in M1-3) and medial geniculate nucleus (rank 0: MGN in M1-3).

Axonal fibers in the hippocampus were estimated based on their location within the CA subfields (CA1-4), the dentate gyrus (Dg) and subiculum (Sub). In two of the animals, the tiny CA2 subfield was almost impossible to distinguish, but in M1 we noticed that his area preferentially received dense expressions (rank 3: CA2, **Figure 2.5Ciii**). The other subfields also contained fiber staining which was higher on average for M3 (rank 3: CA3, rank 2: CA1/4) compared to M1 (rank 2: CA3, rank 1: CA1/4). Similarly, in the remainder of the hippocampal subregions staining for the dentate gyrus and subiculum was higher in M3 (rank 3: Dg, rank 2: Sub) compared to M1 (rank 2: Dg, **Figure 2.5Civ**; rank 1: Sub, **Figure 2.5Cv**). A profoundly aberrant picture of expressions was observed in subject M2, in which, interestingly, none of the

hippocampal subdivisions contained any stained fiber (rank 0: CA1-4, Dg – **Figure 2.5Eiii**, Sub).

Two more posteriorly located subcortical regions that we considered separately in our rankings are the midbrain grey matter area of the periaqueductal grey (PAG) enveloped around the fourth ventricle, and the cerebellum (Cereb). Along the PAG we discovered strong staining that was consistent across monkeys (rank 3: PAG in M1-M3) and even transcended into the contralateral hemisphere in M1 (rank 2: PAG in M1c). We decided not to further split up the cerebellum, since we did not discover a single fiber throughout this large brain structure in any of the animals (rank 0: Cereb M1-M3).

2.3.9 IHC double labelling of nerve terminals

As described above, a substantial portion of VTA neurons transfected with AAV were dopaminergic. It is unclear whether this also applies for the axon terminals in cortical targets. To address this question, we performed IHC double-labeling using anti-RFP and anti-TH antibodies on a handful of coronal slices of M1 (**Figure 2.7**). Within a representative frontal section through dorsal prefrontal cortex including area 46V, only a small number of axons were double-labeled for both the reporter gene and TH (**Figure 2.7A**: as indicated with white arrowheads). This also held

true for axons in the molecular layer of a subregion within DPFC (i.e., area 8B**, Figure 2.7B**). These results seem to imply that a majority of cortical VTA projections are non-dopaminergic. To substantiate such a counterintuitive conclusion, however, we also double-labeled parts of the brain known to contain strong dopaminergic input from the VTA, including the striatum. Surprisingly, even within striatal components, such as the caudate nucleus (**Figure 2.7C**) and the putamen (**Figure 2.7D**), we encountered only a few double-labeled fibers. It is therefore tempting to relate the absence of double-labelling of axons in general, to technical limitations instead, as we will further discuss below.

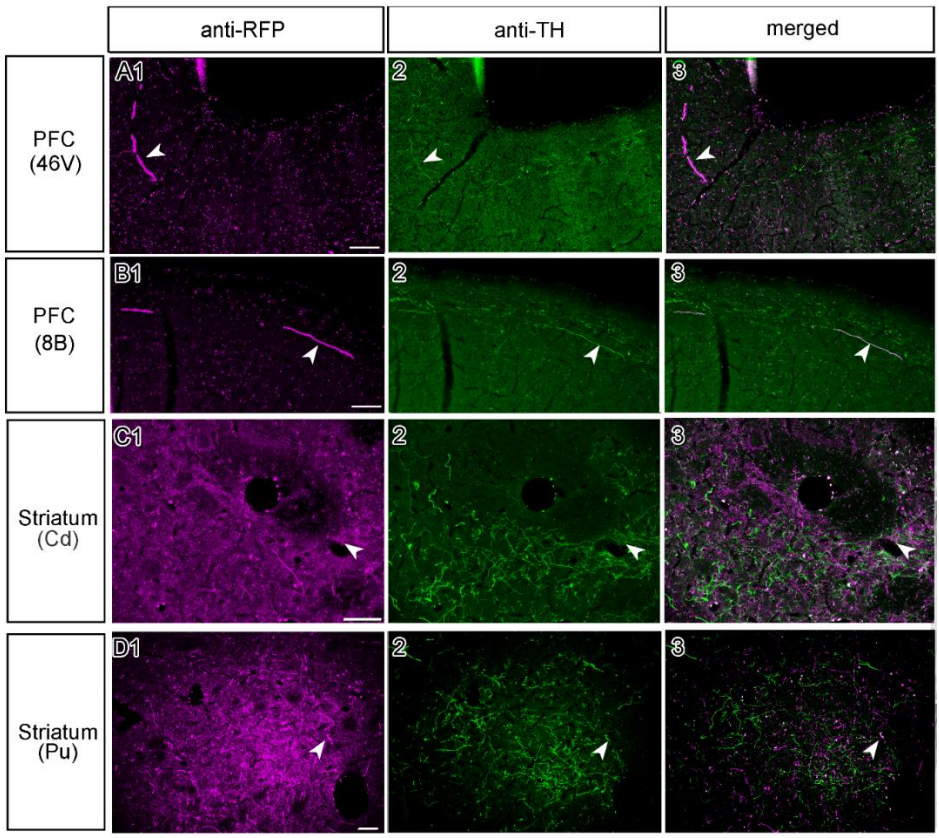


Figure 2.7: Double IHC of axonal terminals originating from the midbrain does not indicate clear co-localization in M1. (A) Selective photomicrographs of the prefrontal cortex (area 46V), showing staining against (1) RFP, (2) TH, and (3) a merged image, with white arrowheads marking an example of terminals that are potentially double labeled. Here, the double-labeling was rare. **(B)** A photomicrograph from area 8B, indicating the potential co-localization with anti-RFP and anti-TH staining, again double-labeling was rare. **(C)** An optical sectioning image of double fluorescent IHC within the caudate nucleus revealed more DAergic (TH^+) terminals, but not necessarily more co-localized (RFP^+) fibers, which was also the case in **(D)** for the putamen. Scale bar: 100 µm.

2.4 Discussion

By employing state-of-the-art anterograde viral tract tracing techniques, this is the first study to provide an overview of the detailed axonal arborization of the VTA throughout the entire brain of macaques. Dopaminergic neuronal projections from the midbrain in non-human primates have been studied extensively, but essentially in reverse, i.e., by using more traditional retrograde tracing techniques. By definition, such retrograde studies can only provide a snapshot of the full connectome from any given structure. Nonetheless, these retrograde studies revealed that the dopaminergic midbrain is preferentially connected to a variety of areas within the frontal cortex (Williams and Goldman-Rakic, 1998, Frankle et al., 2006). Moreover, it was found that these midbrain-frontal projections originated in the three major midbrain nuclei housing dopaminergic neurons: i.e., A10 (VTA), A9 (SNc) and A8 (RRF). To provide a more detailed and comprehensive understanding of the brain-wide distribution of the DA terminals, we aimed to target the VTA using our anterograde vectors. Subsequently, we assessed the relative intensity of VTA projections in individual areas and laminae throughout the brain.

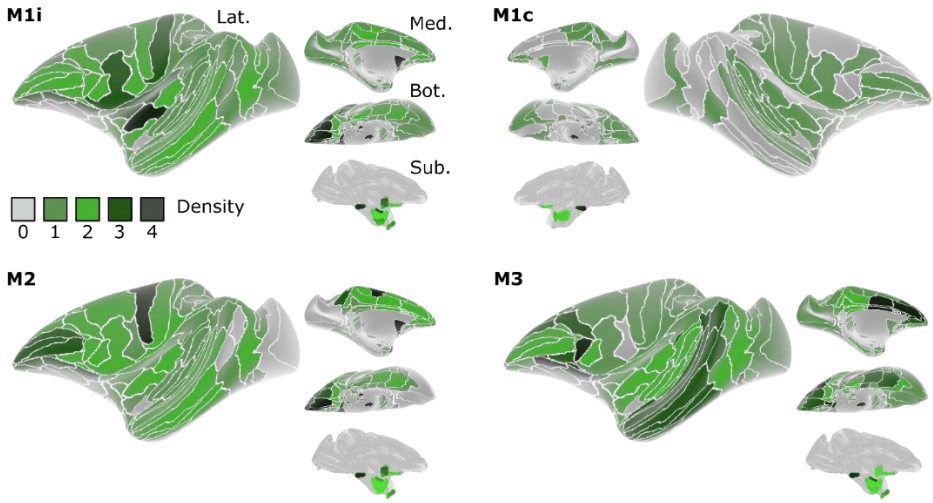


Figure 2.8: Schematic overview of fiber densities on the inflated brains of M1-M3, based on the rankings in figure 2.6. The density of estimated terminals (0-4) in the molecular layer of each region is overlaid on a lateral (Lat.), medial (Med.), bottom (Bot.) and subcortical (Sub.) perspective of the inflated D99 brain (Reveley et al., 2017). For M1, both the ipsilateral (M1i) and contralateral (M1c) hemisphere relative to the injection side are shown.

Previous studies showed that the highest concentrations of cortical catecholaminergic (i.e. dopaminergic and noradrenergic) terminals are found in prefrontal and temporal cortex, with decreasing levels in premotor and occipital cortex (Mac Brown and Goldman, 1977, Björklund et al., 1978). A follow-up study showed widespread distribution of TH^+ fibers, indicative for their dopaminergic or noradrenergic nature, throughout the cerebral

cortex of macaques (Lewis et al., 1987). These studies describe the ubiquity of DA innervations in primates arguing against pronounced regionally restricted projections (i.e. within frontal and striatal regions). However, information regarding the exact nature and origin of the catecholaminergic innervation remained obscure. These TH^+ axons could be dopaminergic projections from either the VTA, SNc, or RRF, or noradrenergic projections from the locus coeruleus, despite morphological differences in nerve terminals were proposed (Levitt et al. 1984). More recently, anatomical features of dopaminergic midbrain nuclei has been investigated in much more detail in rodents, through genetically-defined subgroups that innervate divergent brain targets: the more lateral SNc projects to striatal targets (caudate, putamen), whereas the more medial VTA projects more into the nucleus accumbens, olfactory tubercle and the forebrain (Poulin et al, 2018). Whether these findings can be directly compared to the spatial organization of the DA system in primates, however, is questionable, especially since areal and laminar DA receptor distributions differ profoundly between non-human primates and rodents (Berger et al., 1991). It is reasonable to assume that the DA system has undergone a significant transformation ever since the evolutionary split of the rodent and primate lines. Such a transformation emphasizes the necessity to investigate the exact DA connectivity profile in terms of both their midbrain origins and subsequent projection sites in primates.

Our aim was to target the VTA (A10). Since this nucleus has an irregular border with the neighboring SNc (A9) and RRF (A8) (**Figure 2.1**), however, it is exceedingly difficult to confine an injection to this tiny region. Based on the histological assessment of the exact injection sites and the spread of transduced neurons, we could basically divide our subjects into two groups: (1) M1 and M2, in which the vector transduced neurons in the VTA but also a part of the SNc, and (2) M3, in which expression was present in the more dorsal part of the VTA, in addition to parts of the ventro-medial thalamus but sparing the SNc. It is important to note that in all the animals, the injection avoided the RRF.

In M1 and M2, densest projections were observed in the OFC and sensorimotor regions (with patchy projections in the deeper layers). In prefrontal cortex of M3, on the other hand, strong projections were found in the OFC, DPFC, VLPFC and ACC (**Figure 2.8** for an overview). The consistent presence of dense innervations within OFC of all three subjects is the most resolute evidence that this subdivision is most strongly innervated by the VTA, at least compared to the other PFC subdivisions. Within subcortical regions, a strikingly different expression pattern was observed in the striatum; which received strong projections in subjects M1 and M2, but not in M3. Although speculative, these

differences could be explained by the fact that the dorsal striatum is mainly targeted by the SNc and the ventral striatum by ventral VTA or medial SNc (Gerfen, 1985). A peculiar difference between the two first monkeys was observed in the hippocampus, which received weak versus no projections in M1 and M2, respectively. In M1, slightly more medial portions of the VTA are transduced compared to M2 (**Figure 2.1D and E**). Since in M3 the most medially-located VTA neurons were transduced (**Figure 2.1C**), and since also the hippocampus in M3 was strongly innervated, it may be that the hippocampus is mainly innervated by the most medial part of the VTA, arguing for a specific functional topography within the VTA (Lisman and Grace, 2005).

The main conclusion that we derive from these results is that VTA-originating projections cover the entire brain, with denser innervation in the more frontal regions and sparse projections in the posterior part of the brain, exactly as suggested in previous studies (Williams and Goldman-Rakic, 1998, Berger et al., 1988). We suspect that the hotspots of innervations observed in idiosyncratic cases are the result of the disparity of the injections. For example, the predominantly medial VTA injection in M3 might have resulted in particularly dense projections to the OFC and other prefrontal regions. It is tempting to speculate that the slightly more lateral SNc injection in M1-M2 led to the strong innervations in the striatum and sensorimotor areas,

which were lacking in M3. Of note, the lack of strong striatal innervations within M3 might suggest that the observed projections within the DPFC, ACC, VLPFC partially originated in the ventro-medial thalamus in addition to the medial VTA (Kolb et al., 1982, McFarland and Haber, 2002). The combined results suggest a segregation of midbrain dopaminergic neurons in the lateral VTA and SNc versus medial VTA and ventromedial thalamus in terms of their cortical and subcortical targets. This anatomical segregation is interesting in light of recent behavioral findings on the functional topography in rodents through photostimulation of the more medial VTA versus that of the more lateral VTA/SNc (Keiflin et al., 2019, Saunders et al., 2018a). Similarly, a broad medial-lateral physiological segregation based on variable electrophysiological outcomes in DA neurons has been proposed previously in macaques (Matsumoto and Hikosaka, 2009). The relationship between the observed anatomical and physiological segregation of DA neuron subgroups should be studied in more detail with state-of-the-art selective manipulation techniques (Vancraeyenest et al., 2020) in future primate studies.

It is important to note that the injected vector tracer we used in all our subjects is non cell–type-specific. Although viable TH-specific promoters are in circulation and have been successfully used in previous work (Lerchner et al., 2014, Stauffer et al.,

2016), there are some concerns about the transfection efficiency and specificity of these promoters. Rough estimates indicate that only 40% of the TH^+ cells are infected by these injected cell-type specific vectors (Lohani et al., 2017, Lohani et al., 2018). We used the generic non-cell type-specific CAG promoter as it drives high levels of long term gene expression (Alexopoulou et al., 2008). Our choice for a generic non-cell type-specific promoter means that we cannot be conclusive about the dopaminergic nature of the stained axons in the projection sites. However, representative double-labeled fluorescence samples indicate that at least a substantial fraction of the somata within the midbrain (**Figure 2.1G-I**), and some of their axons in projection sites are dopaminergic (**Figure 2.7A1-D3**), as they are both RFP^+ (i.e., transduced by the vector) and TH^+ (dopaminergic). Previous studies by Goldman-Rakic and colleagues suggested that dopaminergic projections to temporal and frontal lobes exhibit a bimodal distribution: with one peak in more superficial layers (laminae II-III) and a second peak in deeper layers (laminae IV-V) (Levitt et al., 1984). These findings were substantiated by rich expression of D1-type dopaminergic receptors, again both in the superficial and deeper layers in different parts of the neocortex, while expression of D2 receptors was mostly restricted to layer V (Lidow et al., 1991). A more recent study on the other hand, showed a more ubiquitous distribution of D1- and D2-type receptor proteins in the cell bodies of neurons across laminae II-

VI in the frontal eye field of macaques (Mueller et al., 2020). To clarify whether the cortical projection fibers in the superficial and deep layers are dopaminergic, we performed double IHC staining in the cortex. However, observations of double labeled axon terminals were rare (**Figure 2.7A and B**), even when a majority of RFP^+ cell bodies within the VTA were double labeled (**Figure 2.1I**). Surprisingly, even in the striatum only a low number of RFP^+ axons were also stained for TH (**Figure 2.7C and D**). Yet, the majority of striatal axons originating in the ventral midbrain are considered to be dopaminergic, at least in rodents (Ikemoto, 2007). How can we explain these seemingly false negative results? Recently, it has been reported that it is challenging to detect anti-TH immuno-staining in neurons transduced by an AAV vector because of possible downregulation of TH synthesis in the infected neurons (Albert et al., 2019). Therefore, the negative evidence in the present study may be related to unknown technical difficulties to show that RFP^+ axons are TH^+ after transduction with an AAV vector. In conclusion, our axonal double-labeling data have to be interpreted with caution and should not be taken as conclusive evidence that the RFP^+ axons are actually non-dopaminergic (see **Figure 1.2** for possible non-dopaminergic efferents of the dopminergic ventral midbrain nuclei).

When comparing our anatomical connectivity results with those of our previous 'effective connectivity' findings obtained through a combination of electrical stimulation of the VTA (VTA-EM) and fMRI, we found similarities and differences. Major cortical regions showing increased fMRI activity following VTA-EM included frontal areas such as the PFC and OFC, ACC, intraparietal areas, as well as somatomotor regions, insula, and gustatory cortex (Arsenault et al., 2014), exactly as observed in the present tracer study, in particular in subjects M1 and M2. In addition, subcortical regions showing VTA-stimulation induced activity included the caudate, putamen, and parts of the thalamus (Arsenault et al., 2014). The OFC, parts of prefrontal and temporal cortex, and to some extent more posterior parietal and visual areas were activated after VTA stimulation at intermediate stimulation frequencies (Murris et al., 2020), a connectivity map that more closely resembles the findings in M3. In the latter VTA-EM study, activation of somatomotor areas and the striatum was weak, although these areas showed strong midbrain projections in M1 and M2. Hence, it is tempting to relate the differences in vector spread in the present study to the exact positioning of the chronic electrodes in the VTA-EM studies above.

The present study includes an extensive analysis of both cortical and subcortical DA projections revealing interregional and

laminar-specific similarities and differences across injected animals. The differences may be attributed to slight differences in the spread of the vector. The main novelty of this VTA-DA anatomical connectivity study is that by using anterograde tracers, we could provide a detailed efferent connectivity map for the DA in correspondence with midbrain of non-human primates (**Figure 2.6, 2.8**). We observed clear laminar specificity in the projections, with strongest innervation of the molecular layer in many cortical areas, and with sometimes dense patches resembling parts of columnar like structures in deeper layers of specific brain regions. In light of inter-species (Raghanti et al., 2008) and regional differences in D1/D2 receptor distributions (Lidow et al., 1991), these findings will be highly instrumental to guide experiments aimed to study the functional impact of dopaminergic-specific midbrain projections on cortical and sub-cortical processing.

2.5 Supplementary information

Subject	M1	M2	M3
sex	Female	Female	Female
age (year)	4	7	9
body weight (kg)	4.2	6.7	9.4
vector serotype	AAV2.1	AAV DJ	AAV DJ
vector FP-tag	DsRed2	tdTomato	tdTomato
vector titer (unit vg/mL)	$2.2x10^{12}$	$1.1x10^{13}$	$3.8x10^{12}$
injected side	Left	Left	Left
volume /injection site (µL)	1.0	0.5	0.7
injection rate (nL/min)	100	100	100
tracks (#)	3	3	3
injection sites /tracks (#)	1	1	1-2
total number of injection sites	3	3	5
days until perfusion	41	42	42

Table S2.1: Subject and experimental characteristics

A comprehensive overview: which includes specifications of the animals, the viral vectors and the injection procedures in the study. The first four rows refer to the animals (*Macaca fuscata*) that were used in this study and their weight and age at the time of perfusion. Three rows below provide information on the serotype of the vector, the fluorescent tag that could either directly be used in histology for fluorescence staining or through enhanced staining (DAB), and the predetermined vector titer (see Materials & Methods). The bottom six rows relate to details on the injection procedures that differed only

slightly between subjects. In all animals, the left hemisphere was injected, with the main difference being the injected volume, which was more in M3, followed by that in M1 and M2.

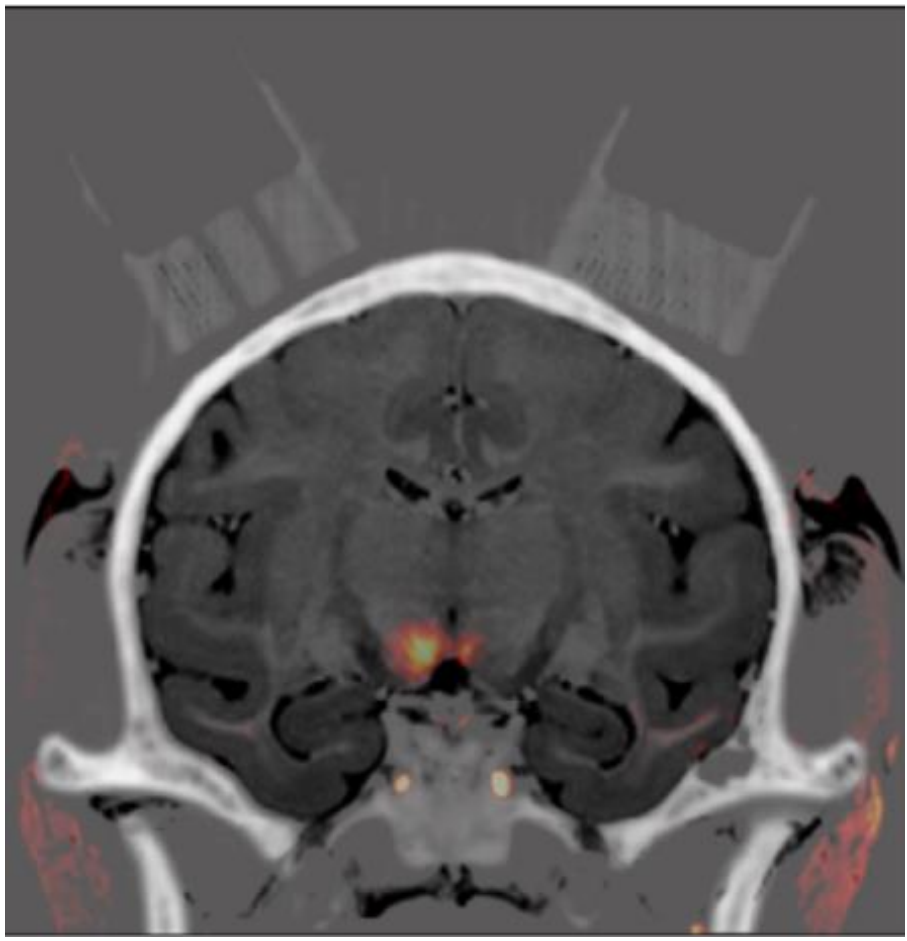
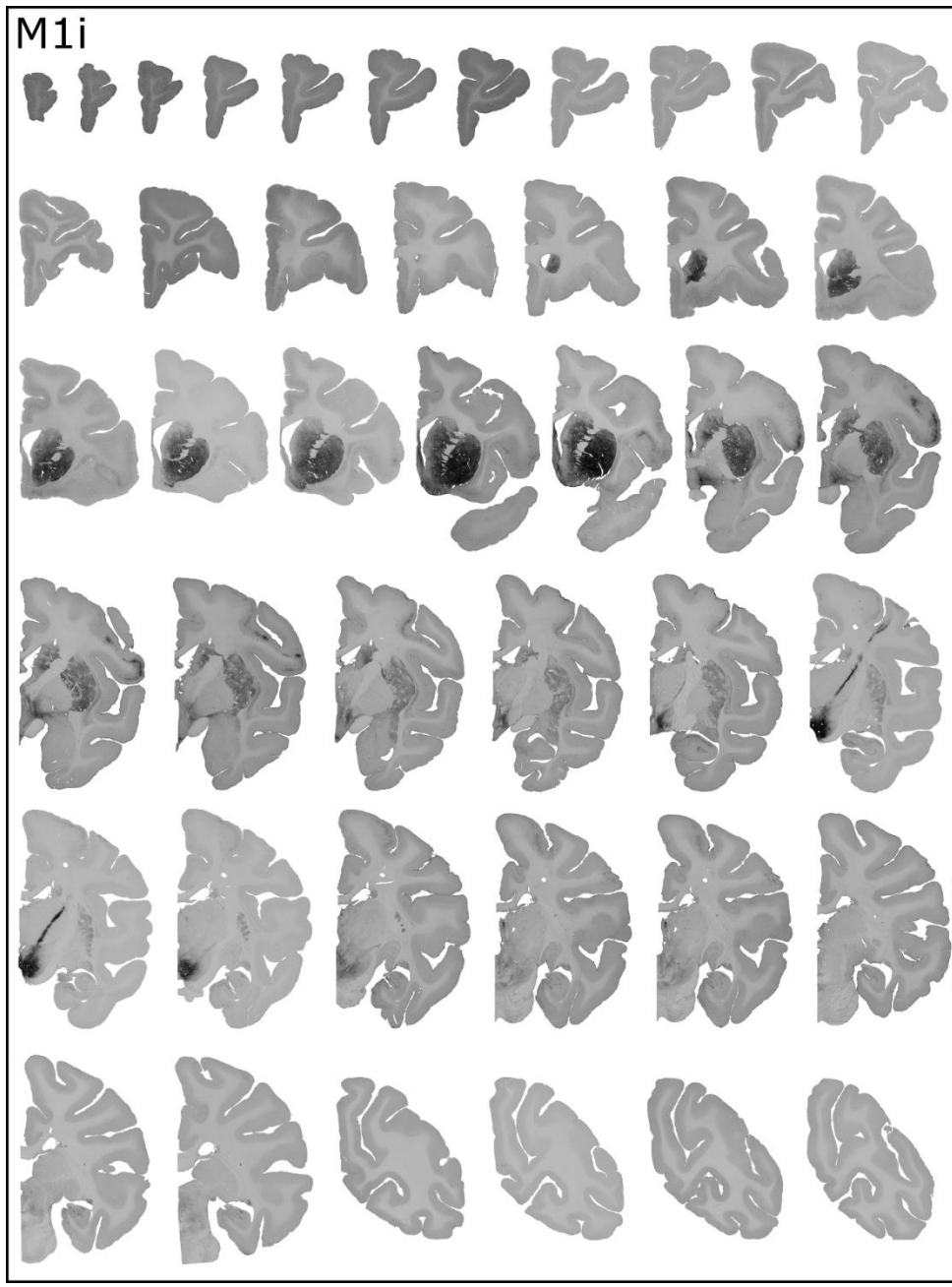


Figure S2.1: Pre-injection targeting of the VTA through a combination of CT and contrast enhanced MR imaging. The midpoint of a gadolinium injection targeting the right VTA (T1 in hot metal color scale) was overlaid on a representative T2-reverse MRI coronal slice and CT (both in gray scale) showing anatomical outlines, the skull and implanted chamber/grids. Individual pre-operative imaging facilitated in determining the exact injection site in each animal, in addition to providing a reliable estimate of potential vector spread when taking gadolinium as a reference, before moving on to the actual viral vector injections.


M1i

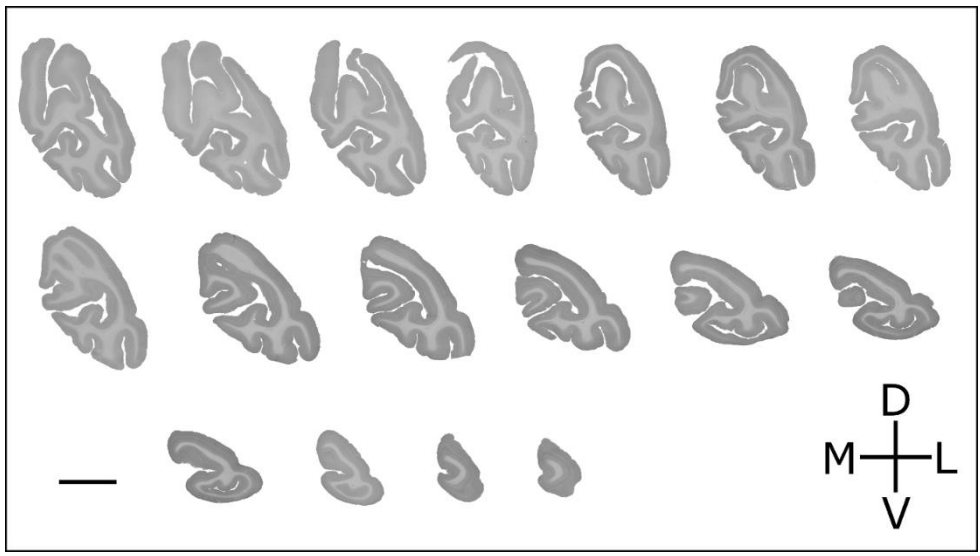
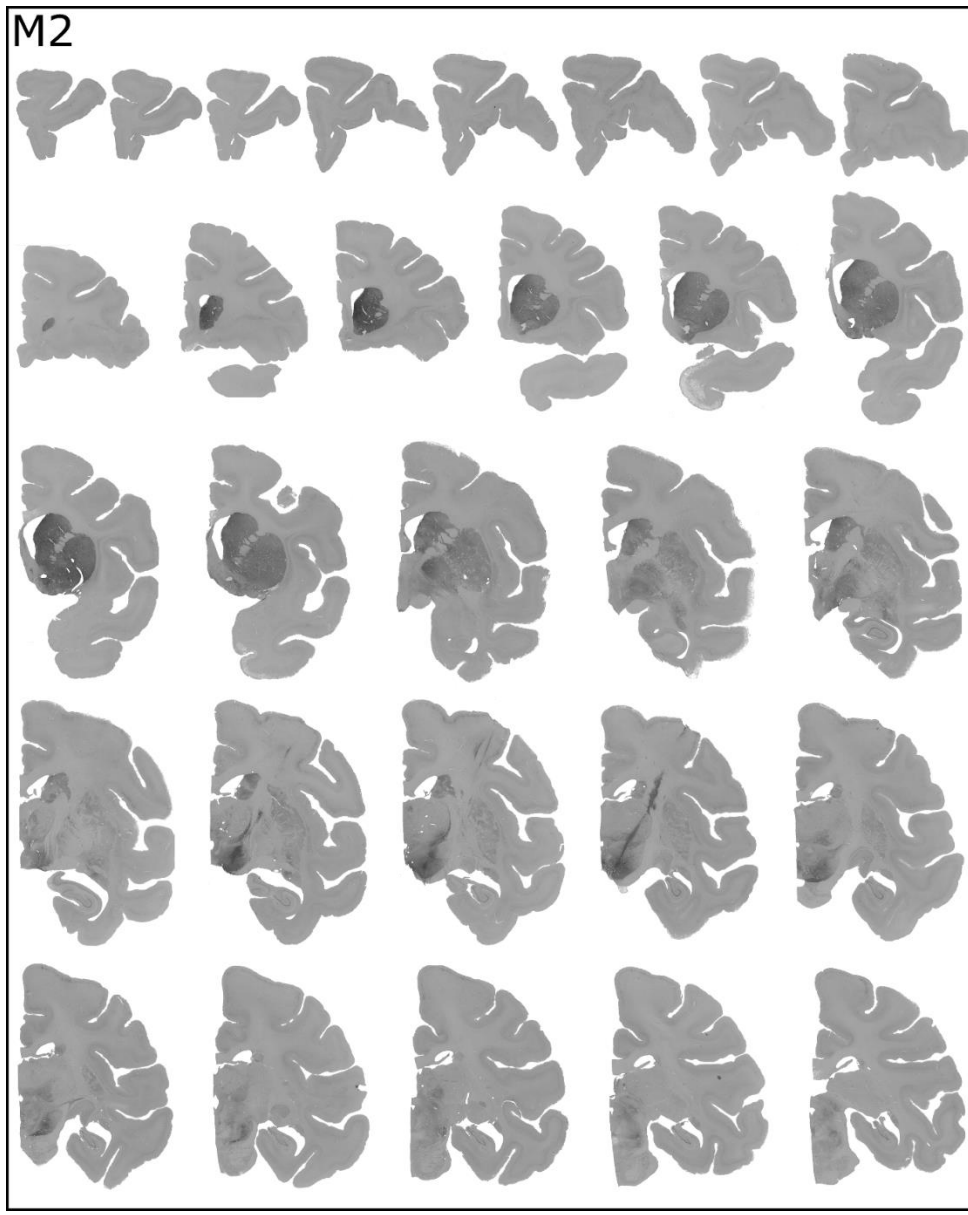


Figure S2.2: Overview of all IHC stained coronal sections of the hemisphere ipsilateral to the injection in M1. The coronal sections shown here at low magnification were used to determine the fiber density from DAB staining throughout the brain in M1 (see Figure 2.6-2.7) and therefore relate to the main findings in this study. The presentation of the coronal slices is from anterior (top left) to posterior (bottom right). Scale bar (bottom left): 10 mm. **Coordinate system**: dorsal (D), lateral (L), ventral (V), medial (M).


M2

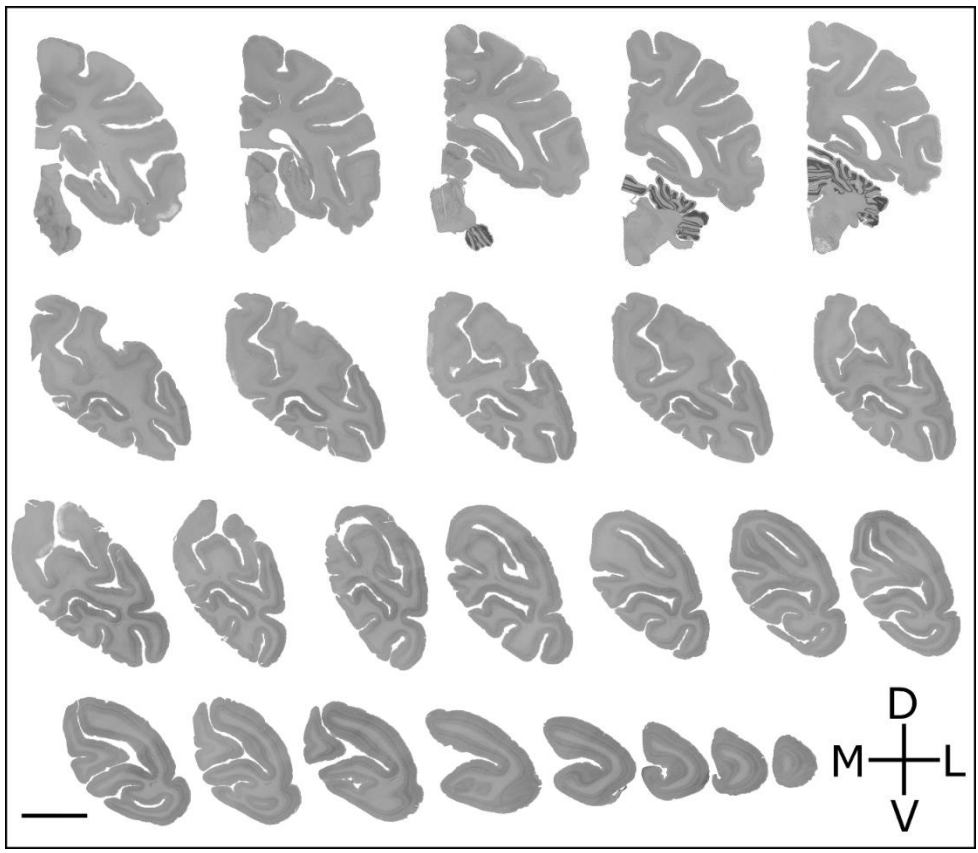
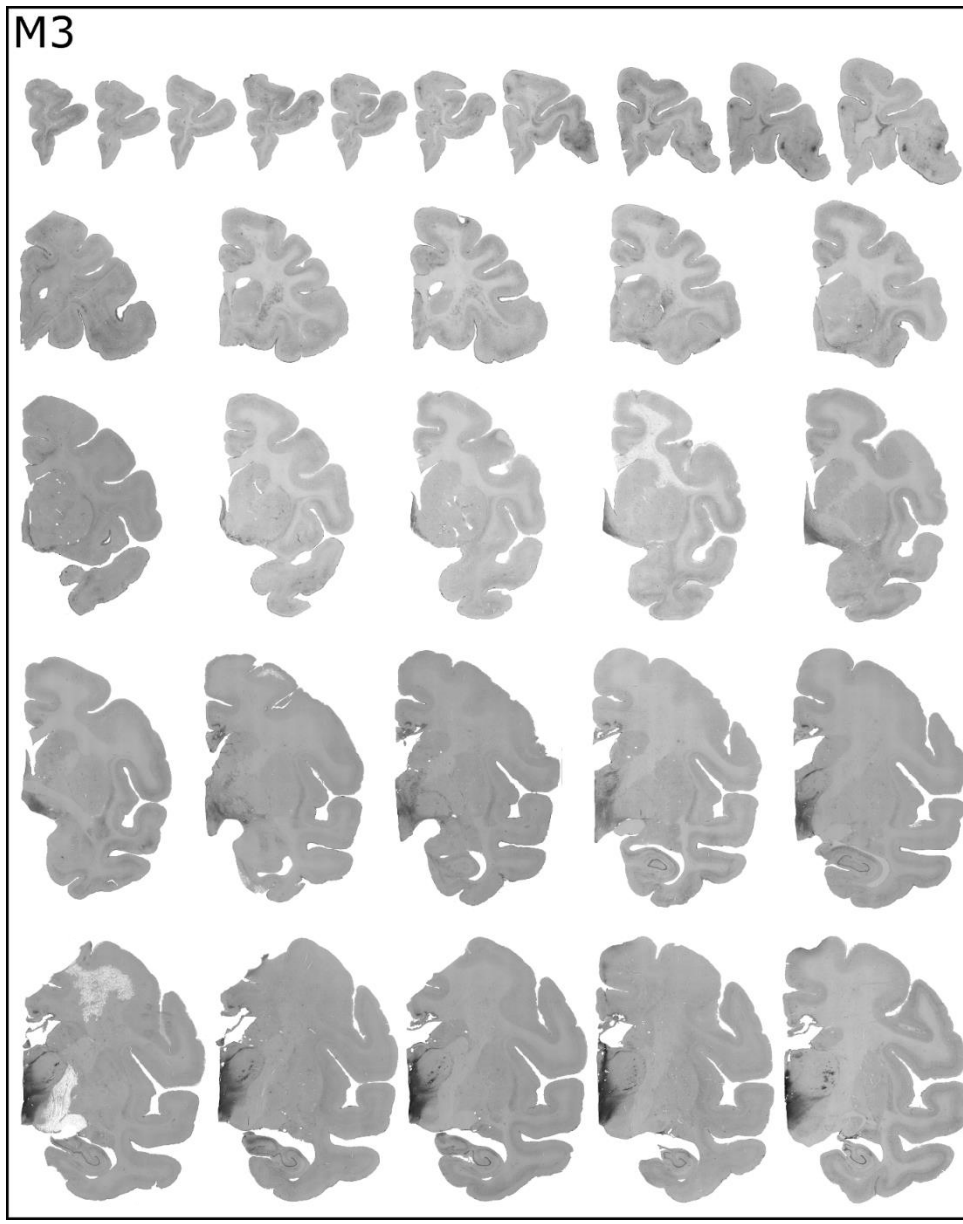


Figure S2.3: Overview of all IHC stained coronal sections of the hemisphere ipsilateral to the injection in M2. Conventions follow those in Supplement 3; but presented coronal slices are from the ipsilateral hemisphere in M2.


M3

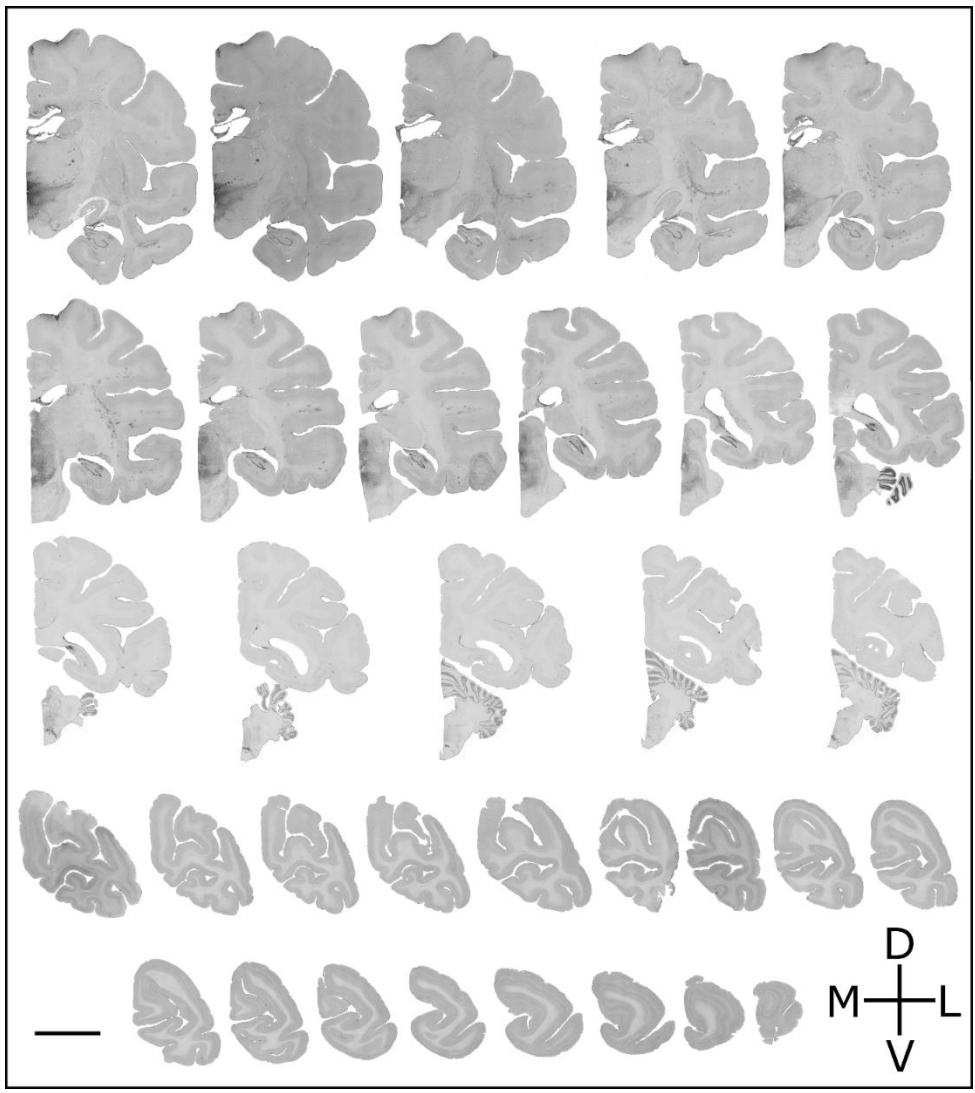
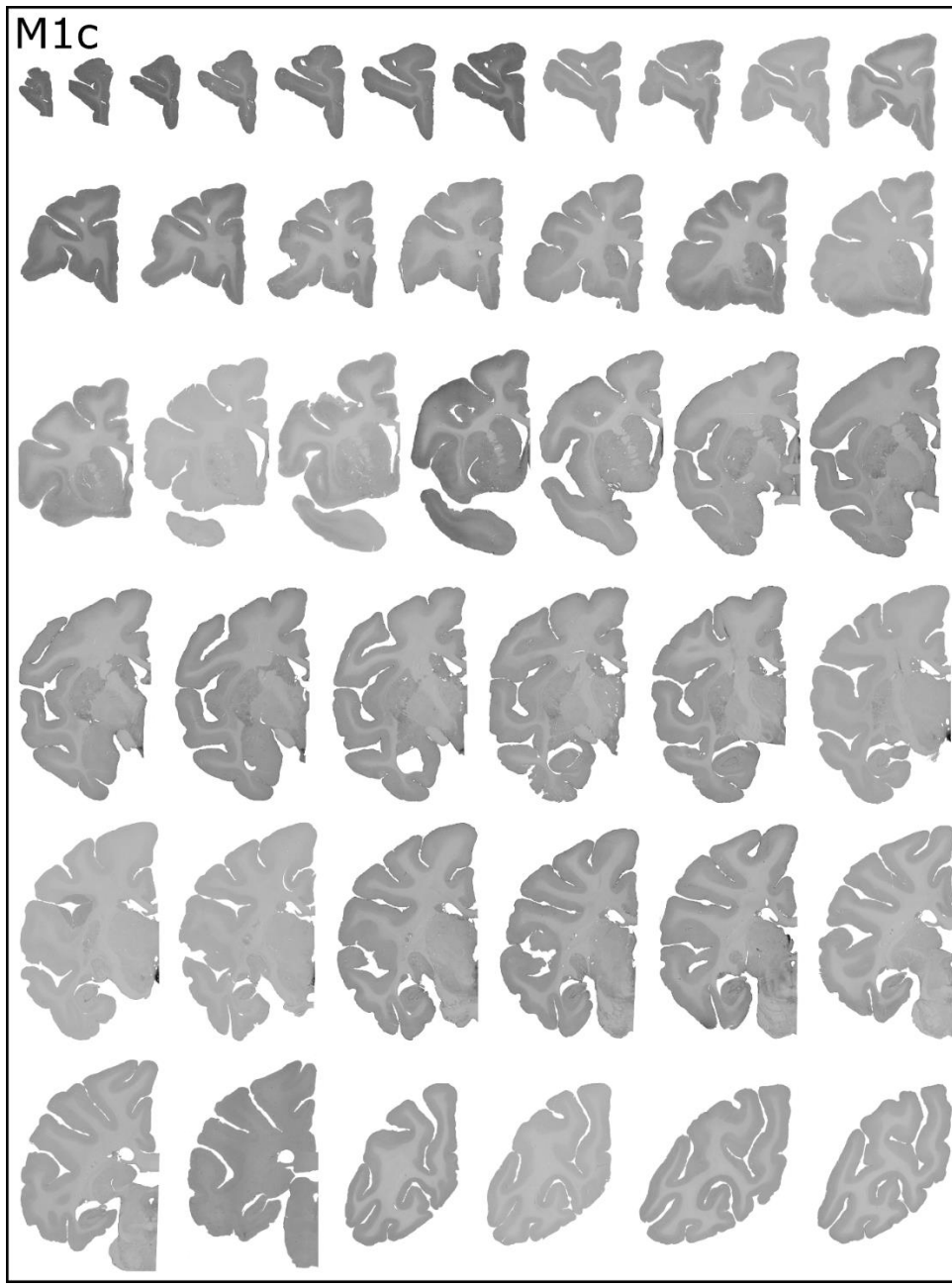


Figure S2.4: Overview of all IHC stained coronal sections of the hemisphere ipsilateral to the injection in M3. Conventions follow those in Supplement 3; but presented coronal slices are from the ipsilateral hemisphere in M3.


M1c

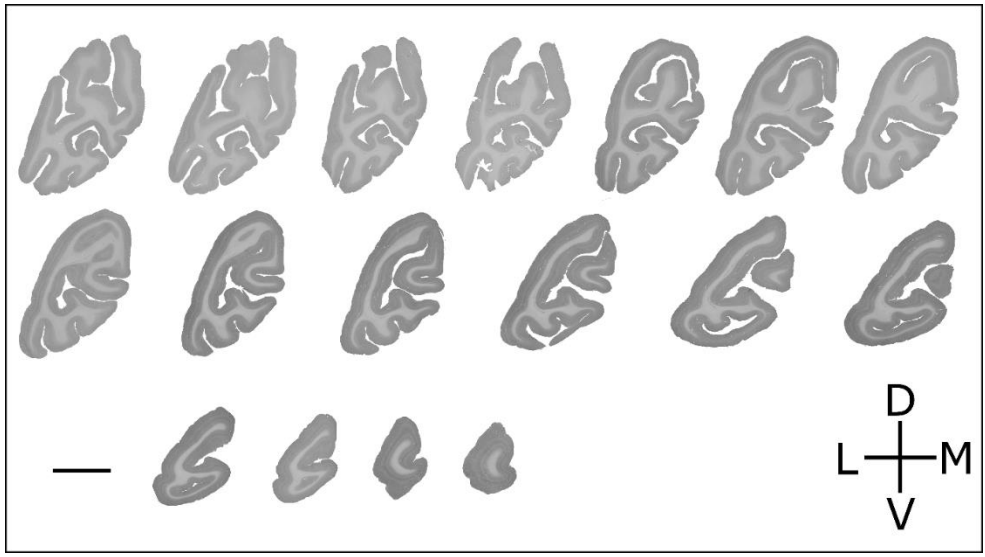


Figure S2.5: Overview of all IHC stained coronal sections of the hemisphere contralateral to the injection in M1. Conventions follow those in Supplement 3; here we present coronal slices from the hemisphere contralateral to the injections in the same animal (M1).

As followers of natural science we know nothing of any relation between thoughts and the brain, except as a gross correlation in time and space.

-Charles Scott Sherrington (1857 – 1952 CE)

LIST OF ABBREVIATIONS

AQL	anterior quadrangular lobule
cu	cuneate fasciculus of the medulla
Gr	gracile nucleus of the medulla
GrL	gracile lobule
ISL	inferior semilunar lobule
Sim	simple lobule
V	lobule V
VI	declive
VIIB	tuber
VIIIB	lobule VIIIB

CHAPTER III:Somatomotor signals modulate early visual cortical activity

Muhammad Zubair[1,2], John T. Arsenault[1,2], Wim Vanduffel[1,2,3,4]

[1] Laboratory of Neuro- and Psychophysiology, Department of Neurosciences, KU Leuven Medical School, Leuven 3000, Belgium

[2] Leuven Brain Institute, KU Leuven, Leuven 3000, Belgium

[3] Athinoula A. Martinos Center for Biomedical Imaging, Massachusetts General Hospital, Charlestown, MA 02129, USA

[4] Department of Radiology, Harvard Medical School, Boston, MA 02144, USA

This chapter is based on:

Zubair, M., Arsenault, J. T., Vanduffel, W. Stimulus-effector associations modulate activity in early visual cortex of monkeys. *(Manuscript in preparation)*

Stimulus-effector associations modulate activity in early visual cortex of monkeys

Retinally-driven activity is modulated by cognitive signals, which originate in higher order brain areas and affect early levels of the visual system via feedback channels. Although oculomotor signals also interact with visual activity in occipital cortex, to stabilize vision and enhance saccadic target detection, modulation of neuronal activity in early visual areas by non-saccadic somatomotor signals is far less understood, especially in primates. Using an event-related fMRI paradigm in monkeys, we show that a learnt association between a visual feature and a unilateral manual action induces lateralized activity changes in early visual cortex (areas V1, V2 and V3). Activity increases and decreases in contralateral and ipsilateral visual areas, respectively, relative to the hand associated with the visual cue. Our results suggest that non-saccadic somatomotor signals can influence processing at very early levels of the visual hierarchy. Such a mechanism may be instrumental to improve or accelerate acquired visuo-motor interactions, analogous to the enhancement of visual signals prior saccadic target selection.

3.1 Introduction

Activity in early visual areas is shaped by a combination of retinal feedforward input and non-retinal influences carried by feedback, lateral and ascending neuro-modulatory axons. These non-retinal signals modulate visually-driven activity depending on context, value, state, attention, internal needs and memory of the subject. Although (pre)saccadic motor activity is also known to influence responses in early visual areas, to stabilize vision (e.g., (Sylvester et al., 2005, Reppas et al., 2002)) and to improve saccadic target selection (Noudoost et al., 2014), the modulatory influences of other types of motor activity is less understood, especially in primates.

Although locomotion changes the gain of V1 responses in a nonspecific manner in mice (Kaneko and Stryker, 2014), information related to locomotion (e.g. speed of running) can also be integrated with visual signals to estimate the velocity of moving stimuli (Saleem et al., 2013, Keller et al., 2012, Niell and Stryker, 2010, Ayaz et al., 2013). In humans, however, the effect of locomotion on low-level features, such as contrast, is not comparable to that in rodents (Bullock et al., 2017, Benjamin et al., 2018). Nevertheless, it has been shown that object features can affect motor activity, and that such affordances occur very fast after stimulus presentation. This inspired the hypothesis

that activity in early human visual cortex might be modulated by a learnt object-action association (Goslin et al., 2012).

Intriguingly, and reminiscent of response properties typically observed in higher-order cortex (e.g. (Rishel et al., 2013), neurons in macaque area V4 indeed show feature-dependent categorization sensitivity (Mirabella et al., 2007). In this case, the learnt behavioral category to which a feature belongs, and not the feature itself, determines the activity of such neurons. An interpretation of such V4 responses as being mere category-selective, however, ignores the possibility that also the effector, used by a subject to indicate the stimulus category, may influence visually-driven activity. Category-dependent modulations of activity should be independent of (pre)motor activity related to the use of a specific effector. In case a unilateral effector (e.g. left hand) is used during the categorization task, and if the effector affects sensory-driven activity, one predicts lateralized modulations in visual cortex in the hemisphere contralateral to the effector (right hemisphere in this example). This is exactly the hypothesis we aimed to test in this study. Can the representation of a visual stimulus in occipital cortex be modulated depending on the association of a stimulus feature with a specific effector? To test this somatomotor-dependent modulation hypothesis, we designed an event-related fMRI paradigm whereby a specific feature

(color) of a peripherally presented and covertly attended stimulus was associated with different hand responses.

3.2 Results

The experiment consisted of two experimental rounds, during which two monkeys had to categorize the color of a stimulus (being more blue or red), using either a left or a right-hand response, respectively. In the second round, the color-hand association was reversed. fMRI was acquired in both rounds and used to detect changes in brain activity depending on the hand associated with both color categories. For example, in the first round, subject M1 had to covertly attend a small blue or red stimulus, presented at 7.5 degrees eccentricity along the vertical meridian. To obtain a reward, M1 had to press a button with its right or left hand, when the stimulus was blue or red, respectively (**Figure 3.1a**). A white stimulus was presented during one third of the trials, and the animal was not allowed to press a button to be rewarded. In the second round, this hand-color association was reversed: i.e., the blue and red color was associated with a left- and righthand response, respectively. These color-hand associations were counterbalanced across both experimental rounds of subject M2 (**Figure 3.1b**). Thus, featural attention and effector use was counterbalanced across conditions since the same feature was associated with both left-

and righthand responses in different experimental rounds within the same individual and across subjects. Animals were first trained and then scanned using the respective color-hand associations of each experimental round.

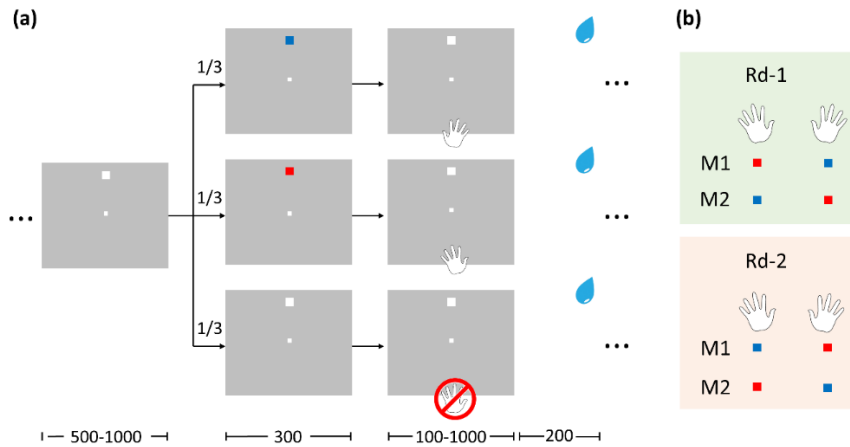


Figure 3.1: Experimental design. (a) Task trial. Each trial started with a randomized fixation period (500-1000 ms) while a peripheral white square was presented at 7.5° eccentricity above the central fixation point. Next, this square turned either red or blue (for 300 ms), or remained white. The colored stimuli required a specific hand response to receive a juice reward (in this example, blue and red were associated with a right- and left-hand response, respectively). Correct responses were rewarded within 100-1000 ms after the colored stimuli were replaced by a white one. When the white stimulus remained on the screen, the monkey had to fixate without pushing a response button, but with both hands inside the response box, to be rewarded. **(b) Color-hand association in each round for both subjects.** Each subject performed two experimental rounds (Rd-1, Rd-2), and the color-hand association was counterbalanced across subjects and rounds.

3.2.1 Hand-color association: behavioral performance

The total number of scan sessions & runs (during experimental rounds 1/2) for M1 and M2 were 5/6 & 102/115 and 6/6 & 118/84, respectively. The mean percentage correctly executed trials for M1 during these sessions was 92.87 ± 0.97%/83.00 ± 1.26% (mean ± standard error of the mean, SEM) for color-A, and 91.20 ± 1.53%/85.6 ± 2.57% for color-B in rounds 1/2, respectively. For M2, this was 93.38 ± 1.82%/91.03 ± 1.75% and 92.47 ± 1.73%/90.34 ± 1.05%, respectively. The average response time (RT) for M1 was 606.47 ± 13.81/701.06 ± 21.54 ms (mean ± SEM) for color-A and 680.69 ± 16.78/691.28 ± 10.67 ms for color-B in rounds 1/2, respectively. For M2 the RT was 556.18 ± 11.46/609.39 ± 26.12 ms for color-A, and 686.60 ± 20.07/496.09 ± 8.27 ms for color-B (**Supplemental Material S3.1**). Interactions between round and color (Kruskal-Wallis non-parametric ANOVA) were significant for performance levels, P = 0.0092 and RTs, P = 3.9×10^{-47} (group-level analysis with 220 and 199 runs for round 1 and 2, respectively).

3.2.2 Eye positions

We analyzed the eye-position data, time-locked to stimulus onset (color-A, color-B; linked to left- or right-hand responses),

after removing eye blinks (see methods). No significant differences in eye-positions (X and Y) were detected between left-and righthand responses (**Figure 3.2** group data, **Supplemental Figure S3.1:** individual data; **Supplemental Figure S3.2:** statistics for 50 ms bin widths, but results are independent of bin width). Hence, differences in eye position are unlikely to explain the fMRI results described below.

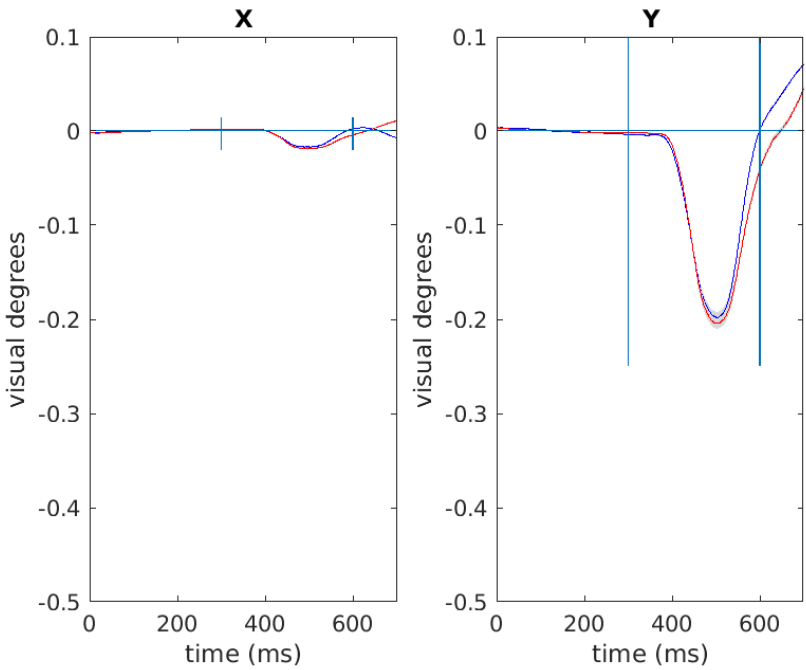


Figure 3.2: eye-position data (group). Blue and red plot curves correspond to trials with left- and righthand responses, respectively. Stimulus interval (300 ms) is indicated by vertical blue lines.

3.2.3 Hand-color association: single subject fMRI activity

The event-related fMRI data were first analyzed for both rounds (Rd-1 and -2) and both subjects, separately (see Methods). T-score maps for the contrast color-A vs color-B (hot colors), corresponding to right versus left hand responses in round 1 of M1 (and round 2 of M2), and left versus right hand responses in round 1 of M2 (and round 2 of M1), are shown on three representative coronal sections (**Figure 3.3,** see **Supplemental Figures S3.3-3.6** for brain-wide overviews). As expected, stronger activity can be observed in primary motor cortex, the anterior parietal lobule and premotor cortex, and primary and secondary somatosensory cortex contralateral to the hand linked with color-A. Also, as predicted, stronger activity, in the hemisphere contralateral to the hand associated with color A, was observed in parts of the basal ganglia, including the putamen, globus pallidus and caudate nucleus, and in the dorsomedial thalamus and ventral striatum. In the cerebellum, opposite activity patterns were observed compared to cortical somatomotor areas: strong positive activity occurred in several cerebellar nuclei ipsilateral relative to the hand associated with color A. These ipsilateral cerebellar activation patterns were measured in both subjects during both rounds of the experiment (**Figure 3.3**, **Supplemental Figures S3.3-3.6**). Deactivations for color-A (or activations for color B) were seen in topologically

corresponding regions of the ipsilateral (relative to the hand associated with color-A) hemisphere of both monkeys in the cerebrum and the contralateral cerebellum. Since the hand associated with color-A switched in the second round, the respective activity patterns were also reversed in this round for both monkeys (**Figure 3.3** (second row) and **Supplemental Figures S3.4,3.6**).

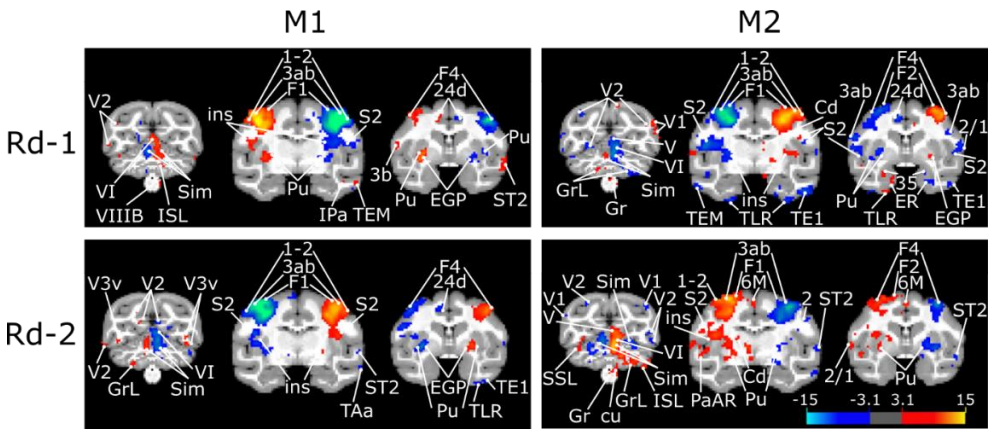


Figure 3.3: fMRI activity in both rounds for each subject for the contrast color-A (blue) vs B (red). Higher fMRI activity for color-A (hot colors) are observed in ipsilateral cerebellum (relative to the hand associated with color A), and contralateral somatomotor cortex and basal ganglia. (t-score maps, uncorrected level, P < 0.001; cluster size: 15 voxels). **Abbreviations:** V, lobule V; VI, declive; VIIIB, lobule VIIIB; ISL, inferior semilunar lobule; Sim, simple lobule; cu, cuneate fasciculus of the medulla; Gr, gracile nucleus of the medulla; GrL, gracile lobule, 1-2, somatosensory areas 1 and 2; 3ab, somatosensory area 3a and 3b; 3b, somatosensory area 3b; ins, insula; F1, primary motor area; F2, premotor area F2; F4, premotor area F4; 24d, area 24d of cortex; Pu, putamen; S2, secondary somatosensory area; EGP, external globus pallidus; IPa, Intraparietal associated area; TEM, temporal area TE

medial part; ST2, superior temporal region 2; 35, subregion of the entorhinal; ER, entorhinal rostral part; TAa, temporal area TAa; TLR, temporal area TL rostral part; TE1, temporal area TE1; PaAR, para-auditory cortex rostral part; 6M, area 6 of cortex; V1, visual area 1; V2, visual area 2; V3v; visual area 3 ventral part.

3.2.4 Hand-color association: group fMRI analysis

The color-hand associations are counterbalanced across rounds and subjects **(Figure 3.1b).** Therefore, to enable group analyses, we flipped the hemispheres of one subject (M2). This simple procedure mitigated analytical issues induced by opposite color-hand associations across subjects within a given experimental round, thereby increasing the statistical power of our analyses **(Figure 3.4a)**. After mirroring M2's hemispheres, we expect higher activity during blue (color A) than red trials (color B) in somatomotor areas of the left hemisphere (of the re-arranged group data) in round 1, and lower activity in the homotopic areas of the right hemisphere. Conversely, in the second experimental round, we expect higher activity in somatomotor regions of the right hemisphere (see **Figure 3.4b)**. More relevant for the present study, however, if the representation of the visual stimulus is modulated based on the associated effector, we predict an interhemispheric difference in visually-driven activity for the same stimulus depending on the experimental round. In that case, one predicts a lateralized modulatory effect of visually-

driven activity: increased activity in the hemisphere ipsilateral to the representation of the effector, thus contralateral to the effector, as schematically presented in **Figure 3.4c**.

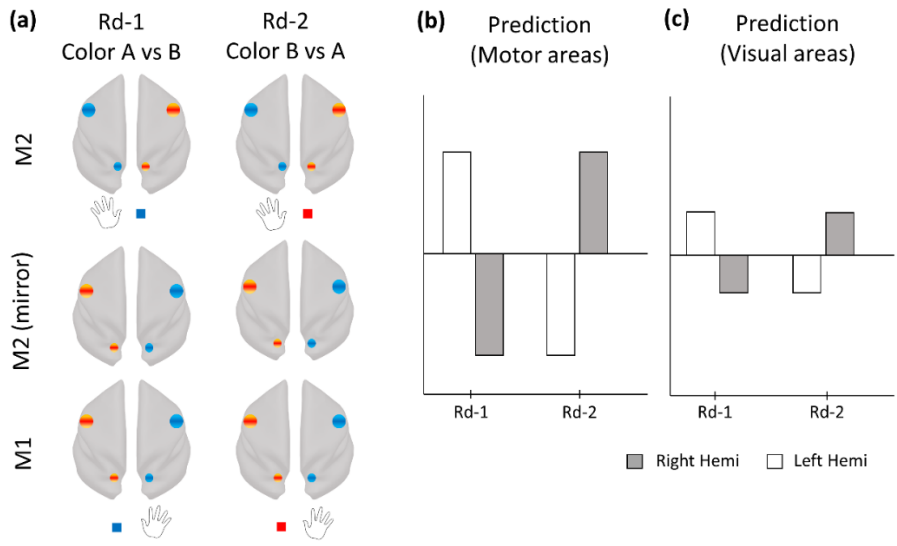


Figure 3.4: Schematic of data mirroring and predicted fMRI activity in somatomotor and visual regions during the two experimental rounds. (a) The top row illustrates the predicted fMRI activity in somatomotor and hypothesized activity in visual areas for both rounds (Rd-1, color-A (blue) associated to the left-hand response; contrast: color-A vs B) (Rd-2, color-B (red) is associated with left-hand responses; contrast: color-B vs A) of monkey M2. The second row represents the flipped hemispheres (right-to-left and vice versa) of M2. The third row illustrates the expected fMRI activity in both experimental rounds of monkey M1 (Rd-1, color-A (blue) associated to the right-hand response; contrast: color-A vs B) (Rd-2, color-B (red) associated to the right-hand response; contrast: color-B vs A). Hot colors reflect putative positive fMRI activations in (pre)motor and visual areas of the hemisphere contralateral to the associated hand. **(b)** Bar graphs indicate the expected group fMRI activity (with M2's

hemispheres mirrored) in somatomotor areas for both rounds in each hemisphere. **(c)** Hypothesized modulation of activity in visual cortex based on activity in ipsilateral motor cortex which is driven by the (contralateral) hand associated with the stimulus. Note that the amplitude of the modulations is not predicted, contrary to the relative sign of the activations during the two rounds. Hemi = hemisphere.

To test this prediction, the data from both subjects were co-registered to D99 (Reveley et al., 2017) after flipping M2's hemispheres (**Figure 3.4a)**, which allowed us to perform a group analysis (using a standard general linear model, GLM) yielding maximal statistical power. Then, we performed a second-level GLM analysis with the per-run beta maps as input (see Methods). The resulting t-score maps, for the contrast color-A vs color-B (whereby color-A is the color associated with right hand button presses), are overlaid on coronal sections **(Figure 3.5,** FWE Bonferroni corrected for multiple comparisons).

As expected, strong contralateral activity relative to the hand associated with color-A is observed in primary motor cortex F1 and primary somatosensory cortex (Brodmann areas 1, 2, 3a and 3b). These positive activations extend into secondary somatosensory cortex within the upper bank of the lateral sulcus. More frontally, we observed activations contralateral to the hand associated with color-A in premotor areas F1, F4, F5p, F7 and ipsilaterally in area F5a. More caudally the activations

contralateral to the hand associated with color-A extended into parietal areas MIP, PGOp and PE. By and large, homotopic ipsilateral cortical regions show negative activity levels when contrasting color-A versus color-B, with the exception of lateral prefrontal/orbitofrontal cortex. Although slightly more extensive, this somatomotor-related cortical network was reminiscent of the grasping-related network described earlier, except for the inclusion of F3 and area 24 (Nelissen and Vanduffel, 2011).

The cerebellar hemispheres show the opposite activity patterns compared to the cerebral cortex. Specifically, several cerebellar regions (Sim, simple lobule; AQL, anterior quadrangular lobule; SSL, superior semilunar lobule; V, lobule V; VI, declive; VIIB, tuber; GrL, gracile lobule; ISL, inferior semilunar lobule) showed strong positive activations ipsilateral relative to the hand associated with color A (Kelly and Strick, 2003). Most of these cerebellar foci showed negative fMRI activity contralateral to the hand associated with color A **(Figure 3.5)**.

Surprisingly, we also observed positive fMRI activity in the secondary visual area (V2) contralateral to the hand associated with color A, which suggests that motor activity can influence visually-driven activity in the same hemisphere. This small but

highly significant hand-specific activity modulation in visual cortex will be further examined in the next analysis.

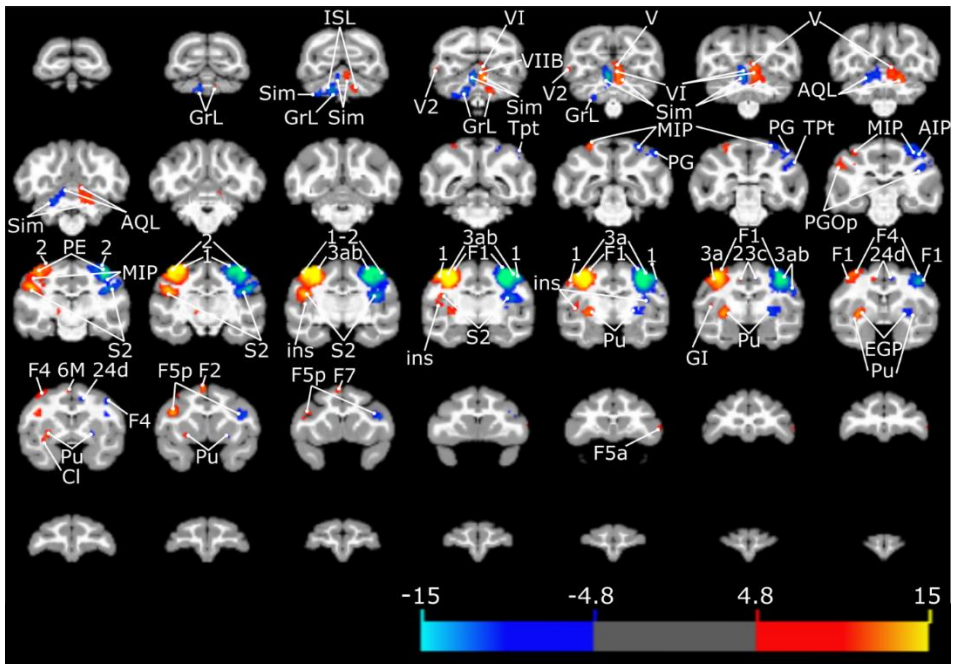


Figure 3.5: fMRI group activity as a result of color-hand association task. T score maps overlaid on coronal slices (top-left: caudal to bottom-right: rostral) in D99 template space, as a result of a second level GLM group analysis. The data are the same as used for figure 3.3. Contrasts: 'color-A versus B': (Rd-1 of monkey M1 whereby color A is associated with the right hand) and M2 (horizontally mirrored data; color A associated with the right hand), hot colors; and 'color-B versus A' of Rd-2 of M1 and M2 (horizontally mirrored data), cold colors. The total number of runs for both rounds (Rd-1 and 2) are 220 and 199, respectively (corrected level, $P < 0.05$; cluster size: 15 voxels). **Abbreviations:** VIIB, tuber; AQL, anterior quadrangular lobule; AIP, anterior intraparietal area; Tpt, temporoparietal area; MIP, medial

intraparietal area; PG, parietal area PG; PGOp, PG opercular part; PE, parietal area; F5p, premotor area F5, posterior part; F7, premotor area F7; 23c, area 23c of cortex; GI, granular insula cortex.

3.2.5 Linear regression model

The previous analyses showed the expected contralateral activations in major somatomotor, premotor and parietal regions relative to the hand associated with color-A (for the contrast color-A versus B), but also some unexpected, yet rather restricted changes in visual cortex contralateral to the effector associated with color-A. To investigate the modulation of activity in visual cortex in more detail and to further increase the power of our statistical analyses, we collapsed all data onto 1 hemisphere. Specifically, all data of the left hemisphere were spatially mirrored to the right-hemisphere and we applied a linear regression (LM) with factors round and hemisphere. This sensitive analysis extracts the information that changes across hemispheres and rounds, yet independent of the specific colors and effectors used, as these are perfectly counterbalanced across rounds and subjects. For example, in somatomotor cortex, effector-driven activity flips from one hemisphere to the other across rounds, which was indeed extracted by the LM analysis (**Figure 3.6a** for group, **Supplemental Figure S3.7** and **S3.8** for individual subjects). The strongest interaction effects between round and hemisphere in the cerebellum was found in

lobule (V) and declive (VI) **(Figure 3.6b,** $P < 0.001$, uncorrected). Thus, the opposite laterality effects in motor and premotor regions of the cerebrum and cerebellum confirm our earlier GLM results, exactly as predicted by the known anatomical motor circuitry. Most importantly for the current study, however, several early visual regions showed a very similar interaction effect as somatomotor cortex (**Figure 3.6a**, V1, V2d, V2v, V3d, V3v).

To illustrate the amplitude of the fMRI responses in a number of regions of interests (ROIs) borne out in the previous LM analysis, we plotted the mean beta values (color-A versus color B) for both rounds, and for both the group and individual animals, separately (**Figure 3.6c** and **Supplement Material S3.2).** In line with the t-score maps of the LM analysis (**Figure 3.6a, b**), all ROIs, except prefrontal area 12 and the cerebellum, show similar responses (positive activity in the left- and negative in right-hemisphere for color-A versus color B) during round 1, when color-A was associated with the right hand (after flipping the data of M2). The opposite pattern (positive activity in the right- and negative in left-hemisphere for color-A versus color B) during round 2 when color-A was associated with a left-hand response (again after flipping the data of M2) (**Figure 3.6c**). The cerebellum shows the opposite activity pattern compared to that of the somatomotor and visual cortex of the same hemisphere.

Thus, the association of a visual stimulus with a specific effector, modulates its neuronal representation in an effector-specific manner: the activity in somatomotor cortex, induced by the contralateral effector that is associated with the stimulus, correlates with activity in several visual areas within the same hemisphere (i.e. contralateral to the effector; see **Figure 3.3**). Critically, the sign of the activity changes (for the contrast color-A versus color B; corresponding to right hand associations versus left hand associations, independent of the actual color) in visual cortex is the same as that in somatomotor areas within the same hemisphere.

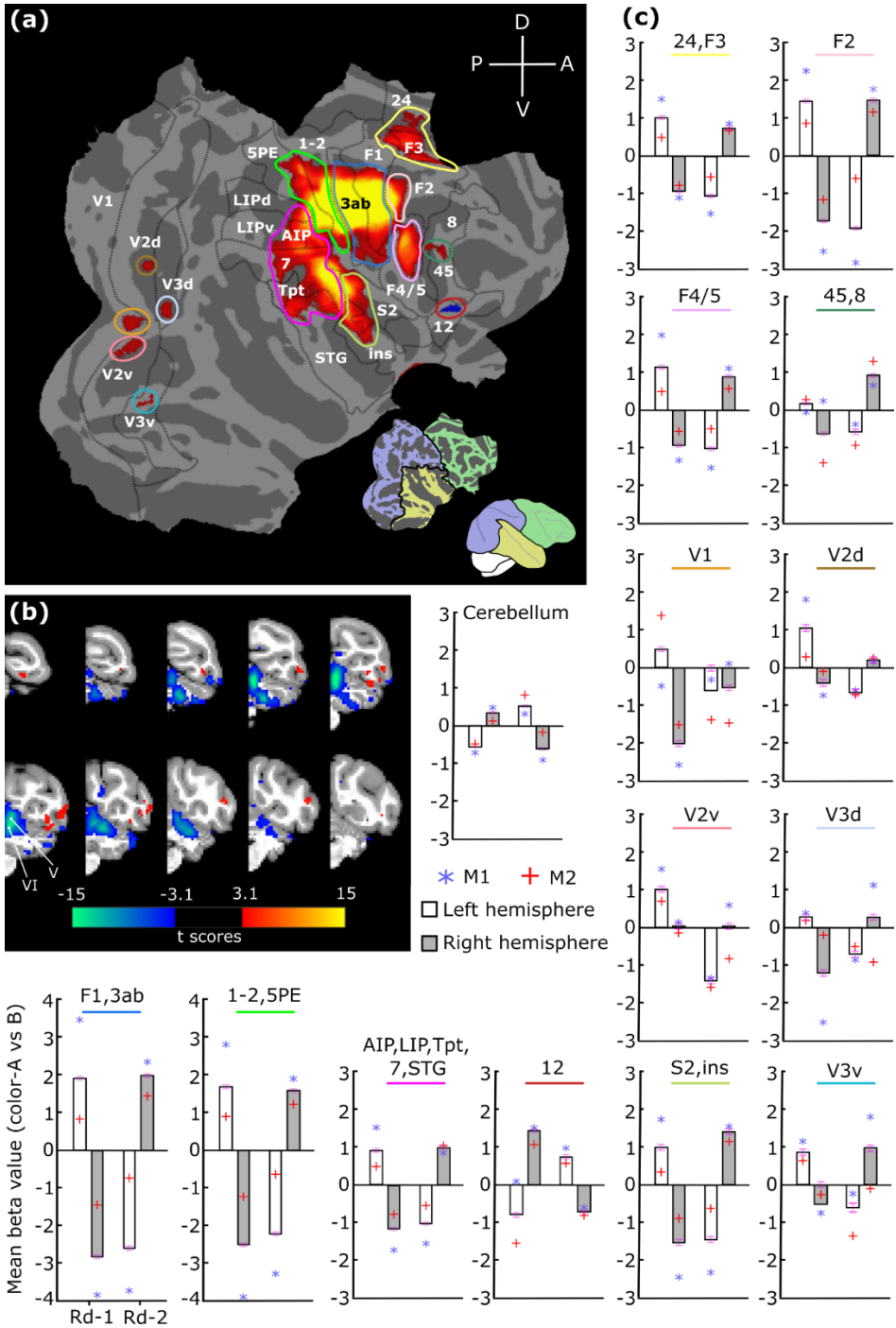

(a)
D
P
A
V
24
5PE
1-2
F1
F3
F2
V1
LIPd
3ab
LIPv
8
V2d
AIP
7
45
V3d
Tpt
F4/5
S2
12
V2v
STG
ins
V3v
(b)
VI
V
-15
-3.1
3.1
15
t scores
Cerebellum
M1
M2
Left hemisphere
Right hemisphere
(c)
24,F3
F2
F4/5
45,8
V1
V2d
V2v
V3d
S2,ins
V3v
Mean beta value (color-A vs B)
F1,3ab
1-2,5PE
AIP,LIP,Tpt,
7,STG
12
Rd-1
Rd-2

Figure 3.6: Interaction between hand response and hemisphere. **(a)** T score values of the interaction between round and hemisphere (LM analysis for the group data; M1: Rd-1 102 runs, Rd-2 115 runs; M2: Rd-1 118 runs, Rd-2 84 runs; uncorrected level, $P < 0.001$; cluster size: 30 voxels) overlaid on a flatmap of the right hemisphere in D99 template space. Some activations spanned multiple areas (F1, 3ab; 24, F3; 45, 8; S2, insula; 1-2, 5PE; AIP, LIP, Tpt, 7, STG), while others were restricted to a single area (F2, F4/5, 12, V1, V2d, V2v, V3d, V3v). Activations are outlined in color (same color code as panels a and c). The inset shows frontal, occipito-parietal and temporal subdivisions onto a 3D surface and 2D flatmap. **(b)** T score maps of the same round X hemisphere interaction overlaid on coronal slices of the right hemisphere, focusing on the cerebellum (uncorrected, $P < 0.001$; cluster correction, 30). **(c)** Mean beta values (from the GLM analysis) for the contrast 'color-A vs B' of regions defined in (a). The average beta values are plotted for individual subjects (M1: *; and M2: +) and the group (bar plots), for both rounds and both hemispheres. The error bar denotes standard error of the mean across runs. **Abbreviations:** LIPd, LIP dorsal part; LIPv, LIP ventral part; AIP, anterior intraparietal area; F3, motor area F3, F4/5, agranular frontal area F4/5, 12; subregion of the OFC; 24; subregion of the ACC, 8; subregion of the DPFC, 45; subregion of the VLPFC, 5PE; superior parietal lobule area, V2d; V2 dorsal part, V2v; V2 ventral part; V3d; V3 dorsal part, STG; superior temporal gyrus, 7; inferior parietal lobule area.

3.3 Discussion

This event-related fMRI study revealed enhanced activity in expected cortical and subcortical somatomotor regions contralateral to an effector associated with a visual feature. The exceptions are cerebellar nuclei showing ipsilateral motor-

related activations, conforming their connections with motor cortex of the opposite hemisphere (Kelly and Strick, 2003). Intriguingly, however, we also found increased activity in early visual areas contralateral to the effector associated with the stimulus (and decreased activity in ipsilateral visual areas). This lateralized modulation of visually-driven activity represents a largely neglected form of extraretinal modulation of sensory input at early levels of the visual system. We argue that this cannot only reflect a category-selective signal at early levels of the visual system, as previously described for V4 neurons (Mirabella et al., 2007). Instead, we propose that the lateralized activity changes in visual cortex result from feedback signals originating in somatomotor regions that modulate sensory input depending on a learnt association between a specific stimulus feature and a specific motor output.

Responses of neurons in early visual cortex primarily depend on the retinal stimulus driving these neurons. Yet, their activity is also influenced by extraretinal signals such as selective attention to either the spatial location (Hayden and Gallant, 2005, Williford and Maunsell, 2006, Sundberg et al., 2009, Connor et al., 1997), or features of the retinal stimulus (McAdams and Maunsell, 1999, Mirabella et al., 2007, McClurkin and Optican, 1996). The present results cannot be explained by differences in selective spatial attention since the stimulus feature associated with

either a left- or right-hand response was presented along the vertical meridian. Covert spatial attention had to be focused to the same location, independent of the effector used. Such a stimulus does not evoke lateralized retinally-driven responses, nor an imbalance in attention to either the left or the right hemifield. Moreover, although the subjects covertly paid attention to a feature of the stimulus, i.e. color, featural attention cannot explain our results, since we carefully balanced the attended features across rounds and subjects. Since color and hand were correlated, it would be difficult to distinguish between a featural attention and somatomotor account of our results using data obtained in a single round. The linear regression analysis, however, extracted these voxels whose activity changed during the two rounds independent of the actual color associated with either the left or right hand. This analysis revealed lateralized activity modulations in visual cortex, refuting a featural attention explanation since this should have induced bilateral activity changes. Finally, eye-positions were also indistinguishable across experimental conditions, indicating that they cannot explain the observed effects.

Previously, it has been shown that about 30% of the neurons in area V4 encode the behavioral response category that is associated with an attended stimulus feature (Mirabella et al., 2007). Interestingly, category-selective V4 responses were

absent in the beginning of the visual response, but increased gradually to peak just before the behavioral response. A potential interpretation is that these late category-selective responses reflect feedback from higher-order regions, such as inferotemporal (Freedman et al., 2003, Kreiman et al., 2000, Thomas et al., 2001), parietal (Freedman and Assad, 2006), and prefrontal cortex (Freedman et al., 2002, Freedman et al., 2003), where behavioral categorical information emerges through associative learning processes. Alternatively, this category-selective response in V4 reflects a (pre)motor-like signal being transmitted from areas encoding the specific operant behavior required to indicate to which category the stimulus feature belongs. Notably, category-selective information in the Mirabella et al. study (2007) was abolished during error trials, suggesting a close link between the motor output and category-selective effects in V4 neurons. The authors of that study, however, disregarded a (pre)-motor account of the category-selective responses for several reasons. Firstly, one would have expected a reverse pattern of activity during error relative to correct trials, which was not the case. Secondly, category-selective responses during control trials were not observed in V4 when the same behavioral response was required from the animal, yet unrelated to the feature driving the neuron's activity -i.e., to indicate the dimming of the fixation point. Category-dependent activity modulations, however, should be

independent of the specific effector used to indicate the category to which a particular stimulus belongs. In the Mirabella study, the same hand was used to push a lever to the right and left, which are different actions using the same effector. If category-selective modulations in early visual cortex are independent of the specific type of motor activity or effector and only depends on the behavioral category, one would not expect lateralized modulatory effects when using bilaterally homologous effectors during the categorization task: it is irrelevant whether a specific feature is linked to a left- or righthand response during categorization. This is contrary to the present findings: activity is higher in visual cortex contralateral to the effector associated with the stimulus, and lower in the ipsilateral hemisphere. The most parsimonious explanation is that somatomotor signals induced by the effector associated with a stimulus feature instigate lateralized activity modulations. This is not a mere reverberation of a general (pre)motor signal, as there must be a learnt association between a stimulus feature and the correct effector (e.g. blue color with the right-hand response during round one of M1, red with right hand response in round two of M1, etc.). This also explains why the category-selective responses in the previous V4 study (Mirabella et al., 2007) are abolished during control trials when the monkey makes a lever response independent of the feature coded in the recorded V4 neuron as there is no association of the coded

feature driving that neuron and a motor response. Moreover, this also explains why these authors did not observe a reverse pattern of V4 activity in error trials. In the latter case, there is an association between a stimulus feature yet with the wrong motor output, different from the learnt one.

It has been shown that extraretinal saccade signals can also modulate activity in early visual cortex and even the LGN (Sylvester et al., 2005) which is another example of a somatomotor signal influencing sensory areas. Such signals suppress peri-saccadic visually-driven activity and are thought to stabilize vision during saccades. Enhanced pre-saccadic activity is also observed in visual cortex when targets located in the receptive field of the neuron are targeted with an ensuing saccadic eye movement (Chelazzi et al., 1993, Buracas and Albright, 2009, Fischer and Boch, 1981, Moore et al., 1998), which is accompanied by perceptual benefits (Moore and Chang, 2009). Moreover, pre-saccadic enhancement of neuronal activity in visual cortex is dependent on activity in areas with oculomotor properties (i.e. the FEF) (Noudoost et al., 2014). It is plausible that the modulatory effects that we observed in visual cortex are highly similar to those observed in the visual-oculomotor system, yet where the visual stimulus is not the target of a motor act (i.e. the monkeys do not reach to the stimulus), but serves as a signal to make a proper hand action. A somatomotor signal which

enhances a visual response can be instrumental to improve accuracy or accelerate visuo-motor interactions whereby a retinal stimulus requires a fast almost habitual action as is often the case in daily life.

3.4 MATERIALS AND METHODS

EXPERIMENTAL PROCEDURES

3.4.1 Subjects

Two male rhesus monkeys (*Macaca mulatta;* 7-9 kg, 4-6 years old) participated in the experiments of this study. Animal care and all experimental procedures were approved by the Animal Ethics Committee KUL's, and are in accordance with the National Institute of Health's Guide for the Care and Use of Laboratory animals and the European guidelines (Directive 2010/63/EU). Following the recommendations of the Weatherall report, animals were allowed extensive locomotor behavior, foraging, and social interactions. Animals were group-housed (cage size at least 16-32m^3) with cage enrichment (toys, foraging devices) at the primate facility of the KU Leuven Medical School. The monkeys were exposed to natural light conditions, with additionally 12 hours of artificial light throughout the year, and with fully-controlled climate conditions. Monkeys were fed daily with standard primate chow supplemented with nuts, breads, raisins, prunes, and fruits. The animals received their daily water supply during the experiments until satiated, with additional water and fruits during the weekends. Monkeys were equipped with an MR compatible headpost. The details of the surgical, initial training and general fMRI procedures of the monkeys have

been described previously (Vanduffel et al., 2001, Arsenault and Vanduffel, 2019).

EXPERIMENTAL DESIGN:

3.4.2 Color-hand association task

Both monkeys were first trained to associate a specific covertly-attended color cue (red or blue) that was presented in the peripheral visual field with a specific hand response (i.e., left or right hand) (**Figure 3.1a**). Monkeys were seated in a sphinx position within a plastic chair with their head restrained to reduce head movements (Vanduffel et al., 2001). The chair was equipped with a small response box containing two response buttons, separated by a plastic divider. Two pairs of optic fibers in the response box allowed us to measure the position of both hands, independent of the response buttons. To start a trial, the monkey was required to keep both hands above the response buttons within the response box and to keep its gaze fixed at the central white fixation dot (0.15^o x 0.15^o, 123 cd/m^2) within a virtual 2 x 2-degree fixation window. Meanwhile, a second white dot (0.5^o x 0.5^o, 123 cd/m^2) was presented, at 7.5 degrees eccentricity in the upper visual field along the vertical axis, on an otherwise grey background with a mean luminance of 60 cd/m^2. Trials were aborted when one or two hands were retracted from the response buttons, or when fixation was interrupted. In case

of an aborted trial, a yellow cross appeared in the center of the screen. This yellow cross served as a cue for the monkey to reposition both hands on the response buttons. Eye positions were monitored with an infrared camera by tracking pupil position and corneal reflection (Iscan, 120Hz). After a variable interval of 500-1000 ms fixation time, the white peripheral dot turned either blue(ish) or red(dish) for 300 ms. Immediately afterwards, the peripheral dot became white again. To receive a juice reward, the animal had to indicate, by either pushing the right or the left response button (with the right and left hand, respectively), whether the covertly attended peripheral dot was more blue or red, respectively. The difference between red and blue was gradually decreased during training, until the monkey reached performance levels of >80% correctly executed trials. In one third of the trials, the peripheral dot did not change color. To receive a juice reward during the latter trial types, the monkey had to keep its fixation centered on the central dot and both hands inside the response box but without pressing any button. Each trial was followed by a 600 ms inter-trial-interval, before the next trial started. The three different trial types were randomly interleaved. Note that the stimulus was always shown for 300 ms, followed by a fixed 100 ms interval during which the animal was not allowed to respond to avoid reflexive responses. This 300 + 100 ms interval is included in the average reaction times.

While the first subject learned the blue-right hand and red-left hand association during the first round of the experiment, this was reversed for the second animal. The first (M1) and second subject (M2) were trained for 62 and 18 days, respectively, for the color-hand association task in the first round of the experiment. The second animal could be trained much faster since this monkey was already trained using hand responses in a previous operant task unrelated to the present experiments. In the second round, the color-hand association was reversed for both monkeys, and M1 and M2 received 7 and 8 days of training, respectively. After training for each round, the monkeys were scanned with the trained color-hand relationship for that round **(Figure 3.1b)**.

3.4.3 fMRI data acquisition

fMRI data were acquired for both monkeys after their performance levels exceeded 80% during the training sessions. Specifically, we collected contrast-agent-enhanced functional images in a 3T horizontal bore full-body scanner (PrismaFit, Siemens Healthcare; Erlangen, Germany), using a gradient-echo T2* weighted echo-planar imaging (EPI) sequence (50 horizontal slices, in-plane 84x84 matrix, TR = 2s, TE = 13ms, 1.25 x 1.25 x 1.2 mm^3 isotropic voxels) with a custom-built external eight-channel phased array receive coil (individual coils 3.5 cm diameter), and

a saddle-shaped radial transmit-only surface coil (Kolster et al., 2009).

Prior to each scan session a contrast agent (monocrystalline iron oxide nanoparticle, MION Molday, Biopal) was injected into the saphenous vein (9-11 mg/kg) of the monkey (Vanduffel et al., 2001).

We next performed a randomized event-related fMRI experiment. The task was exactly the same as during the training sessions and the three trial types were randomly interleaved. The total duration of a run was 10 min 30 s.

3.4.4 GRE and anatomical data acquisition

We took a T2* weighted Gradient Echo (GRE) scan at the onset of each scan session (TR = 5 ms, TE = 2 ms, voxel size = 1.25 x 1.25 x 1.2 mm) to confirm whether all loops of the phased array coil were functional and to aid co-registration with the anatomical images. T1-weighted images (TR = 2.5 s, TE = 4.35 ms, TI = 850 ms, $\alpha = 9°$; 256 sagittal slices, 208 x 208 in-plane matrix, 0.5 mm isotropic voxel size) were collected while the monkey was anesthetized, using a single-loop receive-only surface coil and the standard body transmit coil (Murris et al., 2020).

3.4.5 fMRI preprocessing and analysis

A non-rigid, slice-by-slice realignment of the functional images acquired within runs and an affine realignment between runs of different days was performed to correct for motion (Kolster et al., 2009). A representative mean functional image of 100 EPIs was then non-rigidly co-registered to D99 (Reveley et al., 2017) using ANTs (Advanced Normalization Tools; University of Pennsylvania, USA: (Avants et al., 2011)) following a three-step procedure: 1) The mean functional image was co-registered to a GRE image acquired in the same session. 2) That GRE image was co-registered to a high resolution T1 anatomical from the same monkey. 3) This anatomical was registered to D99. These transformations were then applied to each fMRI time-series acquired within the same session. In a final pre-processing step, we spatially smoothed the images using FSL (FMRIB Software Library; University of Oxford, UK: (Smith et al., 2004)) employing an isotropic Gaussian kernel (FWHM: 4 mm).

A fixed-effect event-related general linear model (GLM) analysis was performed on each run by fitting a GLM using high-pass filtering (128 s), a first-order autoregressive model and restricted maximum likelihood estimation (SPM12; London, UK (Worsley and Friston, 1995)). In addition to the regressors of interest, a single motion regressor (change in correlation with first image in

time-series) and multiple noise regressors (generated by GLMdenoise (Kay et al., 2013)) were added as covariates of no interest. A 1st level GLM analysis yielded beta maps per run, for both rounds of the experiment, for the contrast (color-A vs B) and (color-B vs A). Then a 2nd level GLM was performed across runs for single subject and group analyses (FWE correction, $p < 0.05$). The result of this analysis were then projected onto the coronal slices in D99 atlas space (Reveley et al., 2017) for each individual subject as well as the group.

After the second-level group analysis, we ran a linear mixed effect model (LM) analysis on the per run beta images, but after the left hemispheres from both subjects (M1 and M2) and rounds (1 and 2) was mirrored onto the right hemisphere. The LM was fit with factors hemisphere (right or left), round (1 or 2), with interactions among the factors as main point of interest. In addition, LMs were fit to the data from individual monkeys separately (see **supplemental Figures S3.7-3.8**). T-values showing the interaction effects (for both individual subjects and group) were projected onto the right hemisphere flatmap in D99 atlas space (Reveley et al., 2017) using FreeSurfer (FreeSurfer; Charlestown, USA).

3.5 Supplementary information

		M1				M2			
		Accuracy		RT (ms)		Accuracy		RT (ms)	
		(%)	SEM	Time	SEM	(%)	SEM	Time	SEM
Rd-1	Color-A	92.87	±0.97	606.47	±13.81	93.38	±1.82	556.18	±11.46
	Color-B	91.20	±1.53	680.69	±16.78	92.47	±1.73	686.60	±20.07
Rd-2	Color-A	83.0	±1.26	701.06	±21.54	91.03	±1.75	609.39	±26.12
	Color-B	85.6	±2.57	691.28	±10.67	90.34	±1.05	496.09	±8.27

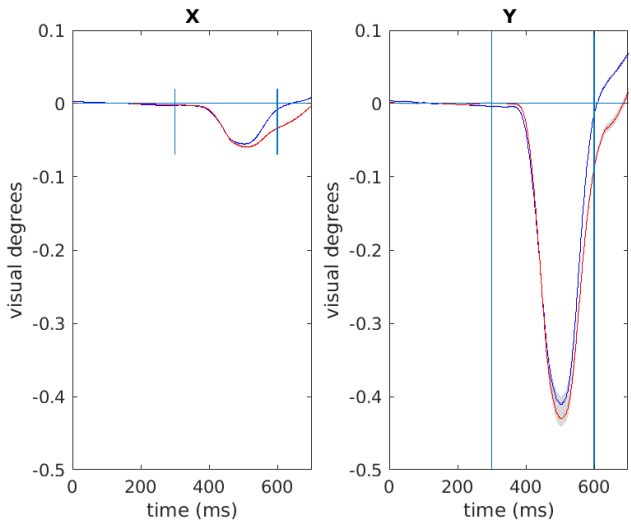
Table S3.1: Behavioral performance of the two monkeys during the recording sessions

ROI	Round	Hemisphere	M1	M2	Group	
			Mean	Mean	Mean	SEM
24, F3	1	L	1.65	0.46	1.01	±0.12
		R	-1.11	-0.86	-0.97	±0.10
	2	L	-1.52	-0.55	-1.11	±0.12
		R	0.83	0.72	0.78	±0.11
F2	1	L	2.17	0.87	1.48	±0.09
		R	-2.63	-1.13	-1.82	±0.09
	2	L	-2.88	-0.68	-1.95	±0.11
		R	1.71	1.26	1.52	±0.09
F4/5	1	L	1.99	0.42	1.14	±0.14
		R	-1.34	-0.64	-0.97	±0.11
	2	L	-1.54	-0.46	-1.08	±0.15
		R	1.05	0.64	0.88	±0.12
45, 8	1	L	-0.02	0.31	0.16	±0.18
		R	0.27	-1.46	-0.66	±0.15
	2	L	-0.38	-0.97	-0.63	±0.20
		R	0.69	1.26	0.93	±0.18
F1	1	L	2.90	0.79	1.82	±0.11
		R	-3.60	-1.48	-2.72	±0.12
	2	L	-3.7	-0.80	-2.76	±0.17
		R	2.5	1.53	2.12	±0.11
3ab	1	L	3.94	0.68	2.12	±0.14
		R	-4.20	-1.26	-3.03	±0.13
	2	L	-4.10	-0.69	-2.84	±0.19
		R	2.20	1.38	1.96	±0.11
1-2, 5PE	1	L	2.87	0.88	1.80	±0.10
		R	-3.96	-1.21	-2.61	±0.13
	2	L	-3.38	-0.66	-2.33	±0.14
		R	1.85	1.26	1.60	±0.10
AIP, LIPv, Tpt, 7, STG	1	L	1.49	0.51	0.96	±0.08
		R	-1.73	-0.88	-1.27	±0.08
	2	L	-1.60	-0.52	-1.14	±0.09
		R	0.85	1.08	0.95	±0.08
12	1	L	-1.60	0.11	-0.80	±0.25

		R	1.64	1.05	1.37	±0.25
	2	L	0.64	0.85	0.73	±0.24
		R	-0.57	-0.86	-0.70	±0.20
S2, insula	1	L	1.77	0.37	1.02	±0.09
		R	-2.58	-0.95	-1.71	±0.10
	2	L	-2.38	-0.59	-1.62	±0.11
		R	1.52	1.12	1.35	±0.10
V1	1	L	-0.43	1.35	0.53	±0.19
		R	-2.65	-1.57	-2.07	±0.25
	2	L	-0.21	-1.30	-0.67	±0.25
		R	0.13	-1.35	-0.50	±0.23
V2d	1	L	1.85	0.29	1.02	±0.23
		R	-0.72	-0.10	-0.38	±0.21
	2	L	-0.73	-0.79	-0.75	±0.23
		R	0.20	0.22	0.21	±0.20
V2v	1	L	1.3	0.78	1.02	±0.21
		R	0.13	-0.08	0.01	±0.25
	2	L	-1.38	-1.57	-1.46	±0.22
		R	0.64	-0.84	0.01	±0.24
V3d	1	L	0.32	0.19	0.25	±0.21
		R	-2.55	-0.23	-1.3	±0.25
	2	L	-0.88	-0.51	-0.72	±0.23
		R	1.16	-0.97	0.26	±0.26
V3v	1	L	1.14	0.70	0.90	±0.26
		R	-0.70	-0.28	-0.47	±0.21
	2	L	-0.25	-1.27	-0.68	±0.31
		R	1.78	-0.10	0.98	±0.26
Cerebellum	1	L	-0.71	-0.50	-0.60	±0.006
		R	0.52	0.11	0.30	±0.06
	2	L	0.27	0.84	0.51	±0.05
		R	-0.98	-0.19	-0.64	±0.07

Table S3.2: Average beta values of M1, M2 and the group data (for contrast, Color-A vs B) in each round and hemisphere for the defined ROIs.

(a)



(b)

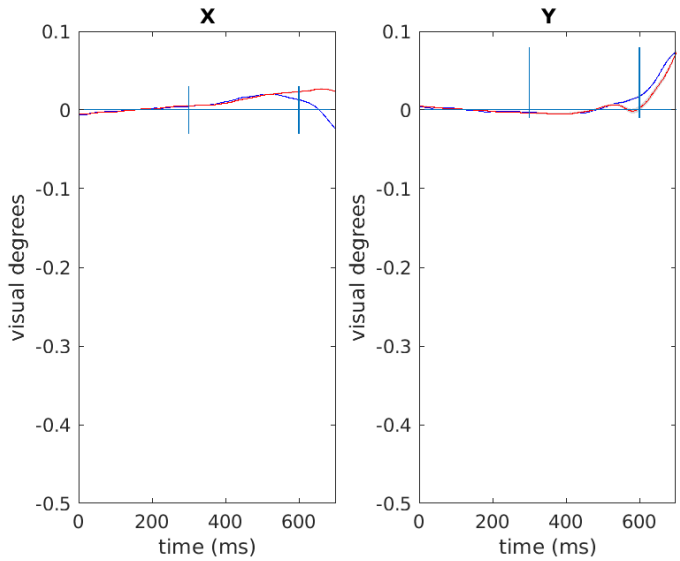
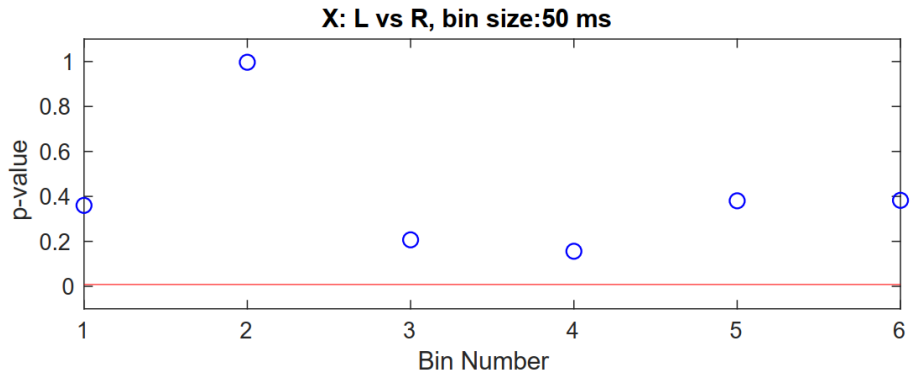


Figure S3.1: Eye-position data. Blue and red plot curves correspond to trials with left- and righthand responses, respectively. Stimulus interval (300 ms) is indicated by vertical blue lines **(a)** M1, **(b)** M2

(a)



(b)

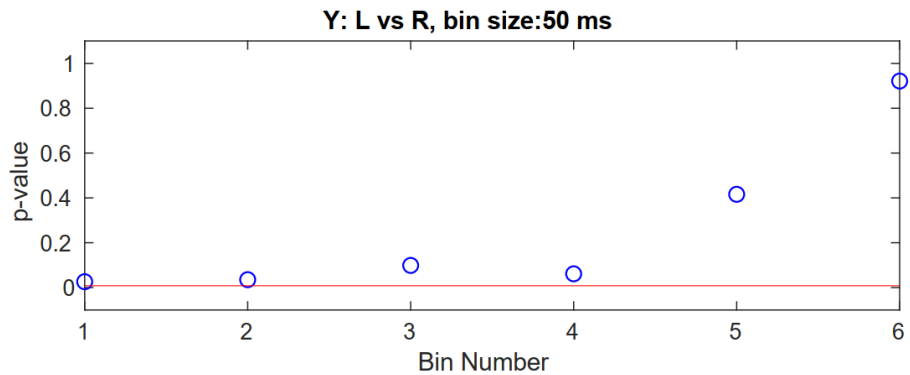


Figure S3.2: Group analysis eye movement data. Wilcoxon test for difference in eye-positions between left-and righthand trials during the 300 ms interval that the color cues were shown (50 ms time bins). All trials included in the fMRI analysis were considered. **(a)** eye positions in the X- and **(b)** in Y-direction. Red line indicates p = 0.05. Note that the comparison of eye positions between left- and righthand trials also yielded no significant differences in the individual monkeys, also independent of the bin size (up to the smallest bins of 16.66 ms) -data not shown.

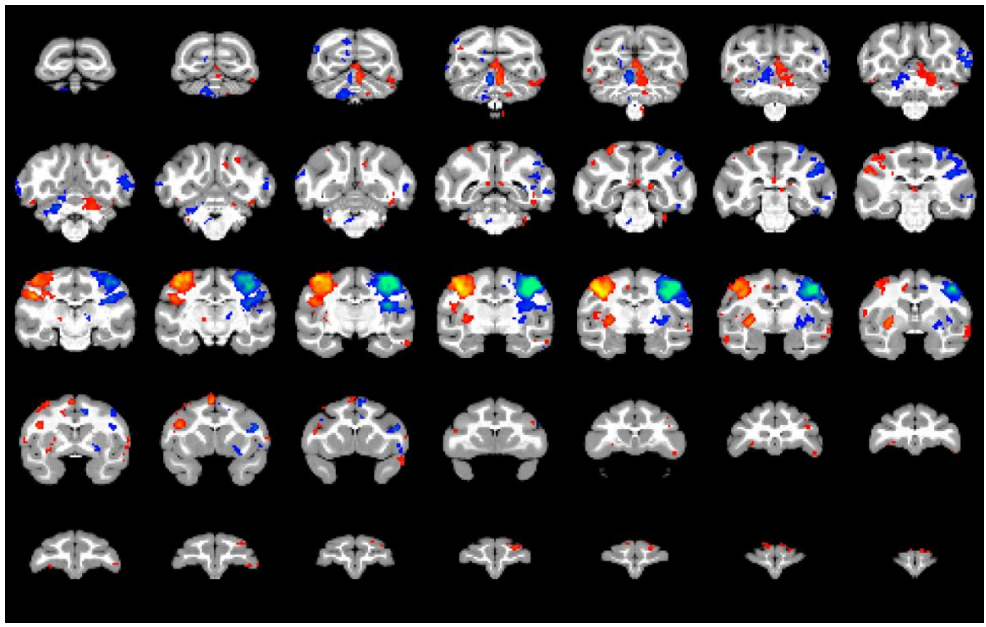


Figure S3.3: Overview of fMRI activity of M1 for Rd-1. T score maps of M1 for Rd-1 overlaid on coronal slices (top-left: caudal to bottom-right: rostral) in the D99 template space as a result of individual subjects' second level GLM analysis for contrast (color-A vs B) and for a total number of 102 runs (uncorrected level, $P < 0.001$; cluster size: 15 voxels).

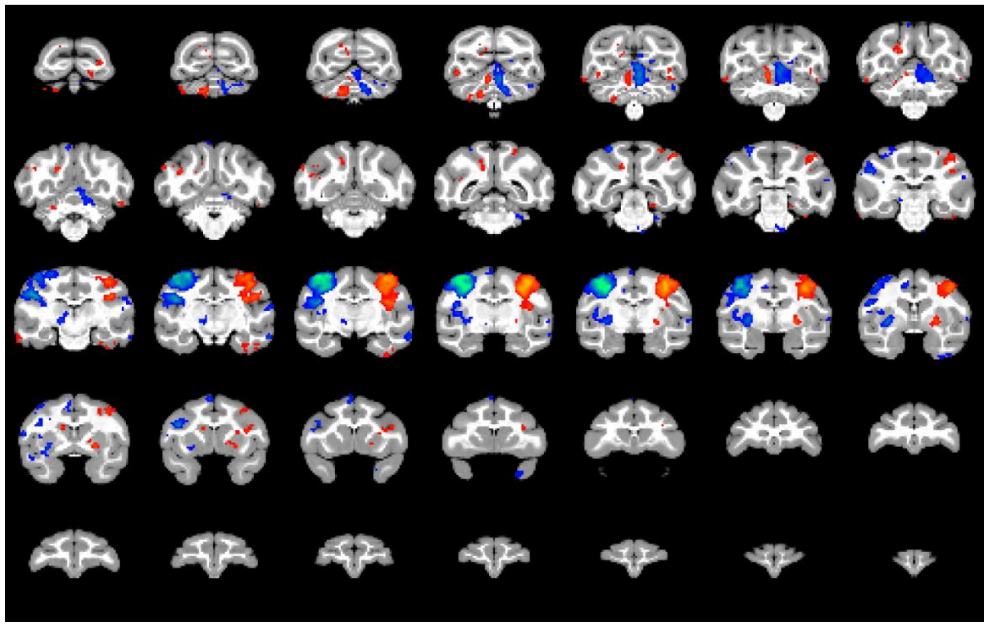


Figure S3.4: Overview of fMRI activity of M1 for Rd-2. T-score map of M1 for Rd-1 overlaid on coronal slices (top-left: caudal to bottom-right: rostral) in the D99 template space as a result of individual subjects' second level GLM analysis for contrast (color-A vs B) and for a total number of 118 runs (uncorrected level, $P < 0.001$; cluster size: 15 voxels).

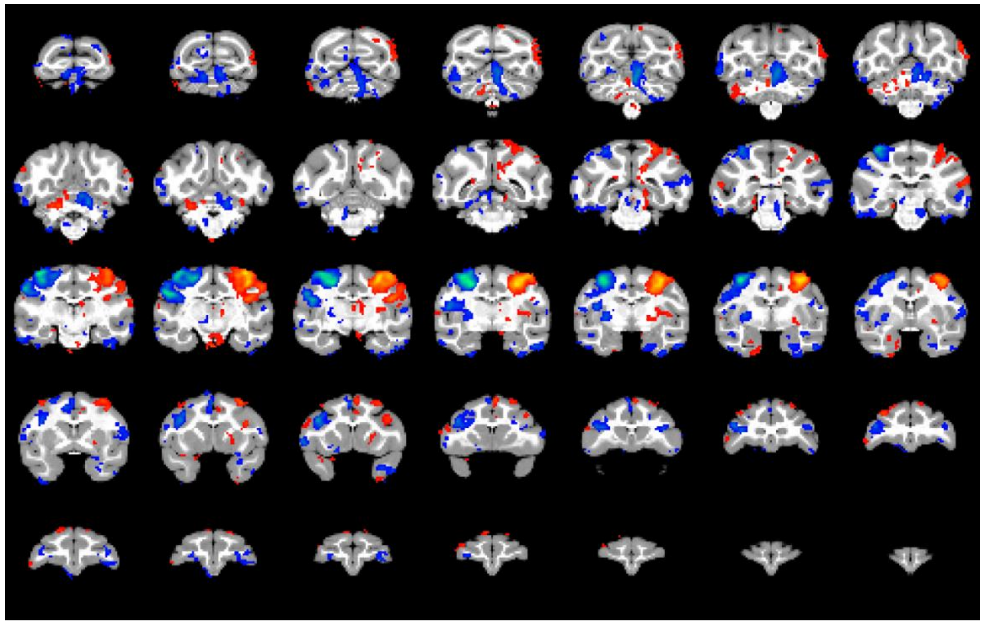


Figure S3.5: Overview of fMRI activity of M2 for Rd-1. T-score map of M1 for round-1 overlaid on coronal slices (top-left: caudal to bottom-right: rostral) in the D99 template space as a result of individual subjects' second level GLM analysis for contrast (color-A vs B) and for a total number of 115 runs (uncorrected level, $P < 0.001$; cluster size: 15 voxels).

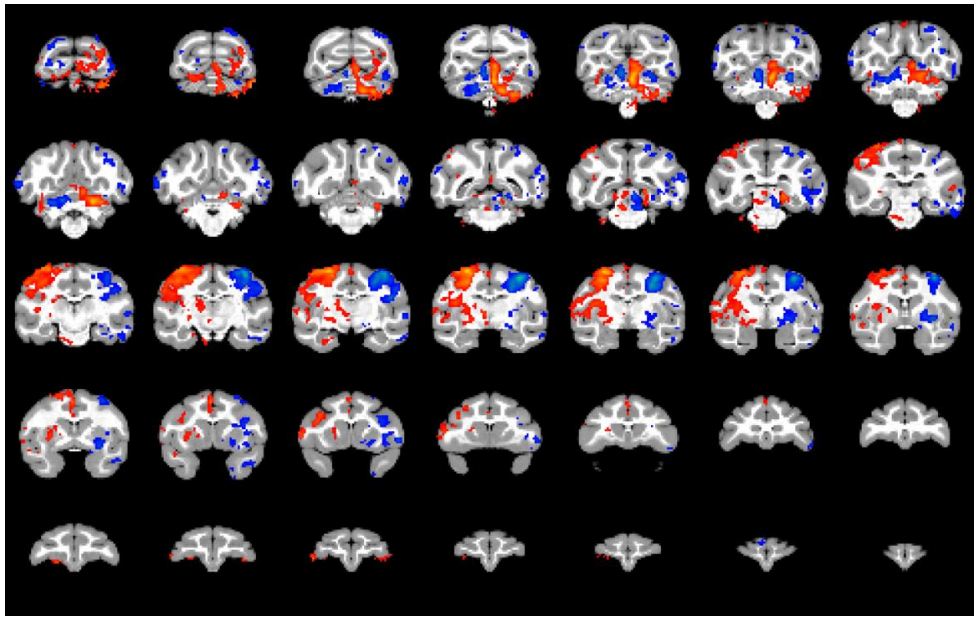


Figure S3.6: Overview of fMRI activity of M2 for Rd-2. T-score map of M1 for round-1 overlaid on coronal slices (top-left: caudal to bottom-right: rostral) in the D99 template space as a result of individual subjects' second level GLM analysis for contrast (color-A vs B) and for a total number of 84 runs (uncorrected level, $P < 0.001$; cluster size: 15 voxels).

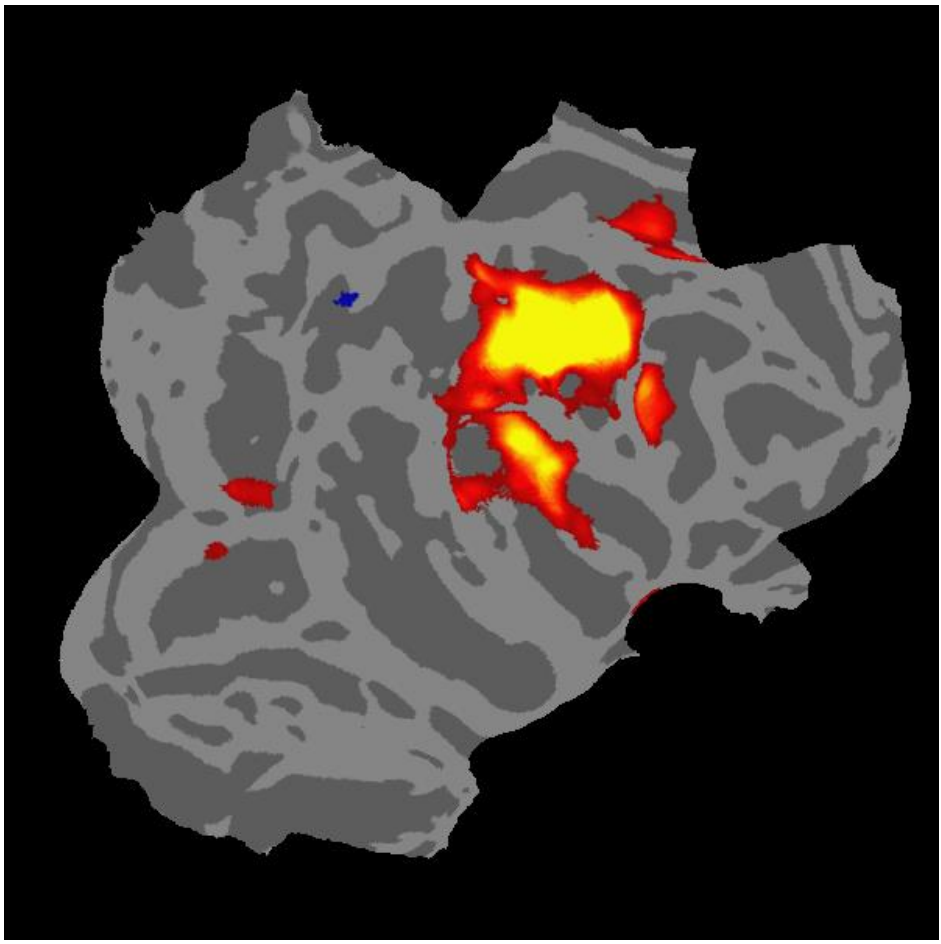


Figure S3.7: Interaction plot between rounds and hemispheres of M1. T-score values of the interaction factor between round and hemisphere as a result of LM analysis on total 220 (Rd-1 102, Rd-2 118) number of runs (uncorrected level, P < 0.001; cluster size, 30 voxels) overlaid onto the right hemisphere cortical flatmap in the D99 template space.

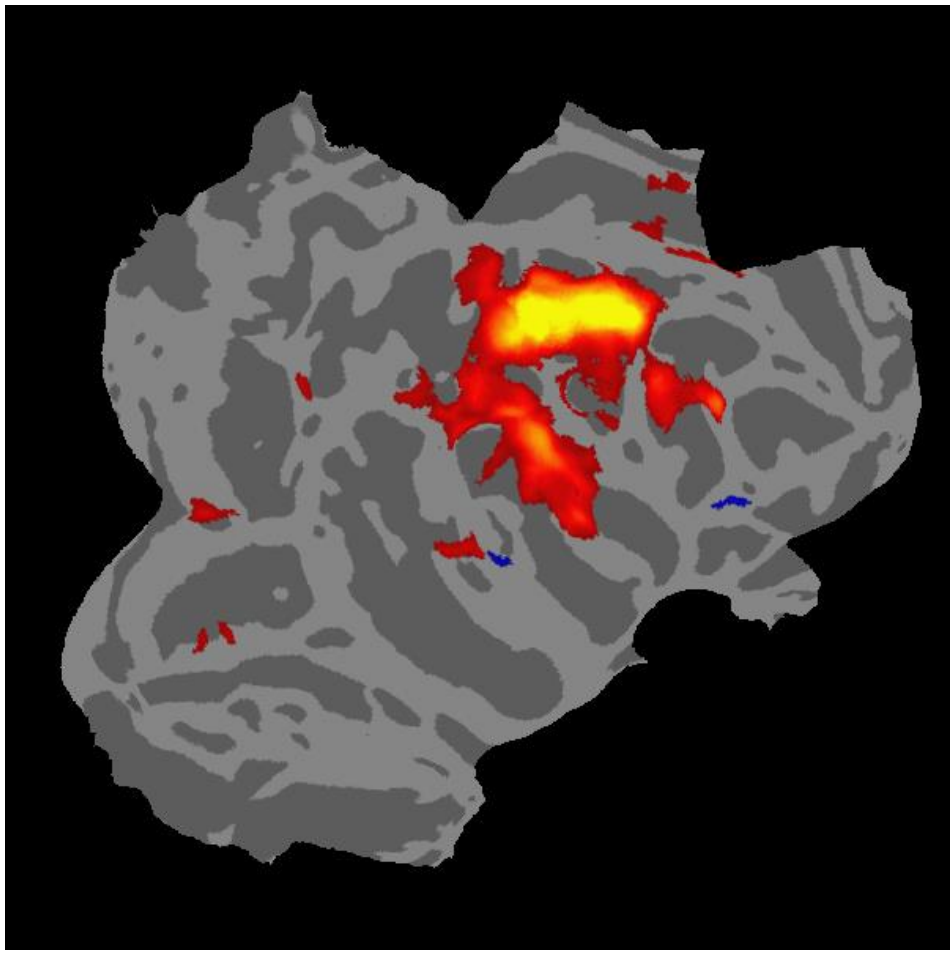


Figure S3.8: Interaction plot between rounds and hemispheres of M2. T-score values of the interaction factor between round and hemisphere as a result of LM analysis on total 199 (Rd-1 115, Rd-2 84) number of runs (uncorrected level, $P < 0.001$; cluster size, 30 voxels) overlaid onto the right hemisphere cortical flatmap in the D99 template space.

3.6 STAR METHODS

KEY RESOURCE TABLE

REAGENT or RESOURCE	SOURCE	IDENTIFIER
Chemicals, Peptides, and Recombinant Proteins		
Molday ION	BioPAL Inc.; Worcester, USA	http://www.biopal.com/molday-ion.htm
Deposited Data		
Functional and structural MRI data, behavioural data	Muhammad Zubair, Wim Vanduffel	Data upload in progress
Experimental Models: Organisms/Strain		
Rhesus macaque *(Macaca mulatta)*	Biomedical Primate Research Centre (BPRC), the Netherlands	http://www.bprc.nl/en
Software and Algorithms		
MATLAB 2017a	MathWorks	RRID: SCR_001622
SPM 12	SPM, University College London, UK	RRID: SCR_007037
FSL		
ANTS – Advanced Normalization ToolS	ANTS, University of Pennsylvania, USA	RRID: SCR_004757
AFNI – Analysis of Functional Images	AFNI, NIMH, USA	RRID: SCR_005927
JIP	JIP Analysis Toolkit	RRID: SCR_009588
GLMdenoise	NITRC, USA	RRID: SCR_014116
Other		
Eye Tracking Device	ISCAN Inc.	http://iscaninc.com

Contact for Reagent and Resource Sharing

Further information and requests for resources and reagents should be directed to and will be fulfilled by the Lead Contact, Wim Vanduffel (wvanduffel@mgh.harvard.edu).

To know how to wonder and question is the first step of the mind toward discovery.

-Louis Pasteur (1822 – 1895 CE)

CHAPTER IV: Discussion

The dopaminergic neurotransmitter system plays a critical role in a wide variety of reward-related processes and is also involved in adult cortical plasticity. In order to increase our understanding of the role of the DA system in the aforementioned processes, we first need to understand its connectome: to which regions of the brain are the dopaminergic nuclei connected? This thesis investigated the whole brain anatomical connections of the ventral midbrain dopamine neurons. Apart from exploring the VTA-DA connectome, in an independent study, we investigated the possible contributions of somatomotor signals on the representation of visual stimuli in early visual areas. Thus, both studies relate to associative learning, the first one looks at the anatomy of the major neuromodulatory system involved, the second one looks at changes in neural representation that occur with associative learning.

In the following section, I will briefly summarize the results of our studies and compare them in the context of previous research. Finally, I will discuss the limitations of our study, what the open questions are and provide future work perspectives.

4.1 Ventral midbrain dopaminergic efferent projections

4.1.1 Significant findings relative to previous studies

In our study, we targeted the VTA with viral vector injections in three macaque monkeys. As a precise and confined injection targeting this tiny deep brain structure (VTA) was challenging, the results were interpreted by categorizing the subjects into two groups based on the injection center and vector spread (M1 and M2 together, and M3 separately). We observed clear differences in the projection patterns across subjects, likely due to minor unintended variations in injection site and vector spread. The major differences found in the efferent projections across our subjects in light of past studies will be summarized in the following section.

We found brain wide heterogenous projections from the ventral midbrain. In general, prefrontal cortex received moderate innervations from the ventral midbrain in M1 and M2, yet dense rather patchy connections in M3. These moderate-to-strong efferent projections in frontal areas resonate with results from previous dopaminergic innervation studies, mainly focusing on frontal cortex in NHPs (Williams and Goldman-Rakic, 1998). A striking difference across our subjects was predominantly observed in somatosensory regions (dense innervations in M1

and M2 while weak in M3), which was interpreted as a result of the inclusion (for M1 and M2) and exclusion (for M3) of parts of the SNc in our injection site. In general, the occipito-parietal cortex was weakly innervated in all subjects, while temporal cortex received moderate projections. Our results showing frontal and temporal areas receiving moderate to strong innervations are in-line with the previous findings in NHPs (Berger et al., 1991, Berger et al., 1988), but in stark contrast with findings in rodents (Berger et al., 1991).

Subcortically, major differences across subjects were found in the basal ganglia. Connection strength in M1 and M2 was nearly the same (darkly expressed vector in the striatum), contrary to M3 (weak to no expressed striatum) likely due to the inclusion and exclusion of SNc in the injection target, respectively. The results (in M1 and M2) coincide with a study in NHP (Lynd-Balta and Haber, 1994) showing that DA neurons from dorsolateral SNc project mainly to the dorsal striatum. The same study shows that projections to the ventral striatum mainly originate in ventromedial SNc and VTA. However, in M3 the vector spread in parts of the rostral VTA and partially also in the medial thalamus, yet excluding the SNc, which explains the sparse projections observed in the ventral striatum. We interpret the major differences of projections in the striatum as a result of the inclusion or exclusion of the SNc. In rodents, the same trend was

reported, where the more lateral parts of the SNc projects to striatal targets (caudate, putamen), whereas the medial VTA projects more to the NAc and the forebrain (Gerfen, 1985, Poulin et al., 2018, Ikemoto, 2007). Recalling, the major differences (cortically and subcortically) in efferent projections across our subjects, it is quite evident that the connectivity profile depends on the precise target and the vector spread.

In brief, the results of our study show that the efferent projections from the lateral portion of the midbrain (which includes SNc) project to the somatomotor regions and the dorsal striatum, whereas the medial midbrain (which excludes SNc but includes part of the medial thalamus) strongly innervates the frontal and temporal regions.

It is important to keep in mind that we cannot be conclusive about the dopaminergic nature of these efferent projections since we used a non-cell type-specific viral vector. Yet, they should not be considered as purely non-dopaminergic, as we validated the targeting of our viral vector for DA neurons by double staining (higher than 75% for M1 and M2, 37% for M3). Although viable cell type-specific promoters have been successfully used in NHP studies (Stauffer et al., 2016, Ruiz et al., 2013, De et al., 2020), with known compromises on their efficiency and specificity (Lohani et al., 2017, Lohani et al., 2018),

technical barriers in the development of such cell type-specific viral vectors exists (see **section 4.1.3**). The above-mentioned differences in double-stained neurons across monkeys (M1 and M2, versus M3) could be another reason for different efferent projection profiles. In theory, the higher the number of double stained neurons (FP^+ and TH^+) the denser would be the projections that could be visualized and vice versa. The relatively low percentage of double stained neurons in M3 could be one of the explanations of observing weak projections in the basal ganglia and sensorimotor areas in M3 compared to the other two subjects. However, in all subjects we used the same generic non-cell type-specific promoter (CAG) which drives high level of gene expression (Alexopoulou et al., 2008). In the following section, we will offer some possible reasons for the difference of double-stained neurons.

A higher dose of viral vector should result in more neurons being transduced. In fact, the total amount of viral vector injected in M3 (3.5 µL in total) is slightly higher than in M1 (3 µL) and M2 (1.5 µL). However, our preliminary data also showed that high-volume injections may cause more inflammation (unpublished data), confirming earlier studies (Kajiwara et al., 1997). In chronological order of the experiments, we injected M3, M2 and M1. In M3, we still observed some local tissue damage. To reduce this, we also used a different serotype, AAV2.1, in our last

subject (M1) which appeared to be less inflammatory. In M3, we found lower percentages of double stained neurons but at the same time very dense projections in the DPFC, VLPFC and temporal cortical areas compared to the other two subjects. In conclusion, we do not believe that major technical issues related to the vector expression in this animal can explain the low percentage of double stained neurons.

After performing the immuno-staining of neurons in the VTA we subsequently performed double IHC staining for the axonal terminals in the cortex, to investigate whether these projections are dopaminergic. However, we rarely found double stained fibers in the cortex. Moreover, contrary to our expectation, we barely found double labeled axonal terminals in the striatum. Although, in NHPs, the transport of viral vector within other deep brain structures (i.e. GP, TH, SN) from the injected site (Pu) has been shown (Hadaczek et al., 2006). A possible explanation for our negative results may be purely technical: it is very challenging to detect anti-TH immune-stained signals because of downregulated TH synthesis after using AAV vectors (Albert et al., 2019).It has been reported that for successful manipulation of cortical cells, the transduction patterns of viral vector systems are dependent on serotype, target area and the promoter sequence (Watakabe et al., 2015, Gerits et al., 2015, Rabinowitz et al., 2002). Possibly, this might be also the case with the

transduction of midbrain neurons, as we were able to detect rare double immune-stained axonal terminals in cortical areas and subcortical structures in M1 (which was injected with serotype AAV2.1). In contrast, we could not find any double stained axonal fibers in the other two subjects (injected with serotype, AAV-DJ). In conclusion, choosing the right serotype is one of the key steps to achieve cell-type specific transduction.

4.1.2 Linking DA anatomical and effective connectivity studies

In this section, I will try to relate and compare results from previous studies from our laboratory focusing on VTA effective connectivity with the anatomical tract tracing study. In our lab, we measured the effective connectivity by combing VTA-EM with fMRI recordings. Stimulation-induced fMRI activations were observed across many cortical regions including PFC, OFC, ACC, intraparietal, somatomotor and insula regions (Arsenault et al., 2014). In a follow-up study, we found that stimulation-induced fMRI activity by VTA-EM is dependent on the stimulation frequency (Murris et al., 2020). In EM studies, it is difficult to define the exact extent of the stimulated brain region, hence other areas in close neighborhood of the VTA may have been stimulated. Moreover, VTA-EM is a non-cell type specific technique, so non-dopaminergic neurons (i.e., glutamatergic and GABAergic) that also reside within the VTA (see **Table 1.3**) are co-

activated during electrical stimulation. Although, our study is also non-cell type-specific, however, by validating our viral vector efficacy for dopamine neurons we go one step ahead. The main concept behind the VTA-DA connectome investigation was to glean better insight into this network to overcome the shortcomings (precise location of stimulation, frequency dependent network activity etc.) we faced in EM studies. In **Chapter 2**, we discussed the physical wiring of the dopaminergic neurons from the VTA (in particular) and ventral midbrain (in general).

The comparison of the midbrain DA anatomical connectivity with the effective connectivity results reveals similarities as well as differences. The major common cortical (includes PFC, OFC, ACC, somatomotor, intraparietal areas, gustatory cortex, insula) and subcortical areas (dorsal striatum, parts of thalamus) identified in the VTA-EM study (Arsenault et al., 2014), also showed dense projections in the tracing study, particularly in subjects M1 and M2. However, when using intermediate VTA-EM frequencies (Murris et al., 2020), activity in some parts of prefrontal and temporal cortex, OFC, posterior parietal and visual areas were observed, which are comparable to the anatomical connectivity results from subject M3. As mentioned earlier, the efferent connectivity differences (between M1 and M2 versus M3) may be explained by small difference in the (precise) injection site

and vector spread. It is tempting to speculate that differences in fMRI activated regions are due to the precise positioning of the chronic electrodes or (unavoidable) triggering of non-dopaminergic (glutamatergic, GABAergic) neurons. Alternatively, they may be caused by diverse functional properties of DA neurons at different locations within the VTA (and SNc) (Matsumoto and Hikosaka, 2009).

Functional effects (measured using fMRI) as a result of artificial perturbation (EM) of an area is dependent on multiple stimulation parameters i.e. frequency (Murris et al., 2020, Kim et al., 2010), amplitude (Backes et al., 2000) and pulse width (Camp et al., 2006). As mentioned earlier, our lab has shown that by varying the external stimulation frequency during VTA-EM the corresponding global functional effects can change (Murris et al., 2020). If we assume that these global functional effects are mediated by dopaminergic neurons, we can speculate that dopaminergic VTA neurons communicate with different brain areas using different frequency channels (Hong, 2013).

4.1.3 Limitations of the study and future perspectives

We used a non-cell type specific promotor which requires a double staining to confirm that the injected vector successfully transduced dopaminergic neurons. The double staining is a proxy

method to validate that the dopaminergic (TH^+) nature of transduced neurons (FP^+). In the future, we hope that advancements in molecular biology enables the development of a sensitive viral vector with a highly selective cell type-specific (dopaminergic) promoter. Currently its challenging to fit some cell type-specific gene promoters into standard viral backbones due to their large size, for example the entire promoter of TH gene (Kessler et al., 2003). Moreover, a large size is also not desirable as it reduces the efficiency of a vector i.e. transportation rate from the injected site. To overcome this technical obstacle, fragments of cell-type specific gene promoters are usually used but they are often less sensitive (weak staining expressions). Besides, a viral vector which transduces neurons well in one brain area (or species) does not necessarily perform well in other parts of the brain (or other species).

The most usual method of transduction is by injecting the viral constructs, like AAV. For viral vector delivery, we used conventional multiple micro-injections technique (details in **Table S2.1**), in which transduction levels also depends on vector diffusion properties. However, an advanced technique known as convection-enhanced delivery (CED) promises improved transduction levels, as shown for deep brain areas of NHPs (Johnston et al., 2009, Cunningham et al., 2008, Bankiewicz et al.,

2000, Hadaczek et al., 2006). The CED method uses a pressure gradient technique that enhance the spread through brain parenchyma and allows faster injection rates and uniform transduction. Though, the conventional vector delivery method also works by locally applying a pressure differential (but in an uncontrolled way) to drive fluid flow. Conventional injection techniques use multiple micro-injections at different locations and depth within the targeted area also results in rather uniform vector spread, but with more tissue damage due to multiple needle insertions and extractions.

In the last decade, the exponential development of genetically-based techniques in NHPs, i.e. optogenetics, allowed neuroscientists to have millisecond resolution control of cell type-specific neural activity (Han et al., 2009) and makes it possible to steer the neuronal activity with high spatial resolution (Deisseroth, 2015). Moreover, subsequent studies took advantage of optogenetics for manipulating behavior in NHPs (Gerits et al., 2012, Jazayeri et al., 2012, Cavanaugh et al., 2012). Advanced tool development and improvements made it possible to successfully apply the technique even for deep brain regions in NHPs (Tamura et al., 2012). However, optogenetic based NHP techniques still demand developments, e.g. to target specific cell-types, reduce tissue inflammation, increase expression levels of opsins, etc. In the last years, progress has

been made to resolve these problems (Galvan et al., 2017, El-Shamayleh and Horwitz, 2019), with contributions from our own lab (Vancraeyenest et al., 2020, Fabbrini et al., 2019, Gerits et al., 2012). Although we had difficulties in replicating this study, we believe that future advancements it would become the primary choice to manipulate neurons in a cell type-specific manner while observing the consequences of these manipulations with high spatial and temporal resolution.

Another limitation in NHPs studies is the limited number of subjects that can be used, (three in our experiments: **Chapter 2**), because NHPs experiments demand more resources, time, and have more technical barriers due to the underdeveloped tools that are already available for rodent studies. Being fully aware of these constraints, it would be interesting to replicate our study in more subjects whereby also neighboring regions of the VTA are systematically targeted (e.g. SNc, SNr, RRF etc.).

As we know using EM technique, it is not possible to perform this systematic targeting of the neighboring areas. Although we believe, the brain areas activated by VTA-EM (showing either positive or negative fMRI activations) can be mono- or multi-synaptically connected with the VTA. However, the nature of these connections (being dopaminergic or not) still remains

unanswered. Given that we did not employ cell-type specific viral vectors, our findings cannot address that question either.

In the future, advancement in the tools could be used to explore different DA nuclei that are distributed in the mesencephalon of NHPs (i.e., RRF, ventral SN, dorsal SN and VTA, see **Table 1.3**). Such studies could provide in-depth knowledge of their respective anatomical connections and how they functionally interact with target sites. Moreover, advancements in technologies, like optogenetics, chemogenetics, calcium imaging etc., would allow to investigate cell type-specific properties of the networks linked with different mesencephalic subregions. We hope that our study on the ventral midbrain's dopaminergic system will provide directions for future studies to gain an even more refined understanding of its brain-wide anatomical and functional connectivity. A better insight in the properties of these DA subgroup neurons may also help to improve our understanding of several neuropsychiatric disorders, including schizophrenia, Parkinson's disease (PD) and addiction, which results from a dysfunctional DA circuitry.

Although our knowledge is still rather limited, we know that degeneration of mesencephalic (DA) neurons (in VTA) and projections to the limbic system and prefrontal cortex may be linked to psychiatric disease like schizophrenia (Carlsson et al.,

2001). However, the functional properties of different DA subgroups in dorsal, dorsolateral and ventromedial VTA are not yet fully explored. It is well established that selective degeneration of DA neurons in the SNc plays an important role in PD (Schallert and Tillerson, 2000, Liu et al., 2017, Vernier et al., 2004, Kish et al., 1988). Besides motor impairment, Parkinson's patients eventually develop impairments in visuospatial functions, memory, attention and executive functions (Zhou et al., 2012, Kudlicka et al., 2011, Wu et al., 2012). Even in early stages of the disease, social behavioral disorders and cognitive impairments were reported (Anderson et al., 2013, Dubois and Pillon, 1996). Possibly, this variety of symptoms may also be linked to different connectional and functional properties of DA neurons in dorsolateral or ventromedial sectors of the SNc (Matsumoto and Hikosaka, 2009). Thus, it is essential to explore the connections and functions of these DA subgroups (within VTA and SNc), in order to understand their respective roles in the normal and pathological brain. Identifying these properties may contribute in developing therapeutic strategies battling neuropsychiatric diseases associated with the dopaminergic system.

4.1.4 Midbrain dopaminergic neurons shaping motor activity

There is increasing evidence that the neuromodulator DA plays a key role in motor related tasks and are involved in movement disorders (notably PD) (Kordower et al., 2013, Shetty et al., 2019). Movement control is accomplished by complex interactions among various cell groups, one is located in SN which communicates with the basal ganglia by releasing DA. In the nigrostriatal pathways (see **Figure 1.1**), DA neurons project to the dorsal striatum and play a primary role in motor skills and their degeneration causes a dysregulation of motor control, a hallmark of PD. Thus, the mesencephalic DA system plays a critical part in generating, shaping and executing motor action sequences (Tanji, 2001, Jin and Costa, 2010, Jin et al., 2014, Hosp and Luft, 2013). In our study, IHC results have shown dense efferent ventral midbrain projections, in particular from the SNc to somatomotor areas, which supports ample previous evidence that this ventral midbrain region plays a significant role in motor action.

4.1.5 Parkinson's Disease and its treatment

The role of DA in motor learning comes to some extent from patient studies with PD, a movement disorder due to the degeneration of mesencephalic DA neurons (Kordower et al.,

2013). Initial symptoms of PD are tremor (shaking body parts), akinesia (loss of voluntary movement), bradykinesia (slowness of movement) and impairment across a range of motor learning tasks (Olson et al., 2019). In PD, neurons in SN progressively degenerates which results in less DA for neurotransmission. To study PD, laboratory animals should feature this typical DA loss associated to PD related symptoms.

Animal models of PD provided indispensable insights into the mechanisms underlying PD, and in possible treatments. Investigation in NHPs modeled for PD, helped out in the understanding of underlying mechanisms associated to PD in humans. The 1-methyl-4-phenyl-1,2,3,6-tetrahydropyridine (MPTP)-treated monkey has been recognized as a gold standard PD model (Porras et al., 2012, Dauer and Przedborski, 2003), as the biochemical and cellular changes that occur following administration of MPTP are remarkably similar to those seen in PD. In both humans and monkeys, MPTP-induced neurodegeneration is a result of damage to the nigrostriatal dopaminergic pathways comparable to damage observed in PD patients. In our study, we found dense efferent projections to the dorsal striatum and somatomotor regions as a result of vector spread to the SNc (in M1 and M2), which depicts the involvement of SN in motor control. A histological evidence in MPTP monkey model supports our interpretation of results by

showing declined number of TH expressed neurons in the SNc in parallel with increased severity of motor deficits. Thus, a close correlation between cell loss in the SNc and striatal dopaminergic depletion exists (Blesa et al., 2012).

Different approaches in the treatment of PD have been introduced by neuroscientists. An invasive methodology, thalamotomy in treating the characteristic tremor of PD almost disappeared from neurological practices due to the associated irreversible complications, and the fading effects with time. As an alternative to this lesion-based surgery, deep brain stimulation (DBS) was introduced and showed a dramatic and stable improvement in animal models and humans with motor control symptoms of PD. Initially, high frequency stimulation in the basal ganglia mimics the effects of lesions to treat PD movement disorders. With the advantage of reversibility, DBS became a very potent tool for functional neurosurgery (Benabid et al., 2003). High frequency stimulation has shown effective results and was extended from the thalamus to STN. Chronic high frequency STN-DBS demonstrated profound clinical benefits in the treatment of motor-related symptoms of PD (Benabid, 2003, Benabid et al., 2009). Importance of screening PD patients to shortlist for DBS surgery is crucial. PD patients with persistent motor disability (Jarraya et al., 2003) and with ongoing mild

cognitive deterioration (Welter et al., 2002) are less considered for subthalamic stimulation treatments.

STN-DBS improves hyperdopaminergic behaviors like impulse control disorders and medication-related complications like dyskinesia (Santin et al., 2021). However, different side effects have been reported in patients, like depression, mood changes (Schneider et al., 2003, Berney et al., 2002, Bejjani et al., 2002), laughter (Krack et al., 2001) and suicidal ideas (Bejjani et al., 1999). These might possibly be explained due to the recruitment of neighboring structures by using high voltages or partially mis-located electrodes. Impact of DBS on behavior and involvement of limbic structures (Schroeder et al., 2002) needs to be thoroughly investigated (Mayberg and Lozano, 2002).

DBS is a complex and risky procedure. A simple and relatively safe alternative approach was demonstrated in MPTP-treated baboons by chronically stimulating (at high frequency) the motor cortex, showing significant alleviation of Parkinson symptoms (Drouot et al., 2004). Efficiency of motor cortex stimulation was apparent, showing improved akinesia and bradykinesia.

A non-invasive treatment is the oral administration of L-dopa which modulates neuronal firing in the striatum by increasing DA concentrations. This very simple effective therapeutic strategy to

treat PD related motor symptoms, however, can lead to complications that include involuntary movements, dyskinesia and cognitive impairments. Off-target effects of L-dopa throughout the dopaminergic system can account for other side effects as well (Fénelon et al., 2000).

Highly interestingly, a multigene therapy protocol was introduced, by injecting a lentiviral vector encoding critical genes for DA synthesis into the striatum of MPTP-treated macaque monkeys which corrected motor deficits without complications of dyskinesia (Jarraya et al., 2009). This injected lentiviral vector comprises critical genes (TH, aromatic L-amino acid decarboxylase and guanosine 5'-triphosphate cylcohydrolase 1) for DA synthesis. Effects of this injected gene-carrying vector were maintained without the complications of motor fluctuations observed in L-dopa-treated patients. Another gene therapy-based study shows clinical improvements in the therapeutic window of L-dopa in MPTP-lesioned NHPs over many years. It shows, by injecting the lesioned striatum with AAV2-human L-amino acid decarboxylase (hAADC) that the activity of AADC restores which results in normalized responses to levodopa (Hadaczek et al., 2010). Immunohistochemical analysis after long-term (8 years of) experimental durations revealed no sign of attenuation of AADC expression and neuroinflammation within the transduced region. The study

suggested the stability of the transferred gene and efficacy of transduction rate by using AAV2 which was also apparent in our study in subject M1 (**Chapter 2**).

4.2 Effector-induced modulations in the early visual processing

Training of animals to detect or discriminate specific sensory stimuli or stimulus features, results in changes of stimulus representations, as observed in rodents (Rutkowski and Weinberger, 2005, Wiest et al., 2010, Goltstein et al., 2013, Gdalyahu et al., 2012, Rainer et al., 2004) and NHPs (Schoups et al., 2001, Yang and Maunsell, 2004, Blake et al., 2006, Yan et al., 2014, Li et al., 2008, Ghose et al., 2002). In primates, the visual system has been studied by focusing mainly on its role in perception (Rainer et al., 2004, Kourtzi et al., 2005, Furmanski et al., 2004) and cognition (Vuilleumier and Driver, 2007, Reynolds and Chelazzi, 2004). However, modulations of stimulus representations also depend on non-retinal inputs to the visual system. In both rodents and primates, studies have shown the involvement of non-retinal inputs (attention, reward, emotion, value, context, audio, oculomotor, locomotion, saccadic eye-movement etc.) in the visual processing (see **section 1.7**).

In NHPs, the involvement of non-retinal inputs is not fully explored. For example, our current knowledge about the involvement of other modalities (e.g. somatomotor) in shaping the visual cortical activity is limited. Therefore, in an event-related fMRI experiment **(Chapter 3)**, subjects were trained to associate a visual stimulus with a motor response, with the goal to identify possible neuronal modulations in the visual areas caused by the associated effector.

4.2.1 Significant findings in light with the previous work

In the following section, we will explain our major findings and discuss how they relate to the existing studies and fill (some of) the current gaps in our knowledge by explaining neuronal modulations in the occipital cortex by merely associating an effector to a visual stimulus.

We trained two subjects (macaque monkeys) to perform a simple visual color discrimination task by presenting a visual cue in the visual peripheral area of the subject. The subjects were trained to answer with the corresponding hand response associated with the stimulus feature (color) by covertly attending the visual stimulus. We observe modulations (enhancement) in

the visual stimulus representation in the early visual areas, summarized below.

In general, as expected we observed, strong positive and negative fMRI activity in the contralateral and ipsilateral primary motor, premotor, primary and secondary somatosensory areas, and parts of basal ganglia relative to the hand response, respectively. The region to most of our interest were the visual areas (V1, V2 and V3), interestingly, we found active contralateral to the hand response. However, the cerebellum was found showing a complete opposite trend (strong positive and negative activations contralateral and ipsilateral to the associated hand, respectively) compared to the cerebral cortex.

Our results were quite similar as reported in humans, where unilateral motor actions produce contralateral activations in sensorimotor cortex and subcortical areas together with ipsilateral deactivations in the sensorimotor and subcortical areas. However, in the cerebellum, this pattern of activations is totally opposite (Hamzei et al., 2002, Allison et al., 2000). Interestingly, it has been reported, that duration of the motor response affects the amplitude of the (negative and positive) fMRI activity (Newton et al., 2005). A short duration motor action results in less ipsilateral deactivation in the primary motor area compared to a long duration motor action. Moreover, the study

also claims the ipsilateral negative activation amplify if the subject uses the dominant hand for action. The fMRI activity trend that we observed in our experiments (for each subject in both rounds and the group) coincides with the above-mentioned studies bilaterally for sensorimotor areas, basal ganglia and the cerebellum. This supports the resultant fMRI (positive and negative) activity we observed, due to the motor response in different parts of the brain.

As expected, we also observe activity in the presupplementary motor (pre-SMA) and premotor areas. Initially, in NHP studies, pre-SMA was associated to sequential movement learning (Shima and Tanji, 1998, Nakamura et al., 1999). In humans, the same function of pre-SMA was reported (Hikosaka et al., 1996). Later the same group presented a modified view of the pre-SMA and suggested its involvement in visuomotor associations (Sakai et al., 1999). Moreover, the pre-SMA response was observed to be effector-independent, as the area was found active while performing an oculomotor (Merriam et al., 2001, Kawashima et al., 1998) or simply a manual motor task (Kurata et al., 2000, Nachev et al., 2007). These studies also support our findings of activity in the pre-SMA region, independent of the involved-effector (right- or left-hand).

In the last two decades, the motor system has been studied beyond its conventional role in simple movements (Rizzolatti and Luppino, 2001) to action understanding (Lingnau and Petris, 2013), imitation learning (Nelissen et al., 2005), action generation etc. Our experiment fMRI results shows activations in premotor area (F5), parietal area AIP, primary- and secondary-somatosensory areas (SI, SII) and motor area (F1), which were reported to respond significantly while performing a grasping task (Nelissen and Vanduffel, 2011). Although, our experiment does not entirely depict the grasping task as the subject has to place the hand above a button throughout the trial, rather transporting the arm and the holding the key. We suspect subject's gripping behavior before pressing the key activates the same circuitry. Other possible explanations for the activity of premotor area F5 and area AIP is the activation of visuomotor neurons that use visual and other sensory input to plan an action. Moreover, the task required high level cognitive functions, which also contributes to premotor activity (Brass and Von Cramon, 2002, Ridderinkhof et al., 2004).

We also predicted activity in parts of basal ganglia (including: putamen, caudate nucleus, globus pallidus) which follow the same fMRI activity trends (positive and negative activations contralateral and ipsilateral to the hand response, respectively) as we found for somatomotor region. The involvement of the

basal ganglia was not surprising to us, as it is known to be involved in motor control tasks (Doya, 2000, Groenewegen, 2003, Takakusaki et al., 2004).

Cerebellar activations have been documented in studies on motor control (Kelly and Strick, 2003, Manto et al., 2012), saccadic eye movements (Ohki et al., 2009), smooth eye movements (Hiramatsu et al., 2008), non-motor tasks, including but not restricted to sensory and cognitive processing (Gao et al., 1996), visual attention (Allen et al., 1997), unsupervised learning (Doya, 2000), and tracking of the movements (Paulin, 1993).

The involvement of non-retinal inputs on visual processing has already been discussed. But, the question is how a non-retinal input (motor action) associated with a retinal stimulus brought up neuronal modulations in the visual system? Though similar findings have been reported in the past (Mirabella et al., 2007), they were interpreted as a result of stimulus categorization, thereby neglecting the associated effector involvement. Contrarily, our study, suggest that these modulations are most likely a result of feedback somatomotor signals induced by a learnt association between a visual stimulus and the effector. Our experimental design excludes the involvement of other possible non-retinal inputs that can modulate neuronal activity in early visual cortex such as selective spatial attention (Hayden

and Gallant, 2005, Sundberg et al., 2009), and selective featural attention (Mirabella et al., 2007, McAdams and Maunsell, 1999). To avoid spatial and feature-based attention, the visual cue was presented at the same location (along the vertical meridian) and was covertly attended by the subject. Though, the color cues associated to different hand responses were very close in the RGB values and associated to different hand response, we balanced the visual feature and the effector (hand response) across rounds and subjects.

The visual system exists of (at least) two visual streams, both having specialized functions: an occipito-temporal 'ventral stream' aids perception by attaching meaning to objects and events and tends to be 'object-centered'. An occipito-parietal 'dorsal stream' is dedicated to the visual control of skilled actions and tends to be 'viewer-centered'. Cells in the dorsal stream are sensitive to spatial information, while those in the ventral stream are sensitive to object identity (Ungerleider, 1982).

The affordance competition hypothesis suggests that the dorsal visual stream specifies actions in parallel to processing sensory information (Cisek, 2007). Recent neurophysiological studies suggest that target selection and movement preparation are performed in an integrated manner (Cisek, 2007, Cisek, 2006, Wang, 2008). The dorsal visual stream is found to have a close

relationship with sensorimotor areas in premotor and parietal cortical areas, which mediate the required sensorimotor transformations necessary for visually guided actions (Goodale and Milner, 1992). This was also supported by studies in patients with damaged posterior parietal cortex (dorsal visual stream), as they were not able to reach correctly towards an object and also fail to posture their hand to reflect the local orientation of the target object (Perenin and Vighetto, 1988). Posterior parietal areas are linked to premotor regions implicated in reaching and grasping movements. Moreover, different networks modulated by motor outputs (fixation, eye movements, reaching, manipulation) in the posterior parietal areas are linked to the corresponding functional areas in premotor cortex. It is believed, that a combination of these networks might be used to perform the desired visuo-motor actions. Visuo-motor control is engaged in situations where rapid responsed to visible targets are required, as in our experiment (**Chapter 3**) where the subject needs to act fast. Our experimental results are in line with the affordance competition hypothesis, showing modulations (enhancement) in the early visual cortical areas as a result of non-visual sensory input involvement due to the associated effector.

4.2.2 Open questions and future work perspectives

In primates, early visual areas are anatomically connected to several parietal and temporal cortical areas (Rockland and Ojima, 2003) and receives non-retinal input signals from higher-order cortical areas. To some extent, these direct connections to early visual areas can be considered as feedback connections. These can play a significant functional role when subjects learn to associate a stimulus feature (i.e. spatial location, shape, size, color etc.) with a behavioral response (saccade, motor action etc.). However, we do not fully know how these feedback signals interact with the visual signals at single cell level, nor which specific pathways that are involved. In the future, exploring the cellular-level mechanism is necessary to fully understand the (extent of) contributions by somatomotor feedback on early visual processing.

4.3 General conclusion

Anatomically the ventral midbrain DA system is heterogeneously connected with all cortical lobes. Frontal and temporal regions are strongly innervated by the medial midbrain (mainly VTA), the lateral midbrain (mainly SNc) densely projects to the parietal areas and dorsal striatum, whereas the occipito-parietal cortex overall receives very weak projections from the ventral midbrain. The current and previous work in our lab increased our

knowledge about the connectome of the ventral midbrain and further supports the evidence for its role in reward processing, learning and perception. We also conclude, that visual processing in early visual cortical areas can be modulated by somatomotor signals, likely via feedback input from somatomotor areas of the brain.

References

ALBERT, K., VOUTILAINEN, M. H., DOMANSKYI, A., PIEPPONEN, T. P., AHOLA, S., TUOMINEN, R. K., RICHIE, C., HARVEY, B. K. & AIRAVAARA, M. 2019. Downregulation of tyrosine hydroxylase phenotype after AAV injection above substantia nigra: Caution in experimental models of Parkinson's disease. *Journal of neuroscience research,* 97**,** 346-361.

ALEXOPOULOU, A. N., COUCHMAN, J. R. & WHITEFORD, J. R. 2008. The CMV early enhancer/chicken β actin (CAG) promoter can be used to drive transgene expression during the differentiation of murine embryonic stem cells into vascular progenitors. *BMC cell biology,* 9**,** 2.

ALLEN, G., BUXTON, R. B., WONG, E. C. & COURCHESNE, E. 1997. Attentional activation of the cerebellum independent of motor involvement. *Science,* 275**,** 1940-1943.

ALLISON, J. D., MEADOR, K. J., LORING, D. W., FIGUEROA, R. E. & WRIGHT, J. C. 2000. Functional MRI cerebral activation and deactivation during finger movement. *Neurology,* 54**,** 135-135.

ANDERSON, R. J., SIMPSON, A. C., CHANNON, S., SAMUEL, M. & BROWN, R. G. 2013. Social problem solving, social cognition, and mild cognitive impairment in Parkinson's disease. *Behavioral neuroscience,* 127**,** 184.

ANGELAKI, D. E., GU, Y. & DEANGELIS, G. C. 2009. Multisensory integration: psychophysics, neurophysiology, and computation. *Current opinion in neurobiology,* 19**,** 452-458.

ANGELAKI, D. E., GU, Y. & DEANGELIS, G. C. 2011. Visual and vestibular cue integration for heading perception in extrastriate visual cortex. *The Journal of physiology,* 589**,** 825-833.

ARANSAY, A., RODRÍGUEZ-LÓPEZ, C., GARCÍA-AMADO, M., CLASCÁ, F. & PRENSA, L. 2015. Long-range projection neurons of the mouse ventral tegmental area: a single-cell axon tracing analysis. *Frontiers in neuroanatomy,* 9**,** 59.

ARNSTEN, A. F., CAI, J. X., STEERE, J. C. & GOLDMAN-RAKIC, P. S. 1995. Dopamine D2 receptor mechanisms contribute to age-related cognitive decline: the effects of quinpirole on

memory and motor performance in monkeys. *Journal of Neuroscience,* 15**,** 3429-3439.

ARSENAULT, J. T., RIMA, S., STEMMANN, H. & VANDUFFEL, W. 2014. Role of the primate ventral tegmental area in reinforcement and motivation. *Current Biology,* 24**,** 1347-1353.

ARSENAULT, J. T. & VANDUFFEL, W. 2019. Ventral midbrain stimulation induces perceptual learning and cortical plasticity in primates. *Nature communications,* 10**,** 1-13.

AVANTS, B. B., TUSTISON, N. J., SONG, G., COOK, P. A., KLEIN, A. & GEE, J. C. 2011. A reproducible evaluation of ANTs similarity metric performance in brain image registration. *NeuroImage*.

AYAZ, A., SALEEM, A. B., SCHÖLVINCK, M. L. & CARANDINI, M. 2013. Locomotion controls spatial integration in mouse visual cortex. *Current Biology,* 23**,** 890-894.

BACKES, W. H., MESS, W. H., VAN KRANEN-MASTENBROEK, V. & REULEN, J. P. H. 2000. Somatosensory cortex responses to median nerve stimulation: fMRI effects of current amplitude and selective attention. *Clinical neurophysiology,* 111**,** 1738-1744.

BANKIEWICZ, K. S., EBERLING, J. L., KOHUTNICKA, M., JAGUST, W., PIVIROTTO, P., BRINGAS, J., CUNNINGHAM, J., BUDINGER, T. F. & HARVEY-WHITE, J. 2000. Convection-enhanced delivery of AAV vector in parkinsonian monkeys; in vivo detection of gene expression and restoration of dopaminergic function using pro-drug approach. *Experimental neurology,* 164**,** 2-14.

BECKSTEAD, R. M., DOMESICK, V. B. & NAUTA, W. J. H. 1979. Efferent connections of the substantia nigra and ventral tegmental area in the rat. *Brain research,* 175**,** 191-217.

BEJJANI, B.-P., DAMIER, P., ARNULF, I., THIVARD, L., BONNET, A.-M., DORMONT, D., CORNU, P., PIDOUX, B., SAMSON, Y. & AGID, Y. 1999. Transient acute depression induced by high-frequency deep-brain stimulation. *New England Journal of Medicine,* 340**,** 1476-1480.

BEJJANI, B. P., HOUETO, J. L., HARIZ, M., YELNIK, J., MESNAGE, V., BONNET, A. M., PIDOUX, B., DORMONT, D., CORNU, P. & AGID, Y. 2002. Aggressive behavior induced by intraoperative stimulation in the triangle of Sano. *Neurology,* 59**,** 1425-1427.

BENABID, A.-L., VERCUCIL, L., KRACK, P., POLLAK, P. & BENAZZOUZ, A. 2003. Deep brain stimulation: What does it offer? *Advances in neurology,* 91**,** 293-302.

BENABID, A. L. 2003. Deep brain stimulation for Parkinson's disease. *Current opinion in neurobiology,* 13**,** 696-706.

BENABID, A. L., CHABARDES, S., MITROFANIS, J. & POLLAK, P. 2009. Deep brain stimulation of the subthalamic nucleus for the treatment of Parkinson's disease. *The Lancet Neurology,* 8**,** 67-81.

BENJAMIN, A. V., WAILES-NEWSON, K., MA-WYATT, A., BAKER, D. H. & WADE, A. R. 2018. The effect of locomotion on early visual contrast processing in humans. *Journal of Neuroscience,* 38**,** 3050-3059.

BERGER, B., GASPAR, P. & VERNEY, C. 1991. Dopaminergic innervation of the cerebral cortex: unexpected differences between rodents and primates. *Trends in neurosciences,* 14**,** 21-27.

BERGER, B., TASSIN, J. P., BLANC, G., MOYNE, M. A. & THIERRY, A. M. 1974. Histochemical confirmation for dopaminergic innervation of the rat cerebral cortex after destruction of the noradrenergic ascending pathways. *Brain research,* 81**,** 332-337.

BERGER, B., TROTTIER, S., VERNEY, C., GASPAR, P. & ALVAREZ, C. 1988. Regional and laminar distribution of the dopamine and serotonin innervation in the macaque cerebral cortex: a radioautographic study. *Journal of Comparative Neurology,* 273**,** 99-119.

BERGER, B., VERNEY, C., ALVAREZ, C., VIGNY, A. & HELLE, K. B. 1985a. New dopaminergic terminal fields in the motor, visual (area 18b) and retrosplenial cortex in the young and adult rat. Immunocytochemical and catecholamine histochemical analyses. *Neuroscience,* 15**,** 983-998.

BERGER, B., VERNEY, C., FEBVRET, A., VIGNY, A. & HELLE, K. B. 1985b. Postnatal ontogenesis of the dopaminergic innervation in the rat anterior cingulate cortex (area 24). Immunocytochemical and catecholamine fluorescence histochemical analysis. *Developmental Brain Research,* 21**,** 31-47.

BERNEY, A., VINGERHOETS, F., PERRIN, A., GUEX, P., VILLEMURE, J. G., BURKHARD, P. R., BENKELFAT, C. & GHIKA, J. 2002. Effect on mood of subthalamic DBS for Parkinson's disease A consecutive series of 24 patients. *Neurology,* 59**,** 1427-1429.

BJÖRKLUND, A., DIVAC, I. & LINDVALL, O. 1978. Regional distribution of catecholamines in monkey cerebral cortex, evidence for a

dopaminergic innervation of the primate prefrontal cortex. *Neuroscience letters,* 7**,** 115-119.

BJÖRKLUND, A., LINDVALL, O. & HÖKFELT, T. 1984. Dopamine containing systems in the CNS. Handbook of Chemical Neuroanatomy, Vol. 2. Classical Transmitters in the CNS, Part 1. *:.* Elsevier Science Publishers.

BLAKE, D. T., HEISER, M. A., CAYWOOD, M. & MERZENICH, M. M. 2006. Experience-dependent adult cortical plasticity requires cognitive association between sensation and reward. *Neuron,* 52**,** 371-381.

BLANCHARD, V., RAISMAN-VOZARI, R., VYAS, S., MICHEL, P. P., JAVOY-AGID, F., UHL, G. & AGID, Y. 1994. Differential expression of tyrosine hydroxylase and membrane dopamine transporter genes in subpopulations of dopaminergic neurons of the rat mesencephalon. *Molecular brain research,* 22**,** 29-38.

BLESA, J., PIFL, C., SÁNCHEZ-GONZÁLEZ, M. A., JURI, C., GARCÍA-CABEZAS, M. A., ADÁNEZ, R., IGLESIAS, E., COLLANTES, M., PEÑUELAS, I. & SÁNCHEZ-HERNÁNDEZ, J. J. 2012. The nigrostriatal system in the presymptomatic and symptomatic stages in the MPTP monkey model: a PET, histological and biochemical study. *Neurobiology of disease,* 48**,** 79-91.

BRASS, M. & VON CRAMON, D. Y. 2002. The role of the frontal cortex in task preparation. *Cerebral cortex,* 12**,** 908-914.

BROMBERG-MARTIN, E. S., MATSUMOTO, M. & HIKOSAKA, O. 2010. Dopamine in motivational control: rewarding, aversive, and alerting. *Neuron,* 68**,** 815-834.

BROWN, R. M., CRANE, A. M. & GOLDMAN, P. S. 1979. Regional distribution of monoamines in the cerebral cortex and subcortical structures of the rhesus monkey: concentrations and in vivo synthesis rates. *Brain research,* 168**,** 133-150.

BULLOCK, T., ELLIOTT, J. C., SERENCES, J. T. & GIESBRECHT, B. 2017. Acute exercise modulates feature-selective responses in human cortex. *Journal of cognitive neuroscience,* 29**,** 605-618.

BULMER, D. 1964. The histochemistry of ovarian macrophages in the rat. *Journal of Anatomy,* 98**,** 313.

BURACAS, G. T. & ALBRIGHT, T. D. 2009. Modulation of neuronal responses during covert search for visual feature conjunctions. *Proceedings of the National Academy of Sciences,* 106**,** 16853-16858.

CAMP, N. V., VERHOYE, M. & DER LINDEN, A. V. 2006. Stimulation of the rat somatosensory cortex at different frequencies and pulse widths. *NMR in Biomedicine: An International Journal Devoted to the Development and Application of Magnetic Resonance In Vivo,* 19**,** 10-17.

CAPPE, C. & BARONE, P. 2005. Heteromodal connections supporting multisensory integration at low levels of cortical processing in the monkey. *European Journal of Neuroscience,* 22**,** 2886-2902.

CARLSSON, A., WATERS, N., HOLM-WATERS, S., TEDROFF, J., NILSSON, M. & CARLSSON, M. L. 2001. Interactions between monoamines, glutamate, and GABA in schizophrenia: new evidence. *Annual review of pharmacology and toxicology,* 41**,** 237-260.

CARR, D. B. & SESACK, S. R. 2000. GABA ‐ containing neurons in the rat ventral tegmental area project to the prefrontal cortex. *Synapse,* 38**,** 114-123.

CAVANAUGH, J., MONOSOV, I. E., MCALONAN, K., BERMAN, R., SMITH, M. K., CAO, V., WANG, K. H., BOYDEN, E. S. & WURTZ, R. H. 2012. Optogenetic inactivation modifies monkey visuomotor behavior. *Neuron,* 76**,** 901-907.

CHAMBERLAIN, S. R., MÜLLER, U., BLACKWELL, A. D., CLARK, L., ROBBINS, T. W. & SAHAKIAN, B. J. 2006. Neurochemical modulation of response inhibition and probabilistic learning in humans. *Science,* 311**,** 861-863.

CHELAZZI, L., MILLER, E. K., DUNCAN, J. & DESIMONE, R. 1993. A neural basis for visual search in inferior temporal cortex. *Nature,* 363**,** 345-347.

CHEN, G., KING, J. A., BURGESS, N. & O'KEEFE, J. 2013. How vision and movement combine in the hippocampal place code. *Proceedings of the National Academy of Sciences,* 110**,** 378-383.

CHINTA, S. J. & ANDERSEN, J. K. 2005. Dopaminergic neurons. *The international journal of biochemistry & cell biology,* 37**,** 942-946.

CHUHMA, N., ZHANG, H., MASSON, J., ZHUANG, X., SULZER, D., HEN, R. & RAYPORT, S. 2004. Dopamine neurons mediate a fast excitatory signal via their glutamatergic synapses. *Journal of Neuroscience,* 24**,** 972-981.

CISEK, P. 2006. Integrated neural processes for defining potential actions and deciding between them: a computational model. *Journal of Neuroscience,* 26**,** 9761-9770.

CISEK, P. 2007. Cortical mechanisms of action selection: the affordance competition hypothesis. *Philosophical Transactions of the Royal Society B: Biological Sciences,* 362**,** 1585-1599.

COCCHI, L., TOEPEL, U., DE LUCIA, M., MARTUZZI, R., WOOD, S. J., CARTER, O. & MURRAY, M. M. 2011. Working memory load improves early stages of independent visual processing. *Neuropsychologia,* 49**,** 92-102.

CONNOR, C. E., PREDDIE, D. C., GALLANT, J. L. & VAN ESSEN, D. C. 1997. Spatial attention effects in macaque area V4. *Journal of Neuroscience,* 17**,** 3201-3214.

CONRAD, L. C. A. & PFAFF, D. W. 1976. Autoradiographic tracing of nucleus accumbens efferents in the rat. *Brain research,* 113**,** 589-596.

CORNWALL, J., COOPER, J. D. & PHILLIPSON, O. T. 1990. Afferent and efferent connections of the laterodorsal tegmental nucleus in the rat. *Brain research bulletin,* 25**,** 271-284.

CRAGG, S. J., BAUFRETON, J., XUE, Y., BOLAM, J. P. & BEVAN, M. D. 2004. Synaptic release of dopamine in the subthalamic nucleus. *European Journal of Neuroscience,* 20**,** 1788-1802.

CUNNINGHAM, J., PIVIROTTO, P., BRINGAS, J., SUZUKI, B., VIJAY, S., SANFTNER, L., KITAMURA, M., CHAN, C. & BANKIEWICZ, K. S. 2008. Biodistribution of adeno-associated virus type-2 in nonhuman primates after convection-enhanced delivery to brain. *Molecular Therapy,* 16**,** 1267-1275.

DAHLSTRÖM, A. 1964. Evidence for the existence of monoamine-containing neurons in the central nervous system. *Acta Physiol Scand,* 62**,** 5-55.

DAUER, W. & PRZEDBORSKI, S. 2003. Parkinson's disease: mechanisms and models. *Neuron,* 39**,** 889-909.

DAVIDSSON, M., WANG, G., ALDRIN-KIRK, P., CARDOSO, T., NOLBRANT, S., HARTNOR, M., MUDANNAYAKE, J., PARMAR, M. & BJÖRKLUND, T. 2019. A systematic capsid evolution approach performed in vivo for the design of AAV vectors with tailored properties and tropism. *Proceedings of the National Academy of Sciences,* 116**,** 27053-27062.

DE, A., EL-SHAMAYLEH, Y. & HORWITZ, G. D. 2020. Fast and reversible neural inactivation in macaque cortex by optogenetic stimulation of GABAergic neurons. *Elife,* 9**,** e52658.

DECOT, H. K., NAMBOODIRI, V. M., GAO, W., MCHENRY, J. A., JENNINGS, J. H., LEE, S.-H., KANTAK, P. A., KAO, Y.-C. J., DAS, M. & WITTEN, I. B. 2017. Coordination of brain-wide activity dynamics by dopaminergic neurons. *Neuropsychopharmacology,* 42**,** 615-627.

DEISSEROTH, K. 2015. Optogenetics: 10 years of microbial opsins in neuroscience. *Nature neuroscience,* 18**,** 1213-1225.

DESCARRIES, L., LEMAY, B., DOUCET, G. & BERGER, B. 1987. Regional and laminar density of the dopamine innervation in adult rat cerebral cortex. *Neuroscience,* 21**,** 807-824.

DOYA, K. 2000. Complementary roles of basal ganglia and cerebellum in learning and motor control. *Current opinion in neurobiology,* 10**,** 732-739.

DROUOT, X., OSHINO, S., JARRAYA, B., BESRET, L., KISHIMA, H., REMY, P., DAUGUET, J., LEFAUCHEUR, J. P., DOLLÉ, F. & CONDÉ, F. 2004. Functional recovery in a primate model of Parkinson's disease following motor cortex stimulation. *Neuron,* 44**,** 769-778.

DUBOIS, B. & PILLON, B. 1996. Cognitive deficits in Parkinson's disease. *Journal of neurology,* 244**,** 2-8.

EL-SHAMAYLEH, Y. & HORWITZ, G. D. 2019. Primate optogenetics: Progress and prognosis. *Proceedings of the National Academy of Sciences,* 116**,** 26195-26203.

ERNST, M. O. & BANKS, M. S. 2002. Humans integrate visual and haptic information in a statistically optimal fashion. *Nature,* 415**,** 429-433.

FABBRINI, F., VAN DEN HAUTE, C., DE VITIS, M., BAEKELANDT, V., VANDUFFEL, W. & VOGELS, R. 2019. Probing the mechanisms of repetition suppression in inferior temporal cortex with optogenetics. *Current Biology,* 29**,** 1988-1998.

FADEL, J. & DEUTCH, A. Y. 2002. Anatomical substrates of orexin–dopamine interactions: lateral hypothalamic projections to the ventral tegmental area. *Neuroscience,* 111**,** 379-387.

FALCHIER, A., CLAVAGNIER, S., BARONE, P. & KENNEDY, H. 2002. Anatomical evidence of multimodal integration in primate striate cortex. *Journal of Neuroscience,* 22**,** 5749-5759.

FALLON, J. H., SCHMUED, L. C., WANG, C., MILLER, R. & BANALES, G. 1984. Neurons in the ventral tegmentum have separate populations projecting to telencephalon and inferior olive, are histochemically different, and may receive direct visual input. *Brain research,* 321**,** 332-336.

FELTEN, D. L., LATIES, A. M. & CARPENTER, M. B. 1974. Monoamine - containing cell bodies in the squirrel monkey brain. *American journal of anatomy,* 139**,** 153-165.

FÉNELON, G., MAHIEUX, F., HUON, R. & ZIÉGLER, M. 2000. Hallucinations in Parkinson's disease: prevalence, phenomenology and risk factors. *Brain,* 123**,** 733-745.

FIORILLO, C. D. 2013. Two dimensions of value: dopamine neurons represent reward but not aversiveness. *Science,* 341**,** 546-549.

FIORILLO, C. D., SONG, M. R. & YUN, S. R. 2013. Multiphasic temporal dynamics in responses of midbrain dopamine neurons to appetitive and aversive stimuli. *Journal of Neuroscience,* 33**,** 4710-4725.

FISCHER, B. & BOCH, R. 1981. Enhanced activation of neurons in prelunate cortex before visually guided saccades of trained rhesus monkeys. *Experimental Brain Research,* 44**,** 129-137.

FRANCOIS, C., YELNIK, J., TANDE, D., AGID, Y. & HIRSCH, E. C. 1999. Dopaminergic cell group A8 in the monkey: anatomical organization and projections to the striatum. *Journal of Comparative Neurology,* 414**,** 334-347.

FRANKLE, W. G., LARUELLE, M. & HABER, S. N. 2006. Prefrontal cortical projections to the midbrain in primates: evidence for a sparse connection. *Neuropsychopharmacology,* 31**,** 1627-1636.

FREEDMAN, D. J. & ASSAD, J. A. 2006. Experience-dependent representation of visual categories in parietal cortex. *Nature,* 443**,** 85-88.

FREEDMAN, D. J., RIESENHUBER, M., POGGIO, T. & MILLER, E. K. 2002. Visual categorization and the primate prefrontal cortex: neurophysiology and behavior. *Journal of neurophysiology,* 88**,** 929-941.

FREEDMAN, D. J., RIESENHUBER, M., POGGIO, T. & MILLER, E. K. 2003. A comparison of primate prefrontal and inferior temporal cortices during visual categorization. *Journal of Neuroscience,* 23**,** 5235-5246.

FURMANSKI, C. S., SCHLUPPECK, D. & ENGEL, S. A. 2004. Learning strengthens the response of primary visual cortex to simple patterns. *Current Biology,* 14**,** 573-578.

FUXE, K., HÖKFELT, T., JOHANSSON, O., JONSSON, G., LIDBRINK, P. & LJUNDAHL, Å. 1974. The origin of the dopamine nerve terminals in limbic and frontal cortex. Evidence for meso-cortico dopamine neurons. *Brain research,* 82**,** 349-355.

GALVAN, A., STAUFFER, W. R., ACKER, L., EL-SHAMAYLEH, Y., INOUE, K.-I., OHAYON, S. & SCHMID, M. C. 2017. Nonhuman primate optogenetics: recent advances and future directions. *Journal of Neuroscience,* 37**,** 10894-10903.

GAMO, N. J., WANG, M. & ARNSTEN, A. F. 2010. Methylphenidate and atomoxetine enhance prefrontal function through α2-adrenergic and dopamine D1 receptors. *Journal of the American Academy of Child & Adolescent Psychiatry,* 49**,** 1011-1023.

GAO, J.-H., PARSONS, L. M., BOWER, J. M., XIONG, J., LI, J. & FOX, P. T. 1996. Cerebellum implicated in sensory acquisition and discrimination rather than motor control. *Science,* 272**,** 545-547.

GASBARRI, A., VERNEY, C., INNOCENZI, R., CAMPANA, E. & PACITTI, C. 1994. Mesolimbic dopaminergic neurons innervating the hippocampal formation in the rat: a combined retrograde tracing and immunohistochemical study. *Brain research,* 668**,** 71-79.

GASPAR, P., BERGER, B., FEBVRET, A., VIGNY, A. & HENRY, J. P. 1989. Catecholamine innervation of the human cerebral cortex as revealed by comparative immunohistochemistry of tyrosine hydroxylase and dopamine‐beta‐hydroxylase. *Journal of Comparative Neurology,* 279**,** 249-271.

GASPAR, P., STEPNIEWSKA, I. & KAAS, J. H. 1992. Topography and collateralization of the dopaminergic projections to motor and lateral prefrontal cortex in owl monkeys. *Journal of Comparative Neurology,* 325**,** 1-21.

GATTASS, R., GALKIN, T. W., DESIMONE, R. & UNGERLEIDER, L. G. 2014. Subcortical connections of area V4 in the macaque. *Journal of Comparative Neurology,* 522**,** 1941-1965.

GDALYAHU, A., TRING, E., POLACK, P.-O., GRUVER, R., GOLSHANI, P., FANSELOW, M. S., SILVA, A. J. & TRACHTENBERG, J. T. 2012.

Associative fear learning enhances sparse network coding in primary sensory cortex. *Neuron,* 75**,** 121-132.
GEISLER, S. & ZAHM, D. S. 2005. Afferents of the ventral tegmental area in the rat‐anatomical substratum for integrative functions. *Journal of Comparative Neurology,* 490**,** 270-294.
GERFEN, C. R. 1985. The neostriatal mosaic. I. Compartmental organization of projections from the striatum to the substantia nigra in the rat. *Journal of Comparative Neurology,* 236**,** 454-476.
GERITS, A., FARIVAR, R., ROSEN, B. R., WALD, L. L., BOYDEN, E. S. & VANDUFFEL, W. 2012. Optogenetically induced behavioral and functional network changes in primates. *Current Biology,* 22**,** 1722-1726.
GERITS, A., VANCRAEYENEST, P., VREYSEN, S., LARAMÉE, M.-E., MICHIELS, A., GIJSBERS, R., VAN DEN HAUTE, C., MOONS, L., DEBYSER, Z. & BAEKELANDT, V. 2015. Serotype-dependent transduction efficiencies of recombinant adeno-associated viral vectors in monkey neocortex. *Neurophotonics,* 2**,** 031209.
GERMAN, D., DUBACH, M., ASKARI, S., SPECIALE, S. & BOWDEN, D. 1988. 1-Methyl-4-phenyl-1, 2, 3, 6-tetrahydropyridine-induced parkinsonian syndrome in Macaca fascicularis: which midbrain dopaminergic neurons are lost? *Neuroscience,* 24**,** 161-174.
GERMAN, D. C., MANAYE, K., SMITH, W. K., WOODWARD, D. J. & SAPER, C. B. 1989. Midbrain dopaminergic cell loss in Parkinson's disease: computer visualization. *Annals of Neurology: Official Journal of the American Neurological Association and the Child Neurology Society,* 26**,** 507-514.
GERMAN, D. C. & MANAYE, K. F. 1993. Midbrain dopaminergic neurons (nuclei A8, A9, and A10): three‐dimensional reconstruction in the rat. *Journal of Comparative Neurology,* 331**,** 297-309.
GHAZANFAR, A. A. & SCHROEDER, C. E. 2006. Is neocortex essentially multisensory? *Trends in cognitive sciences,* 10**,** 278-285.
GHOSE, G. M., YANG, T. & MAUNSELL, J. H. R. 2002. Physiological correlates of perceptual learning in monkey V1 and V2. *Journal of neurophysiology,* 87**,** 1867-1888.

GILBERT, C., ITO, M., KAPADIA, M. & WESTHEIMER, G. 2000. Interactions between attention, context and learning in primary visual cortex. *Vision research,* 40**,** 1217-1226.
GOLDMAN-RAKIC, P. S. 1997. The cortical dopamine system: role in memory and cognition. *Advances in pharmacology,* 42**,** 707-711.
GOLTSTEIN, P. M., COFFEY, E. B. J., ROELFSEMA, P. R. & PENNARTZ, C. M. A. 2013. In vivo two-photon Ca2+ imaging reveals selective reward effects on stimulus-specific assemblies in mouse visual cortex. *Journal of Neuroscience,* 33**,** 11540-11555.
GOODALE, M. A. & MILNER, A. D. 1992. Separate visual pathways for perception and action. *Trends in neurosciences,* 15**,** 20-25.
GOSLIN, J., DIXON, T., FISCHER, M. H., CANGELOSI, A. & ELLIS, R. 2012. Electrophysiological examination of embodiment in vision and action. *Psychological science,* 23**,** 152-157.
GROENEWEGEN, H. J. 2003. The basal ganglia and motor control. *Neural plasticity,* 10.
HABER, S. N. 2014. The place of dopamine in the cortico-basal ganglia circuit. *Neuroscience,* 282**,** 248-257.
HABER, S. N., FUDGE, J. L. & MCFARLAND, N. R. 2000. Striatonigrostriatal pathways in primates form an ascending spiral from the shell to the dorsolateral striatum. *Journal of Neuroscience,* 20**,** 2369-2382.
HADACZEK, P., EBERLING, J. L., PIVIROTTO, P., BRINGAS, J., FORSAYETH, J. & BANKIEWICZ, K. S. 2010. Eight years of clinical improvement in MPTP-lesioned primates after gene therapy with AAV2-hAADC. *Molecular Therapy,* 18**,** 1458-1461.
HADACZEK, P., KOHUTNICKA, M., KRAUZE, M. T., BRINGAS, J., PIVIROTTO, P., CUNNINGHAM, J. & BANKIEWICZ, K. 2006. Convection-enhanced delivery of adeno-associated virus type 2 (AAV2) into the striatum and transport of AAV2 within monkey brain. *Human gene therapy,* 17**,** 291-302.
HAMZEI, F., DETTMERS, C., RZANNY, R., LIEPERT, J., BÜCHEL, C. & WEILLER, C. 2002. Reduction of excitability ("inhibition") in the ipsilateral primary motor cortex is mirrored by fMRI signal decreases. *Neuroimage,* 17**,** 490-496.
HAN, X., QIAN, X., BERNSTEIN, J. G., ZHOU, H.-H., FRANZESI, G. T., STERN, P., BRONSON, R. T., GRAYBIEL, A. M., DESIMONE, R. &

BOYDEN, E. S. 2009. Millisecond-timescale optical control of neural dynamics in the nonhuman primate brain. *Neuron,* 62**,** 191-198.
HARRISON, S. A. & TONG, F. 2009. Decoding reveals the contents of visual working memory in early visual areas. *Nature,* 458**,** 632-635.
HAYDEN, B. Y. & GALLANT, J. L. 2005. Time course of attention reveals different mechanisms for spatial and feature-based attention in area V4. *Neuron,* 47**,** 637-643.
HIKOSAKA, O., SAKAI, K., MIYAUCHI, S., TAKINO, R., SASAKI, Y. & PUTZ, B. 1996. Activation of human presupplementary motor area in learning of sequential procedures: a functional MRI study. *Journal of neurophysiology,* 76**,** 617-621.
HIRAMATSU, T., OHKI, M., KITAZAWA, H., XIONG, G., KITAMURA, T., YAMADA, J. & NAGAO, S. 2008. Role of primate cerebellar lobulus petrosus of paraflocculus in smooth pursuit eye movement control revealed by chemical lesion. *Neuroscience research,* 60**,** 250-258.
HONG, S. 2013. Dopamine system: manager of neural pathways. *Frontiers in human neuroscience,* 7**,** 854.
HOSP, J. A. & LUFT, A. R. 2013. Dopaminergic meso-cortical projections to m1: role in motor learning and motor cortex plasticity. *Frontiers in neurology,* 4**,** 145.
HUBBARD, J. E. & DI CARLO, V. 1973. Fluorescence histochemistry of monoamine ‐ containing cell bodies in the brain stem of the squirrel monkey (Saimiri sciureus). The locus caeruleus. *Journal of comparative neurology,* 147**,** 553-565.
IBRAHIM, L. A., MESIK, L., JI, X.-Y., FANG, Q., LI, H.-F., LI, Y.-T., ZINGG, B., ZHANG, L. I. & TAO, H. W. 2016. Cross-modality sharpening of visual cortical processing through layer-1-mediated inhibition and disinhibition. *Neuron,* 89**,** 1031-1045.
IKEMOTO, S. 2007. Dopamine reward circuitry: two projection systems from the ventral midbrain to the nucleus accumbens–olfactory tubercle complex. *Brain research reviews,* 56**,** 27-78.
ISRAEL, I., GRASSO, R., GEORGES-FRANCOIS, P., TSUZUKU, T. & BERTHOZ, A. 1997. Spatial memory and path integration studied by self-driven passive linear displacement. I. Basic properties. *Journal of neurophysiology,* 77**,** 3180-3192.

ITO, M. & GILBERT, C. D. 1999. Attention modulates contextual influences in the primary visual cortex of alert monkeys. *Neuron,* 22**,** 593-604.

IURILLI, G., GHEZZI, D., OLCESE, U., LASSI, G., NAZZARO, C., TONINI, R., TUCCI, V., BENFENATI, F. & MEDINI, P. 2012. Sound-driven synaptic inhibition in primary visual cortex. *Neuron,* 73**,** 814-828.

JARRAYA, B., BONNET, A. M., DUYCKAERTS, C., HOUETO, J. L., CORNU, P., HAUW, J. J. & AGID, Y. 2003. Parkinson's disease, subthalamic stimulation, and selection of candidates: a pathological study. *Movement disorders: official journal of the Movement Disorder Society,* 18**,** 1517-1520.

JARRAYA, B., BOULET, S., RALPH, G. S., JAN, C., BONVENTO, G., AZZOUZ, M., MISKIN, J. E., SHIN, M., DELZESCAUX, T. & DROUOT, X. 2009. Dopamine gene therapy for Parkinson's disease in a nonhuman primate without associated dyskinesia. *Science translational medicine,* 1**,** 2ra4-2ra4.

JAZAYERI, M., LINDBLOOM-BROWN, Z. & HORWITZ, G. D. 2012. Saccadic eye movements evoked by optogenetic activation of primate V1. *Nature neuroscience,* 15**,** 1368-1370.

JHOU, T. C., FIELDS, H. L., BAXTER, M. G., SAPER, C. B. & HOLLAND, P. C. 2009. The rostromedial tegmental nucleus (RMTg), a GABAergic afferent to midbrain dopamine neurons, encodes aversive stimuli and inhibits motor responses. *Neuron,* 61**,** 786-800.

JIN, X. & COSTA, R. M. 2010. Start/stop signals emerge in nigrostriatal circuits during sequence learning. *Nature,* 466**,** 457-462.

JIN, X., TECUAPETLA, F. & COSTA, R. M. 2014. Basal ganglia subcircuits distinctively encode the parsing and concatenation of action sequences. *Nature neuroscience,* 17**,** 423-430.

JOHNSTON, L. C., EBERLING, J., PIVIROTTO, P., HADACZEK, P., FEDEROFF, H. J., FORSAYETH, J. & BANKIEWICZ, K. S. 2009. Clinically relevant effects of convection-enhanced delivery of AAV2-GDNF on the dopaminergic nigrostriatal pathway in aged rhesus monkeys. *Human gene therapy,* 20**,** 497-510.

JONES, E. G. & POWELL, T. P. S. 1970. An anatomical study of converging sensory pathways within the cerebral cortex of the monkey. *Brain,* 93**,** 793-820.

KAJIWARA, K., BYRNES, A. P., CHARLTON, H. M., WOOD, M. J. A. & WOOD, K. J. 1997. Immune responses to adenoviral vectors

during gene transfer in the brain. *Human gene therapy,* 8**,** 253-265.

KANEKO, M. & STRYKER, M. P. 2014. Sensory experience during locomotion promotes recovery of function in adult visual cortex. *Elife,* 3**,** e02798.

KAWANO, M., KAWASAKI, A., SAKATA‐HAGA, H., FUKUI, Y., KAWANO, H., NOGAMI, H. & HISANO, S. 2006. Particular subpopulations of midbrain and hypothalamic dopamine neurons express vesicular glutamate transporter 2 in the rat brain. *Journal of Comparative Neurology,* 498**,** 581-592.

KAWASHIMA, R., TANJI, J., OKADA, K., SUGIURA, M., SATO, K., KINOMURA, S., INOUE, K., OGAWA, A. & FUKUDA, H. 1998. Oculomotor sequence learning: a positron emission tomography study. *Experimental brain research,* 122**,** 1-8.

KAY, K. N., ROKEM, A., WINAWER, J., DOUGHERTY, R. F. & WANDELL, B. A. 2013. GLMdenoise: A fast, automated technique for denoising task-based fMRI data. *Frontiers in Neuroscience*.

KEIFLIN, R., PRIBUT, H. J., SHAH, N. B. & JANAK, P. H. 2019. Ventral tegmental dopamine neurons participate in reward identity predictions. *Current Biology,* 29**,** 93-103.

KELLER, G. B., BONHOEFFER, T. & HÜBENER, M. 2012. Sensorimotor mismatch signals in primary visual cortex of the behaving mouse. *Neuron,* 74**,** 809-815.

KELLY, R. M. & STRICK, P. L. 2003. Cerebellar loops with motor cortex and prefrontal cortex of a nonhuman primate. *Journal of neuroscience,* 23**,** 8432-8444.

KESSLER, M. A., YANG, M., GOLLOMP, K. L., JIN, H. & IACOVITTI, L. 2003. The human tyrosine hydroxylase gene promoter. *Molecular brain research,* 112**,** 8-23.

KIM, T., MASAMOTO, K., FUKUDA, M., VAZQUEZ, A. & KIM, S.-G. 2010. Frequency-dependent neural activity, CBF, and BOLD fMRI to somatosensory stimuli in isoflurane-anesthetized rats. *Neuroimage,* 52**,** 224-233.

KISH, S. J., SHANNAK, K. & HORNYKIEWICZ, O. 1988. Uneven pattern of dopamine loss in the striatum of patients with idiopathic Parkinson's disease. *New England Journal of Medicine,* 318**,** 876-880.

KOBAYASHI, K., SANO, H., KATO, S., KURODA, K., NAKAMUTA, S., ISA, T., NAMBU, A., KAIBUCHI, K. & KOBAYASHI, K. 2016. Survival

of corticostriatal neurons by Rho/Rho-kinase signaling pathway. *Neuroscience Letters,* 630**,** 45-52.

KOLB, B., PITTMAN, K., SUTHERLAND, R. J. & WHISHAW, I. Q. 1982. Dissociation of the contributions of the prefrontal cortex and dorsomedial thalamic nucleus to spatially guided behavior in the rat. *Behavioural brain research,* 6**,** 365-378.

KOLSTER, H., MANDEVILLE, J. B., ARSENAULT, J. T., EKSTROM, L. B., WALD, L. L. & VANDUFFEL, W. 2009. Visual field map clusters in macaque extrastriate visual cortex. *Journal of Neuroscience,* 29**,** 7031-7039.

KORDOWER, J. H., OLANOW, C. W., DODIYA, H. B., CHU, Y., BEACH, T. G., ADLER, C. H., HALLIDAY, G. M. & BARTUS, R. T. 2013. Disease duration and the integrity of the nigrostriatal system in Parkinson's disease. *Brain,* 136**,** 2419-2431.

KOURTZI, Z., BETTS, L. R., SARKHEIL, P. & WELCHMAN, A. E. 2005. Distributed neural plasticity for shape learning in the human visual cortex. *PLoS Biol,* 3**,** e204.

KRACK, P., KUMAR, R., ARDOUIN, C., DOWSEY, P. L., MCVICKER, J. M., BENABID, A. L. & POLLAK, P. 2001. Mirthful laughter induced by subthalamic nucleus stimulation. *Movement Disorders,* 16**,** 867-875.

KREIMAN, G., KOCH, C. & FRIED, I. 2000. Category-specific visual responses of single neurons in the human medial temporal lobe. *Nature neuroscience,* 3**,** 946-953.

KUDLICKA, A., CLARE, L. & HINDLE, J. V. 2011. Executive functions in Parkinson's disease: Systematic review and meta‐analysis. *Movement disorders,* 26**,** 2305-2315.

KUNORI, N., KAJIWARA, R. & TAKASHIMA, I. 2014. Voltage-sensitive dye imaging of primary motor cortex activity produced by ventral tegmental area stimulation. *Journal of Neuroscience,* 34**,** 8894-8903.

KURATA, K., TSUJI, T., NARAKI, S., SEINO, M. & ABE, Y. 2000. Activation of the dorsal premotor cortex and pre-supplementary motor area of humans during an auditory conditional motor task. *Journal of neurophysiology,* 84**,** 1667-1672.

KUYPERS, H. G. J. M., SZWARCBART, M. K., MISHKIN, M. & ROSVOLD, H. E. 1965. Occipitotemporal corticocortical connections in the rhesus monkey. *Experimental neurology,* 11**,** 245-262.

LAVIN, A., NOGUEIRA, L., LAPISH, C. C., WIGHTMAN, R. M., PHILLIPS, P. E. M. & SEAMANS, J. K. 2005. Mesocortical dopamine neurons operate in distinct temporal domains using multimodal signaling. *Journal of Neuroscience,* 25**,** 5013-5023.

LERCHNER, W., CORGIAT, B., DER MINASSIAN, V., SAUNDERS, R. C. & RICHMOND, B. J. 2014. Injection parameters and virus dependent choice of promoters to improve neuron targeting in the nonhuman primate brain. *Gene therapy,* 21**,** 233-241.

LEVITT, P., RAKIC, P. & GOLDMAN‐RAKIC, P. 1984. Region‐specific distribution of catecholamine afferents in primate cerebral cortex: A fluorescence histochemical analysis. *Journal of Comparative Neurology,* 227**,** 23-36.

LEWIS, D., CAMPBELL, M., FOOTE, S., GOLDSTEIN, M. & MORRISON, J. 1987. The distribution of tyrosine hydroxylase-immunoreactive fibers in primate neocortex is widespread but regionally specific. *Journal of Neuroscience,* 7**,** 279-290.

LEWIS, D. A., FOOTE, S. L., GOLDSTEIN, M. & MORRISON, J. H. 1988. The dopaminergic innervation of monkey prefrontal cortex: a tyrosine hydroxylase immunohistochemical study. *Brain research,* 449**,** 225-243.

LI, W., PIËCH, V. & GILBERT, C. D. 2008. Learning to link visual contours. *Neuron,* 57**,** 442-451.

LIDOW, M. S., GOLDMAN-RAKIC, P. S., GALLAGER, D. W. & RAKIC, P. 1991. Distribution of dopaminergic receptors in the primate cerebral cortex: quantitative autoradiographic analysis using [3H] raclopride,[3H] spiperone and [3H] SCH23390. *Neuroscience,* 40**,** 657-671.

LINDVALL, O., BJÖRKLUND, A. & DIVAC, I. 1978. Organization of catecholamine neurons projecting to the frontal cortex in the rat. *Brain research,* 142**,** 1-24.

LINGNAU, A. & PETRIS, S. 2013. Action understanding within and outside the motor system: the role of task difficulty. *Cerebral Cortex,* 23**,** 1342-1350.

LISMAN, J. E. & GRACE, A. A. 2005. The hippocampal-VTA loop: controlling the entry of information into long-term memory. *Neuron,* 46**,** 703-713.

LIU, T., HU, P., CAO, R., YE, X., TIAN, Y., CHEN, X. & WANG, K. 2017. Dopaminergic Modulation of Biological Motion Perception in patients with Parkinson's disease. *Scientific reports,* 7**,** 1-9.

LOHANI, S., MARTIG, A. K., UNDERHILL, S. M., DEFRANCESCO, A., ROBERTS, M. J., RINAMAN, L., AMARA, S. & MOGHADDAM, B. 2018. Burst activation of dopamine neurons produces prolonged post-burst availability of actively released dopamine. *Neuropsychopharmacology,* 43**,** 2083-2092.

LOHANI, S., POPLAWSKY, A. J., KIM, S.-G. & MOGHADDAM, B. 2017. Unexpected global impact of VTA dopamine neuron activation as measured by opto-fMRI. *Molecular psychiatry,* 22**,** 585-594.

LYND‐BALTA, E. & HABER, S. N. 1994. Primate striatonigral projections: a comparison of the sensorimotor‐related striatum and the ventral striatum. *Journal of Comparative Neurology,* 345**,** 562-578.

MAC BROWN, R. & GOLDMAN, P. S. 1977. Catecholamines in neocortex of rhesus monkeys: regional distribution and ontogenetic development. *Brain research,* 124**,** 576-580.

MANTO, M., BOWER, J. M., CONFORTO, A. B., DELGADO-GARCÍA, J. M., DA GUARDA, S. N. F., GERWIG, M., HABAS, C., HAGURA, N., IVRY, R. B. & MARIËN, P. 2012. Consensus paper: roles of the cerebellum in motor control—the diversity of ideas on cerebellar involvement in movement. *The Cerebellum,* 11**,** 457-487.

MARTINEZ, A., ANLLO-VENTO, L., SERENO, M. I., FRANK, L. R., BUXTON, R. B., DUBOWITZ, D. J., WONG, E. C., HINRICHS, H., HEINZE, H. J. & HILLYARD, S. A. 1999. Involvement of striate and extrastriate visual cortical areas in spatial attention. *Nature neuroscience,* 2**,** 364-369.

MATSUDA, W., FURUTA, T., NAKAMURA, K. C., HIOKI, H., FUJIYAMA, F., ARAI, R. & KANEKO, T. 2009. Single nigrostriatal dopaminergic neurons form widely spread and highly dense axonal arborizations in the neostriatum. *Journal of Neuroscience,* 29**,** 444-453.

MATSUMOTO, M. & HIKOSAKA, O. 2009. Two types of dopamine neuron distinctly convey positive and negative motivational signals. *Nature,* 459**,** 837-841.

MAYBERG, H. S. & LOZANO, A. M. 2002. Penfield revisited?: Understanding and modifying behavior by deep brain stimulation for PD. *Neurology,* 59**,** 1298-1299.

MCADAMS, C. J. & MAUNSELL, J. H. R. 1999. Effects of attention on orientation-tuning functions of single neurons in macaque cortical area V4. *Journal of Neuroscience,* 19**,** 431-441.
MCADAMS, C. J. & REID, R. C. 2005. Attention modulates the responses of simple cells in monkey primary visual cortex. *Journal of Neuroscience,* 25**,** 11023-11033.
MCCLURKIN, J. W. & OPTICAN, L. M. 1996. Primate striate and prestriate cortical neurons during discrimination. I. Simultaneous temporal encoding of information about color and pattern. *Journal of Neurophysiology,* 75**,** 481-495.
MCFARLAND, N. R. & HABER, S. N. 2002. Thalamic relay nuclei of the basal ganglia form both reciprocal and nonreciprocal cortical connections, linking multiple frontal cortical areas. *Journal of Neuroscience,* 22**,** 8117-8132.
MERRIAM, E. P., COLBY, C. L., THULBORN, K. R., LUNA, B., OLSON, C. R. & SWEENEY, J. A. 2001. Stimulus–response incompatibility activates cortex proximate to three eye fields. *Neuroimage,* 13**,** 794-800.
MILNER, D. & GOODALE, M. 2006. *The visual brain in action*, OUP Oxford.
MIRABELLA, G., BERTINI, G., SAMENGO, I., KILAVIK, B. E., FRILLI, D., DELLA LIBERA, C. & CHELAZZI, L. 2007. Neurons in area V4 of the macaque translate attended visual features into behaviorally relevant categories. *Neuron,* 54**,** 303-318.
MOORE, T. & CHANG, M. H. 2009. Presaccadic discrimination of receptive field stimuli by area V4 neurons. *Vision research,* 49**,** 1227-1232.
MOORE, T., TOLIAS, A. S. & SCHILLER, P. H. 1998. Visual representations during saccadic eye movements. *Proceedings of the National Academy of Sciences,* 95**,** 8981-8984.
MORALES, M. & ROOT, D. H. 2014. Glutamate neurons within the midbrain dopamine regions. *Neuroscience,* 282**,** 60-68.
MUELLER, A., KROCK, R. M., SHEPARD, S. & MOORE, T. 2020. Dopamine Receptor Expression Among Local and Visual Cortex-Projecting Frontal Eye Field Neurons. *Cerebral Cortex,* 30**,** 148-164.
MURRAY, E. A., BUSSEY, T. J. & WISE, S. P. 2000. Role of prefrontal cortex in a network for arbitrary visuomotor mapping. *Executive Control and the Frontal Lobe: Current Issues.* Springer.

MURRIS, S. 2020. Neural and behavioural modifications from stimulation of the macaque brainstem.
MURRIS, S. R., ARSENAULT, J. T., RAMAN, R., VOGELS, R. & VANDUFFEL, W. 2021. Electrical stimulation of the macaque ventral tegmental area drives category-selective learning without attention. *Neuron,* 109**,** 1381-1395.
MURRIS, S. R., ARSENAULT, J. T. & VANDUFFEL, W. 2020. Frequency- and State-Dependent Network Effects of Electrical Stimulation Targeting the Ventral Tegmental Area in Macaques. *Cerebral Cortex,* 30**,** 4281-4296.
NACHEV, P., WYDELL, H., O'NEILL, K., HUSAIN, M. & KENNARD, C. 2007. The role of the pre-supplementary motor area in the control of action. *Neuroimage,* 36**,** T155-T163.
NADELHAFT, I. 1984. The sessile drop method for immunohistochemical processing of unmounted sections of nervous tissue. *Journal of Histochemistry & Cytochemistry,* 32**,** 1344-1346.
NAIR-ROBERTS, R. G., CHATELAIN-BADIE, S. D., BENSON, E., WHITE-COOPER, H., BOLAM, J. P. & UNGLESS, M. A. 2008. Stereological estimates of dopaminergic, GABAergic and glutamatergic neurons in the ventral tegmental area, substantia nigra and retrorubral field in the rat. *Neuroscience,* 152**,** 1024-1031.
NAKAMURA, K., SAKAI, K. & HIKOSAKA, O. 1999. Effects of local inactivation of monkey medial frontal cortex in learning of sequential procedures. *Journal of Neurophysiology,* 82**,** 1063-1068.
NELISSEN, K., LUPPINO, G., VANDUFFEL, W., RIZZOLATTI, G. & ORBAN, G. A. 2005. Observing others: multiple action representation in the frontal lobe. *Science,* 310**,** 332-336.
NELISSEN, K. & VANDUFFEL, W. 2011. Grasping-related functional magnetic resonance imaging brain responses in the macaque monkey. *Journal of Neuroscience,* 31**,** 8220-8229.
NEWTON, J. M., SUNDERLAND, A. & GOWLAND, P. A. 2005. fMRI signal decreases in ipsilateral primary motor cortex during unilateral hand movements are related to duration and side of movement. *Neuroimage,* 24**,** 1080-1087.
NIELL, C. M. & STRYKER, M. P. 2010. Modulation of visual responses by behavioral state in mouse visual cortex. *Neuron,* 65**,** 472-479.

NOBIN, A. 1973. Topography of the monoamine neuron systems in the human brain as revealed in fetuses.
NOUDOOST, B., CLARK, K. L. & MOORE, T. 2014. A distinct contribution of the frontal eye field to the visual representation of saccadic targets. *Journal of Neuroscience,* 34**,** 3687-3698.
NOUDOOST, B. & MOORE, T. 2011. Control of visual cortical signals by prefrontal dopamine. *Nature,* 474**,** 372-375.
OAKMAN, S. A., FARIS, P. L., KERR, P. E., COZZARI, C. & HARTMAN, B. K. 1995. Distribution of pontomesencephalic cholinergic neurons projecting to substantia nigra differs significantly from those projecting to ventral tegmental area. *Journal of Neuroscience,* 15**,** 5859-5869.
OGAWA, S., MENON, R. S., TANK, D. W., KIM, S. G., MERKLE, H., ELLERMANN, J. M. & UGURBIL, K. 1993. Functional brain mapping by blood oxygenation level-dependent contrast magnetic resonance imaging. A comparison of signal characteristics with a biophysical model. *Biophysical journal,* 64**,** 803-812.
OHKI, M., KITAZAWA, H., HIRAMATSU, T., KAGA, K., KITAMURA, T., YAMADA, J. & NAGAO, S. 2009. Role of primate cerebellar hemisphere in voluntary eye movement control revealed by lesion effects. *Journal of neurophysiology,* 101**,** 934-947.
OLSON, M., LOCKHART, T. E. & LIEBERMAN, A. 2019. Motor learning deficits in Parkinson's disease (PD) and their effect on training response in gait and balance: A narrative review. *Frontiers in neurology,* 10**,** 62.
OTT, T. & NIEDER, A. 2019. Dopamine and cognitive control in prefrontal cortex. *Trends in Cognitive Sciences,* 23**,** 213-234.
PARENT, A. 1986. *Comparative neurobiology of the basal ganglia*, J. Wiley.
PARENT, A., MACKEY, A. & DE BELLEFEUILLE, L. 1983. The subcortical afferents to caudate nucleus and putamen in primate: a fluorescence retrograde double labeling study. *Neuroscience,* 10**,** 1137-1150.
PASSINGHAM, R. E. & TONI, I. 2001. Contrasting the dorsal and ventral visual systems: guidance of movement versus decision making. *Neuroimage,* 14**,** S125-S131.

PASSINGHAM, R. E., TONI, I., SCHLUTER, N. & RUSHWORTH, M. F. S. 1998. How do visual instructions influence the motor system? , 1998 1998. Wiley Online Library, 129-140.
PAULIN, M. G. 1993. The role of the cerebellum in motor control and perception. *Brain, behavior and evolution,* 41**,** 39-50.
PAXINOS, G., HUANG, X.-F. & TOGA, A. W. 2000. The rhesus monkey brain in stereotaxic coordinates.
PERENIN, M. T. & VIGHETTO, A. 1988. Optic ataxia: A specific disruption in visuomotor mechanisms: I. Different aspects of the deficit in reaching for objects. *Brain,* 111**,** 643-674.
PESSOA, L. & UNGERLEIDER, L. G. 2004. Neuroimaging studies of attention and the processing of emotion-laden stimuli. *Progress in brain research,* 144**,** 171-182.
PETRIDES, M. 1997. Visuo-motor conditional associative learning after frontal and temporal lesions in the human brain. *Neuropsychologia,* 35**,** 989-997.
PHILLIPSON, O. T. 1979. Afferent projections to the ventral tegmental area of Tsai and interfascicular nucleus: a horseradish peroxidase study in the rat. *Journal of Comparative Neurology,* 187**,** 117-143.
PORRAS, G., LI, Q. & BEZARD, E. 2012. Modeling Parkinson's disease in primates: the MPTP model. *Cold Spring Harbor perspectives in medicine,* 2**,** a009308.
PORRINO, L. J. & GOLDMAN‐RAKIC, P. S. 1982. Brainstem innervation of prefrontal and anterior cingulate cortex in the rhesus monkey revealed by retrograde transport of HRP. *Journal of Comparative Neurology,* 205**,** 63-76.
POSNER, M. I. & GILBERT, C. D. 1999. Attention and primary visual cortex. *Proceedings of the National Academy of Sciences,* 96**,** 2585-2587.
POUGET, A., DENEVE, S. & DUHAMEL, J.-R. 2002. A computational perspective on the neural basis of multisensory spatial representations. *Nature Reviews Neuroscience,* 3**,** 741-747.
POULIN, J.-F., CARONIA, G., HOFER, C., CUI, Q., HELM, B., RAMAKRISHNAN, C., CHAN, C. S., DOMBECK, D. A., DEISSEROTH, K. & AWATRAMANI, R. 2018. Mapping projections of molecularly defined dopamine neuron subtypes using intersectional genetic approaches. *Nature neuroscience,* 21**,** 1260-1271.

QUEK, G. L. & PEELEN, M. V. 2020. Contextual and spatial associations between objects interactively modulate visual processing. *Cerebral Cortex,* 30**,** 6391-6404.

RABINOWITZ, J. E., ROLLING, F., LI, C., CONRATH, H., XIAO, W., XIAO, X. & SAMULSKI, R. J. 2002. Cross-packaging of a single adeno-associated virus (AAV) type 2 vector genome into multiple AAV serotypes enables transduction with broad specificity. *Journal of virology,* 76**,** 791-801.

RAGHANTI, M. A., STIMPSON, C. D., MARCINKIEWICZ, J. L., ERWIN, J. M., HOF, P. R. & SHERWOOD, C. C. 2008. Cortical dopaminergic innervation among humans, chimpanzees, and macaque monkeys: a comparative study. *Neuroscience,* 155**,** 203-220.

RAINER, G., LEE, H. & LOGOTHETIS, N. K. 2004. The effect of learning on the function of monkey extrastriate visual cortex. *PLoS Biol,* 2**,** e44.

REPPAS, J. B., USREY, W. M. & REID, R. C. 2002. Saccadic eye movements modulate visual responses in the lateral geniculate nucleus. *Neuron,* 35**,** 961-974.

REVELEY, C., GRUSLYS, A., YE, F. Q., GLEN, D., SAMAHA, J., E. RUSS, B., SAAD, Z., K. SETH, A., LEOPOLD, D. A. & SALEEM, K. S. 2017. Three-dimensional digital template atlas of the macaque brain. *Cerebral cortex,* 27**,** 4463-4477.

REYNOLDS, J. H. & CHELAZZI, L. 2004. Attentional modulation of visual processing. *Annu. Rev. Neurosci.,* 27**,** 611-647.

RIDDERINKHOF, K. R., ULLSPERGER, M., CRONE, E. A. & NIEUWENHUIS, S. 2004. The role of the medial frontal cortex in cognitive control. *science,* 306**,** 443-447.

RIGOTTI, M., BARAK, O., WARDEN, M. R., WANG, X.-J., DAW, N. D., MILLER, E. K. & FUSI, S. 2013. The importance of mixed selectivity in complex cognitive tasks. *Nature,* 497**,** 585-590.

RISHEL, C. A., HUANG, G. & FREEDMAN, D. J. 2013. Independent category and spatial encoding in parietal cortex. *Neuron,* 77**,** 969-979.

RIZZOLATTI, G. & LUPPINO, G. 2001. The cortical motor system. *Neuron,* 31**,** 889-901.

ROBERTS, M., DELICATO, L. S., HERRERO, J., GIESELMANN, M. A. & THIELE, A. 2007. Attention alters spatial integration in macaque V1 in an eccentricity-dependent manner. *Nature neuroscience,* 10**,** 1483-1491.

ROCKLAND, K. S. & OJIMA, H. 2003. Multisensory convergence in calcarine visual areas in macaque monkey. *International Journal of Psychophysiology,* 50**,** 19-26.

ROELFSEMA, P. R., LAMME, V. A. F. & SPEKREIJSE, H. 1998. Object-based attention in the primary visual cortex of the macaque monkey. *Nature,* 395**,** 376-381.

ROSIN, D. L., WESTON, M. C., SEVIGNY, C. P., STORNETTA, R. L. & GUYENET, P. G. 2003. Hypothalamic orexin (hypocretin) neurons express vesicular glutamate transporters VGLUT1 or VGLUT2. *Journal of Comparative Neurology,* 465**,** 593-603.

RUIZ, O., LUSTIG, B. R., NASSI, J. J., CETIN, A., REYNOLDS, J. H., ALBRIGHT, T. D., CALLAWAY, E. M., STONER, G. R. & ROE, A. W. 2013. Optogenetics through windows on the brain in the nonhuman primate. *Journal of neurophysiology,* 110**,** 1455-1467.

RUTKOWSKI, R. G. & WEINBERGER, N. M. 2005. Encoding of learned importance of sound by magnitude of representational area in primary auditory cortex. *Proceedings of the National Academy of Sciences,* 102**,** 13664-13669.

SAKAI, K., HIKOSAKA, O., MIYAUCHI, S., SASAKI, Y., FUJIMAKI, N. & PÜTZ, B. 1999. Presupplementary motor area activation during sequence learning reflects visuo-motor association. *Journal of Neuroscience,* 19**,** RC1-RC1.

SALEEM, A. B., AYAZ, A., JEFFERY, K. J., HARRIS, K. D. & CARANDINI, M. 2013. Integration of visual motion and locomotion in mouse visual cortex. *Nature neuroscience,* 16**,** 1864-1869.

SANTIN, M. D. N., VOULLEMINOT, P., VRILLON, A., HAINQUE, E., BÉREAU, M., LAGHA‐BOUKBIZA, O., WIRTH, T., MONTAUT, S., BARDINET, E. & KYHENG, M. 2021. Impact of Subthalamic Deep Brain Stimulation on Impulse Control Disorders in Parkinson's Disease: A Prospective Study. *Movement Disorders,* 36**,** 750-757.

SATOH, T., NAKAI, S., SATO, T. & KIMURA, M. 2003. Correlated coding of motivation and outcome of decision by dopamine neurons. *Journal of neuroscience,* 23**,** 9913-9923.

SAUNDERS, A., MACOSKO, E. Z., WYSOKER, A., GOLDMAN, M., KRIENEN, F. M., DE RIVERA, H., BIEN, E., BAUM, M., BORTOLIN, L. & WANG, S. 2018a. Molecular diversity and specializations among the cells of the adult mouse brain. *Cell,* 174**,** 1015-1030.

SAUNDERS, B. T., RICHARD, J. M., MARGOLIS, E. B. & JANAK, P. H. 2018b. Dopamine neurons create Pavlovian conditioned stimuli with circuit-defined motivational properties. *Nature neuroscience,* 21**,** 1072-1083.

SAWAGUCHI, T. & GOLDMAN-RAKIC, P. S. 1991. D1 dopamine receptors in prefrontal cortex: involvement in working memory. *Science,* 251**,** 947-950.

SCHALLERT, T. & TILLERSON, J. L. 2000. Intervention strategies for degeneration of dopamine neurons in parkinsonism. *Central nervous system diseases.* Springer.

SCHNEIDER, F., HABEL, U., VOLKMANN, J., REGEL, S., KORNISCHKA, J., STURM, V. & FREUND, H.-J. 2003. Deep brain stimulation of the subthalamic nucleus enhances emotional processing in Parkinson disease. *Archives of general psychiatry,* 60**,** 296-302.

SCHOUPS, A., VOGELS, R., QIAN, N. & ORBAN, G. 2001. Practising orientation identification improves orientation coding in V1 neurons. *Nature,* 412**,** 549-553.

SCHROEDER, U., KUEHLER, A., HASLINGER, B., ERHARD, P., FOGEL, W., TRONNIER, V. M., LANGE, K. W., BOECKER, H. & CEBALLOS‐BAUMANN, A. O. 2002. Subthalamic nucleus stimulation affects striato‐anterior cingulate cortex circuit in a response conflict task: a PET study. *Brain,* 125**,** 1995-2004.

SCHULTZ, W. 1997. Dopamine neurons and their role in reward mechanisms. *Current opinion in neurobiology,* 7**,** 191-197.

SCHULTZ, W. 1998. Predictive reward signal of dopamine neurons. *Journal of neurophysiology,* 80**,** 1-27.

SCHULTZ, W. 2007. Multiple dopamine functions at different time courses. *Annu. Rev. Neurosci.,* 30**,** 259-288.

SCHULTZ, W. 2015. Neuronal reward and decision signals: from theories to data. *Physiological reviews,* 95**,** 853-951.

SCHULTZ, W. 2016. Dopamine reward prediction-error signalling: a two-component response. *Nature Reviews Neuroscience,* 17**,** 183.

SCHULTZ, W., DAYAN, P. & MONTAGUE, P. R. 1997. A neural substrate of prediction and reward. *Science,* 275**,** 1593-1599.

SEMBA, K. & FIBIGER, H. C. 1992. Afferent connections of the laterodorsal and the pedunculopontine tegmental nuclei in the rat: a retro‐and antero‐grade transport and

immunohistochemical study. *Journal of Comparative Neurology,* 323**,** 387-410.
SESACK, S. R. & PICKEL, V. M. 1992. Prefrontal cortical efferents in the rat synapse on unlabeled neuronal targets of catecholamine terminals in the nucleus accumbens septi and on dopamine neurons in the ventral tegmental area. *Journal of Comparative Neurology,* 320**,** 145-160.
SHETTY, A. S., BHATIA, K. P. & LANG, A. E. 2019. Dystonia and Parkinson's disease: what is the relationship? *Neurobiology of disease,* 132**,** 104462.
SHIMA, K. & TANJI, J. 1998. Both supplementary and presupplementary motor areas are crucial for the temporal organization of multiple movements. *Journal of neurophysiology,* 80**,** 3247-3260.
SHULER, M. G. & BEAR, M. F. 2006. Reward timing in the primary visual cortex. *Science,* 311**,** 1606-1609.
SMITH, A. T., SINGH, K. D. & GREENLEE, M. W. 2000. Attentional suppression of activity in the human visual cortex. *Neuroreport,* 11**,** 271-278.
SMITH, S. M., JENKINSON, M., WOOLRICH, M. W., BECKMANN, C. F., BEHRENS, T. E. J., JOHANSEN-BERG, H., BANNISTER, P. R., DE LUCA, M., DROBNJAK, I., FLITNEY, D. E., NIAZY, R. K., SAUNDERS, J., VICKERS, J., ZHANG, Y., DE STEFANO, N., BRADY, J. M. & MATTHEWS, P. M. 2004. Advances in functional and structural MR image analysis and implementation as FSL. *NeuroImage.*
SOMERS, D. C., DALE, A. M., SEIFFERT, A. E. & TOOTELL, R. B. H. 1999. Functional MRI reveals spatially specific attentional modulation in human primary visual cortex. *Proceedings of the National Academy of Sciences,* 96**,** 1663-1668.
STĂNIŞOR, L., VAN DER TOGT, C., PENNARTZ, C. M. A. & ROELFSEMA, P. R. 2013. A unified selection signal for attention and reward in primary visual cortex. *Proceedings of the National Academy of Sciences,* 110**,** 9136-9141.
STAUFFER, W. R., LAK, A., YANG, A., BOREL, M., PAULSEN, O., BOYDEN, E. S. & SCHULTZ, W. 2016. Dopamine neuron-specific optogenetic stimulation in rhesus macaques. *Cell,* 166**,** 1564-1571.
STEINBERG, E. E., KEIFLIN, R., BOIVIN, J. R., WITTEN, I. B., DEISSEROTH, K. & JANAK, P. H. 2013. A causal link between

prediction errors, dopamine neurons and learning. *Nature neuroscience,* 16**,** 966-973.
SULZER, D., JOYCE, M. P., LIN, L., GELDWERT, D., HABER, S. N., HATTORI, T. & RAYPORT, S. 1998. Dopamine neurons make glutamatergic synapses in vitro. *Journal of Neuroscience,* 18**,** 4588-4602.
SUNDBERG, K. A., MITCHELL, J. F. & REYNOLDS, J. H. 2009. Spatial attention modulates center-surround interactions in macaque visual area v4. *Neuron,* 61**,** 952-963.
SWANSON, L. W. 1982. The projections of the ventral tegmental area and adjacent regions: a combined fluorescent retrograde tracer and immunofluorescence study in the rat. *Brain research bulletin,* 9**,** 321-353.
SYLVESTER, R., HAYNES, J.-D. & REES, G. 2005. Saccades differentially modulate human LGN and V1 responses in the presence and absence of visual stimulation. *Current Biology,* 15**,** 37-41.
TAKAKUSAKI, K., SAITOH, K., HARADA, H. & KASHIWAYANAGI, M. 2004. Role of basal ganglia–brainstem pathways in the control of motor behaviors. *Neuroscience research,* 50**,** 137-151.
TAKIKAWA, Y., KAWAGOE, R. & HIKOSAKA, O. 2004. A possible role of midbrain dopamine neurons in short-and long-term adaptation of saccades to position-reward mapping. *Journal of neurophysiology,* 92**,** 2520-2529.
TAMURA, K., OHASHI, Y., TSUBOTA, T., TAKEUCHI, D., HIRABAYASHI, T., YAGUCHI, M., MATSUYAMA, M., SEKINE, T. & MIYASHITA, Y. 2012. A glass-coated tungsten microelectrode enclosing optical fibers for optogenetic exploration in primate deep brain structures. *Journal of neuroscience methods,* 211**,** 49-57.
TANJI, J. 2001. Sequential organization of multiple movements: involvement of cortical motor areas. *Annual review of neuroscience,* 24**,** 631-651.
THOMAS, E., VAN HULLE, M. M. & VOGEL, R. 2001. Encoding of categories by noncategory-specific neurons in the inferior temporal cortex. *Journal of cognitive neuroscience,* 13**,** 190-200.
TONI, I., RUSHWORTH, M. F. & PASSINGHAM, R. E. 2001. Neural correlates of visuomotor associations. *Experimental brain research,* 141**,** 359-369.

TSAI, H.-C., ZHANG, F., ADAMANTIDIS, A., STUBER, G. D., BONCI, A., DE LECEA, L. & DEISSEROTH, K. 2009. Phasic firing in dopaminergic neurons is sufficient for behavioral conditioning. *Science,* 324**,** 1080-1084.

UNGERLEIDER, L. G. 1982. Two cortical visual systems. *Analysis of visual behavior***,** 549-586.

VAN BOCKSTAELE, E. J. & PICKEL, V. M. 1995. GABA-containing neurons in the ventral tegmental area project to the nucleus accumbens in rat brain. *Brain research,* 682**,** 215-221.

VANCRAEYENEST, P., ARSENAULT, J. T., LI, X., ZHU, Q., KOBAYASHI, K., ISA, K., ISA, T. & VANDUFFEL, W. 2020. Selective Mesoaccumbal Pathway Inactivation Affects Motivation but Not Reinforcement-Based Learning in Macaques. *Neuron,* 108**,** 568-581.

VANDUFFEL, W., FIZE, D., MANDEVILLE, J. B., NELISSEN, K., VAN HECKE, P., ROSEN, B. R., TOOTELL, R. B. H. & ORBAN, G. A. 2001. Visual motion processing investigated using contrast agent-enhanced fMRI in awake behaving monkeys. *Neuron,* 32**,** 565-577.

VANDUFFEL, W., FIZE, D., PEUSKENS, H., DENYS, K., SUNAERT, S., TODD, J. T. & ORBAN, G. A. 2002. Extracting 3D from motion: differences in human and monkey intraparietal cortex. *Science,* 298**,** 413-415.

VERNIER, P., MORET, F., CALLIER, S., SNAPYAN, M., WERSINGER, C. & SIDHU, A. 2004. The degeneration of dopamine neurons in Parkinson's disease: insights from embryology and evolution of the mesostriatocortical system. *Annals of the New York Academy of Sciences,* 1035**,** 231-249.

VUILLEUMIER, P. & DRIVER, J. 2007. Modulation of visual processing by attention and emotion: windows on causal interactions between human brain regions. *Philosophical Transactions of the Royal Society B: Biological Sciences,* 362**,** 837-855.

VUILLEUMIER, P., RICHARDSON, M. P., ARMONY, J. L., DRIVER, J. & DOLAN, R. J. 2004. Distant influences of amygdala lesion on visual cortical activation during emotional face processing. *Nature neuroscience,* 7**,** 1271-1278.

WAELTI, P., DICKINSON, A. & SCHULTZ, W. 2001. Dopamine responses comply with basic assumptions of formal learning theory. *Nature,* 412**,** 43-48.

WALKER, S., ROBBINS, T. & ROBERTS, A. 2009. Differential contributions of dopamine and serotonin to orbitofrontal cortex function in the marmoset. *Cerebral Cortex,* 19**,** 889-898.
WALLACE, D. M., MAGNUSON, D. J. & GRAY, T. S. 1992. Organization of amygdaloid projections to brainstem dopaminergic, noradrenergic, and adrenergic cell groups in the rat. *Brain research bulletin,* 28**,** 447-454.
WALTON, M. E. & BOURET, S. 2019. What is the relationship between dopamine and effort? *Trends in neurosciences,* 42**,** 79-91.
WANG, M., VIJAYRAGHAVAN, S. & GOLDMAN-RAKIC, P. S. 2004. Selective D2 receptor actions on the functional circuitry of working memory. *Science,* 303**,** 853-856.
WANG, X.-J. 2008. Decision making in recurrent neuronal circuits. *Neuron,* 60**,** 215-234.
WATAKABE, A., OHTSUKA, M., KINOSHITA, M., TAKAJI, M., ISA, K., MIZUKAMI, H., OZAWA, K., ISA, T. & YAMAMORI, T. 2015. Comparative analyses of adeno-associated viral vector serotypes 1, 2, 5, 8 and 9 in marmoset, mouse and macaque cerebral cortex. *Neuroscience research,* 93**,** 144-157.
WEINER, D. M., LEVEY, A. I., SUNAHARA, R. K., NIZNIK, H. B., O'DOWD, B. F., SEEMAN, P. & BRANN, M. 1991. D1 and D2 dopamine receptor mRNA in rat brain. *Proceedings of the national academy of sciences,* 88**,** 1859-1863.
WELTER, M. L., HOUETO, J. L., TEZENAS DU MONTCEL, S., MESNAGE, V., BONNET, A. M., PILLON, B., ARNULF, I., PIDOUX, B., DORMONT, D. & CORNU, P. 2002. Clinical predictive factors of subthalamic stimulation in Parkinson's disease. *Brain,* 125**,** 575-583.
WIEST, M. C., THOMSON, E., PANTOJA, J. & NICOLELIS, M. A. L. 2010. Changes in S1 neural responses during tactile discrimination learning. *Journal of neurophysiology,* 104**,** 300-312.
WILLIAMS, G. V. & GOLDMAN-RAKIC, P. S. 1995. Modulation of memory fields by dopamine Dl receptors in prefrontal cortex. *Nature,* 376**,** 572-575.
WILLIAMS, S. M. & GOLDMAN-RAKIC, P. S. 1998. Widespread origin of the primate mesofrontal dopamine system. *Cerebral cortex (New York, NY: 1991),* 8**,** 321-345.

WILLIFORD, T. & MAUNSELL, J. H. R. 2006. Effects of spatial attention on contrast response functions in macaque area V4. *Journal of neurophysiology,* 96**,** 40-54.
WITTEN, I. B., STEINBERG, E. E., LEE, S. Y., DAVIDSON, T. J., ZALOCUSKY, K. A., BRODSKY, M., YIZHAR, O., CHO, S. L., GONG, S. & RAMAKRISHNAN, C. 2011. Recombinase-driver rat lines: tools, techniques, and optogenetic application to dopamine-mediated reinforcement. *Neuron,* 72**,** 721-733.
WOLPERT, D. M., GHAHRAMANI, Z. & JORDAN, M. I. 1995. An internal model for sensorimotor integration. *Science,* 269**,** 1880-1882.
WORSLEY, K. J. & FRISTON, K. J. 1995. Analysis of fMRI time-series revisited—again. *Neuroimage,* 2**,** 173-181.
WU, Q., CHEN, L., ZHENG, Y., ZHANG, C., HUANG, L., GUO, W., FANG, Y., ZHOU, H., LIU, Y. & CHEN, J. 2012. Cognitive impairment is common in Parkinson's disease without dementia in the early and middle stages in a Han Chinese cohort. *Parkinsonism & related disorders,* 18**,** 161-165.
YAN, Y., RASCH, M. J., CHEN, M., XIANG, X., HUANG, M., WU, S. & LI, W. 2014. Perceptual training continuously refines neuronal population codes in primary visual cortex. *Nature neuroscience,* 17**,** 1380-1387.
YANG, T. & MAUNSELL, J. H. R. 2004. The effect of perceptual learning on neuronal responses in monkey visual area V4. *Journal of Neuroscience,* 24**,** 1617-1626.
YETNIKOFF, L., LAVEZZI, H. N., REICHARD, R. A. & ZAHM, D. S. 2014. An update on the connections of the ventral mesencephalic dopaminergic complex. *Neuroscience,* 282**,** 23-48.
ZEEB, F. D., FLORESCO, S. B. & WINSTANLEY, C. A. 2010. Contributions of the orbitofrontal cortex to impulsive choice: interactions with basal levels of impulsivity, dopamine signalling, and reward-related cues. *Psychopharmacology,* 211**,** 87-98.
ZHOU, S., CHEN, X., WANG, C., YIN, C., HU, P. & WANG, K. 2012. Selective attention deficits in early and moderate stage Parkinson's disease. *Neuroscience letters,* 509**,** 50-55.

APPENDIX

SCIENTIFIC ACKNOWLEGEMENT AND PERSONAL CONTRIBUTION

Chapter II: Ventral midbrain projections in the macaque brain

Authors: Muhammad Zubair (M.Z.), Sjoerd R Murris (S.R.M.), Kaoru Isa (K.I.), Hirotaka Onoe (H.O.), Yoshinori Koshimizu (Y.K.), Wim Vanduffel (W.V.), Tadashi Isa (T.I.)

Acknowledgements: The animals (*Macaca fuscata*) were provided by the National BioResearch Project-Nihonzaru (Japanese macaque) at the Kyoto University Primate Research Institute with support in part by the National BioResource Project of the Japan Agency for Medical Research and Development (NBRP). We thank M. Takada and K. Inoue for providing us the plasmids of the AAV2.1 vector. We thank K. Svoboda for providing the gene AAV-CAG-hChR2-H134R-tdTomato. We also thank J. Yamashita, M. Nakamura and Y. Shinto for technical assistance. We thank X. Li and Q. Zhu for their assistance in generating the Figure 2.8.

Funding: Japanese KAKENHI Grants from MEXT (26112008, 19H05723 and 19KK0192), JSPS International Bilateral Joint Research Program, JST/CREST (JPMJCR1651), AMED (20DM0107151 and 20DM0307005). KU Leuven (C14/17/109); Fonds Wetenschappelijk Onderzoek-Vlaanderen (FWO-Flanders) (G0D5817N, G0B8617N, G090714N, G088813N and Odysseus G0007.12); and the European Union's Horizon 2020 Framework Programme for Research and Innovation under Grant Agreement No 785907 (Human Brain Project SGA2).

Contributions: Conceptualization, **M.Z.**, S.R.M., W.V., K.I. and T.I., Methodology, **M.Z.**, K.I., Y.K., S.R.M., and H.O., Investigation, **M.Z.**, K.I. and S.R.M., Reviewing and editing, **M.Z.**, S.R.M., W.V.

and T.I., Funding acquisition, T.I. and W.V., Supervision, T.I., K.I., and W.V.

Conflict of Interests: None declared

Chapter III: Somatomotor signals modulate early visual cortical activity

Authors: Muhammad Zubair (M.Z.), John T. Arsenault (J.T.A.), Wim Vanduffel (W.V.)

Acknowledgements: We thank R. Pretorius for his contribution in the eye data analysis and C. Fransen, A. Coeman, P. Kayenbergh, I. Puttemans, C. Ulens, A. Hermans, G. Meulemans, M. Depaep, W. Depuydt, and S. Verstraeten for technical and administrative support.

Funding: This work received funding from KU Leuven C14/17/109; Fonds Wetenschappelijk Onderzoek-Vlaanderen (FWO-Flanders) G0D5817N, G0B8617N, G090714N, G0E0520N, and Odysseus G0007.12; and the European Union's Horizon 2020 Framework Programme for Research and Innovation under Grant Agreement No 945539 (Human Brain Project SGA3).

Contribution: Conceptualization, **M.Z.**, J.T.A., and W.V., Methodology, **M.Z.**, J.T.A., and W.V., Investigation, **M.Z.** and J.T.A., Reviewing and editing, **M.Z.**, and W.V., Funding acquisition, W.V., Supervision, W.V., and J.T.A.

Conflict of Interests: None declared

Muhammad Zubair

+32-485-15-01-89
muhammad.zubair@kuleuven.be
Leuven, Belgium
www.linkedin.com/in/muzubair/

EDUCATION

2017-2021 Ph.D. Biomedical Sciences (Neuroscience), Katholiek University Leuven (KUL), Belgium

2011-2013 MS Computer Engineering, National University of Science & Technology (NUST), Pakistan

2006-2010 B.Sc. Computer System Engineering, The Islamia University of Bahawalpur (IUB), Pakistan

EXPERIENCE

Guest researcher, Lab of neurobiology and physiology, Kyoto university, Japan (**2018 - 2020,** 18 months)

Studied the whole-brain anatomical connectivity of the midbrain dopamine network in detail by injecting an adeno-associated viral vector into monkey's midbrain

Lecturer/medical imaging specialist, Dept. of computer science, HITEC Uni., Pakistan (**2013 - 2017**)

Conducted labs: Introduction to computing, data structure and algorithm, programming fundamentals, database and management system, digital signal processing, digital image processing.

Courses taught: Introduction to computing, discrete structures, digital image processing, data structure and algorithm, numerical computing, software engineering, digital signal processing, operating systems.

Research & Development:

- Implemented a computer-based tool using support vector machine for early brain tumor detection using brain anatomical MRI scan as a system input.
- Develop a program for automated extraction of the optic disc from the retinal fundus images.
- Develop a program to detect the hard exudates using retinal photographs (with extracted optic disc) as system input to detect the diabetic retinopathy.

Guest researcher, Health Science and Technology dept., Aalborg Uni., Denmark (**Mar 2015 - Aug 2015**)
Developed a semi-automated computer program to detect any abnormal cervical vertebrae (C1-C6) motion and calculate the translational and rotational oddity to assist the chiropractitioners.

Visiting faculty, University of Lahore, Islamabad campus, Pakistan **(2013,** 6 months**)**
Conduct lectures on digital image processing and computer architecture.

Teacher Assistant, National University of Sciences & Technology, Pakistan (**2011 - 2013,** 20 months)
Team member of the college campus management system (CMS), providing support and future module development and their integration in the pre-existing system.

PUBLICATIONS

- **Zubair, M.,** Murris, S. R., Isa, K., Onoe, H., Koshimizu, Y., Kobayashi, K., Vanduffel, W., Isa., T. (2021). *Divergent whole brain projections from the ventral midbrain in macaques.* Cerebral Cortex, 31(6), 2913-2931.
- **Zubair, M.**, Ali, H., & Javed, M. Y. (2016). *Automated Segmentation of Hard Exudates Using Dynamic Thresholding to Detect Diabetic Retinopathy in Retinal Photographs*. Journal of Multimedia Processing and Technologies., 7(3), 109-116.
- **Zubair, M.**, Khan, S. A., & Yasin, U. U. (2014). *Classification of Diabetic Macular Edema and Its Stages Using Color Fundus Image*. Journal of Electronic Science and Technology, 12(2), 187-190.
- **Zubair, M**., Yamin, A., & Khan, S. A. (2013, October). *Automated detection of optic disc for the analysis of retina using color fundus image*. In 2013 IEEE International Conference on Imaging Systems and Techniques (IST) (pp. 239-242).
- **Zubair, M.** Vanduffel, W. *Modulations in the neural representation of a visual stimuli as a result of visuomotor association*. (Manuscript submitted).